NUMERICAL ANALYSIS OF FIXED-ENDED MULTILAYER AND FGM ELASTIC TUBES UNDER THERMAL AND MECHANICAL LOADS

A THESIS SUBMITTED TO
THE GRADUATE SCHOOL OF NATURAL AND APPLIED SCIENCES
OF
ATILIM UNIVERSITY

BY

HAITHEM MOHAMMED AHMED AL-MASHHADANI

IN PARTIAL FULFILLMENT OF THE REQUIREMENTS
FOR
THE DEGREE OF MASTER OF SCIENCE
IN
THE DEPARTMENT OF CIVIL ENGINEERING

JANUARY 2019

Approval of the Graduate School of Natural and Applied Sciences, Atılım University.

_____

Prof. Dr. Ali Kara
Director

I certify that this thesis satisfies all the requirements as a thesis for the degree of **Master of Science in Civil Engineering, Atılım University.**

_____

Asst. Prof. Dr. Gökhan Tunç
Head of Department

This is to certify that we have read the thesis NUMERICAL ANALYSIS OF FIXED-ENDED MULTILAYER AND FGM ELASTIC TUBES UNDER THERMAL AND MECHANICAL LOADS submitted by HAITHEM AL-MASHHADANI and that in our opinion it is fully adequate, in scope and quality, as a thesis for the degree of Master of Science.

_____

Prof. Dr. Tolga Akış
Supervisor

Examining Committee Members:

Assoc. Prof. Dr. Hakan Argeşo
Manufacturing Eng. Department, Atılım University _____

Prof. Dr. Tolga Akış
Civil Eng. Department, Atılım University _____

Assoc. Prof. Dr. Tunç Apatay
Mechanical Eng. Department, Gazi University _____

Date: January 25, 2019

I hereby declare that all information in this document has been obtained and presented in accordance with academic rules and ethical conduct. I also declare that, as required by these rules and conduct, I have fully cited and referenced all material and results that are not original to this work.

Name, Last Name: Haithem Al-Mashhadani

Signature:

ABSTRACT

NUMERICAL ANALYSIS OF FIXED-ENDED MULTILAYER AND FGM ELASTIC TUBES UNDER THERMAL AND MECHANICAL LOADS

Al-Mashhadani, Haithem
M.S., Civil Engineering Department
Supervisor: Prof. Dr. Tolga Akış

January 2019, 76 pages

A numerical procedure is presented in this study in order to determine the elastic behavior of multilayer and FGM cylindrical thick-walled tubes with fixed ends under thermal and mechanical loads. In the first part of the study, using the symbolic computation software MATHEMATICA, the expressions of temperature distribution, stress components and radial displacement are derived for single layer tubes with different loading and boundary conditions. Then, using the numerical solution option of MATHEMATICA, the stress response of the fixed-ended multilayer tubes under thermal and mechanical loads are obtained by the simultaneous solution of a series of nonlinear equations. The validity of the numerical procedure is checked by comparing the solutions of several multilayer and FGM tube problems given in different studies with the solutions obtained by the proposed method. For multilayer tubes, almost identical results are obtained, while for FGM tubes, closer results are obtained when the numbers of the layers are increased. The proposed method is easy to be implemented and can be used especially for axisymmetric FGM tube, shaft, and disk problems where the analytical solutions cannot be obtained.

Keywords: Stress Analysis, Multilayer Tubes, Elasticity, FGM Tubes.

ÖZ

ISIL VE MEKANİK YÜKLER ALTINDAKİ ÇOK KATMANLI VE FONKSİYONEL DERECELENDİRİLMİŞ MALZEMEDEN YAPILMIŞ ELASTİK TÜPLERİN SAYISAL ANALİZİ

Al-Mashhadani, Haithem
Yüksek Lisans, İnşaat Mühendisliği Bölümü
Tez Yöneticisi: Prof. Dr. Tolga Akış

Ocak 2019, 76 sayfa

Uçları sabitlenmiş çok katmanlı ve fonksiyonel derecelendirilmiş malzemeden yapılmış kalın silindirik tüplerin ısıl ve mekanik yükler altındaki elastik davranışlarını belirlemek için sayısal bir yöntem geliştirilmiştir. Çalışmanın ilk kısmında MATHEMATICA sembolik yazılım programı kullanılarak tek katmanlı tüplere ait sıcaklık dağılımı, gerilme ve radyal yönde yer değiştirme ifadeleri farklı yükleme ve sınır koşulları için elde edilmiştir. Daha sonra MATHEMATICA programının sayısal denklem çözüm opsiyonu kullanılarak, çok katmanlı tüplerin ısıl ve mekanik yükler altındaki davranışı bir dizi lineer olmayan denklemin çözümüyle elde edilmiştir. Sayısal yöntemin doğruluğunu kontrol etmek amacıyla çeşitli çalışmalarda yer alan çok katmanlı ve fonksiyonel derecelendirilmiş malzemeden yapılmış tüp problemleri ele alınmıştır. Çok katmanlı tüplerde neredeyse aynı sonuçlar bulunurken, fonksiyonel derecelendirilmiş malzemeden yapılmış tüp problemlerinde katman sayısının artırılması ile daha yakın sonuçlar elde edildiği görülmüştür. Kolay kullanımının yanı sıra, önerilen yöntem ile özellikle analitik çözümü bulunmayan eksenel simetriye sahip fonksiyonel derecelendirilmiş tüp, şaft ve disk problemlerinin sayısal çözümlerinin bulunabileceği düşünülmektedir.

Anahtar Kelimeler: Gerilme Analizi, Çok Katmanlı Tüpler, Elastisite, Fonksiyonel Derecelendirilmiş Malzemeden Yapılmış Tüpler.

To My Father Dr. Mohammed Al-Mashhadani

ACKNOWLEDGEMENTS

First of all, I would like to thank to my supervisor Prof. Dr. Tolga Akış for his guidance during this study. To my Father, Dr. Mohammed Al-Mashhadani, I offer sincere thanks for his continuous encouragement to study master's degree. I also want to thank to my wife, Ghada, for her patience during this period. Lastly, I want to thank to my family, friends and my baby boy, Karam, just them presence has been enough for me.

TABLE OF CONTENTS

LIST OF TABLES

TABLES

LIST OF FIGURES

FIGURES

LIST OF SYMBOLS

a, b	inner and outer layer coordinates of the tube assembly, respectively
A_i, C_i	integration constants
E	modulus of elasticity
E_0	the reference of modulus of elasticity
k	thermal conductivity
k_0	the reference thermal conductivity
m, n	functionally grading parameters
Q	constant heat load
q	heat generation rate
r, θ, z	cylindrical coordinates
T	temperature
T_i	reference temperature
u	radial displacement
α	coefficient of thermal expansion
ε_i	strain components
v	Poisson's ratio
σ_i	stress components
σ_0	yield stress

CHAPTER 1

INTRODUCTION

Axisymmetric cylindrical structural members such as shafts, pipes, and tubes are commonly used structures that have a wide range of applications in engineering. Chemical and nuclear industry, automotive industry, power plants, pipelines, and military equipment are the major areas of usage of these assemblies. Due to this reason, the analysis and design of such assemblies under different loading conditions are quite important. On the other hand, in recent years, the investigations on the tubes, shafts and disks made of composite and functionally graded materials have been made by many researchers. As having many advantages while compared with homogenous ones, mechanical analysis, design, and production of them is quite popular.

The theoretical basis for the analysis of infinitely long cylindrical tubes under different loading and boundary conditions can be found in many textbooks such as Timoshenko and Goodier [1], Boresi et al. [2], Mendelson [3], Boley and Weiner [4], and Nadai [5]. In these books, the analytical expression of stresses and displacement in elastic, elastoplastic or elastic-perfectly plastic stress states can be found under different assumptions. For example, Timoshenko and Goodier [1] obtained the stresses and radial displacement of cylindrical tubes under internal and/or external pressure. Mendelson [3] studied the elastic-perfectly plastic tubes under pressure. On the other hand, the stress response of single layer tubes in elastic stress state under different thermal loading cases can be found in [5].

In addition to these studies, Durban and Kubi [6] investigated the internally pressurized tube problem in elastic-plastic stress state. Lazzarin and Livieri [7], Parker [8], and Perry and Aboudi [9] also studied the internally pressurized tubes and focused on the autofrettage process of these tubes.

As stated above, multilayer tubes have several advantages while compared with single layer homogenous tubes. Some examples of analytical studies on multilayer

assemblies that were performed by different researchers in the past are summarized below.

Akış and Eraslan [10] investigated the yielding of infinitely long tightly-fitted two-layer concentric tubes with fixed ends subjected to either internal or external pressure. Using von Mises yield criterion, critical values of pressure that commences the plastic flow are determined in terms of material properties and tube dimensions. In a similar study by the same authors [11] von Mises yield criterion was used for the determination of the yielding behavior of shrink-fitted two-layer tubes. The numerical results were obtained for shrink-fitted tubes made of steel and aluminum. In a similar work, the analyses of two and three-layer shrink fitted composite tubes were studied analytically and by finite element method by Qui and Zhou [12].

Stress analysis in strain hardening tightly fitted two-layer composite tubes subject to cyclic loading of internal pressure was studied by Eraslan and Akis [13]. In their study, they examined fixed-ended cyclically loaded tubes having two layers in the elastic and elastic-plastic stress states. Their analytical solution was based on Tresca's yield criterion and its associated flow rule and they gave numerical results for the assemblies having steel inner and aluminum outer layers. In a similar study by the same authors [14], tightly-fitted two-layer concentric tubes having fixed ends under cyclic external pressure was studied. Elastic and elastic-plastic solutions are obtained and some numerical results were presented for the tubes with steel and aluminum layers.

Stress distributions in energy generating two-layer tubes subjected to free and radially constrained boundary conditions was investigated by Eraslan, Sener and Argeso [15]. The analytical solutions were obtained in that study for thermally induced elastic and elastic plastic deformations in heat generating composite tubes having free inner and radially constrained outer boundaries. Tresca's yield condition and its associated flow rule were used to determine the elastic-plastic response of the assemblies.

As stated before, cylindrical tubes made of functionally graded materials (FGM) have several advantages and due to these reason researchers investigated these assemblies under thermal and mechanical loads in the elastic, partially plastic and elastic-plastic stress states in the past. The studies of Horgan and Chan [16], Tutuncu and Ozturk

[17], Jabbari et al. [18], Ma et al. [19], Zhifei, Taota and Hongjun [20], and Chen and Lin [21] are some examples for analytical studies performed in the past.

Analytical solutions for a functionally graded elastic–plastic pressurized tube under plane strain assumption was obtained by Eraslan and Akis [22], In their study, the analytical plastic model was based on Tresca's yield criterion, its associated flow rule and ideally plastic material behavior. Elastic, partially plastic and fully plastic stress states was investigated and it was shown that the stress response of the FGM pressurized tube is affected significantly by the material no homogeneity.

Pressurized functionally graded hollow cylinders with arbitrarily varying material properties was studied by Li and Peng [23]. In their study, an efficient approach was suggested, which reduces the problem to solving a Fredholm integral equation. The resulting equation was approximately solved by expanding the solution as series of Legendre polynomials and the numerical results of the distribution of the radial and circumferential stresses are presented graphically. Nie, Zhong and Batra [24] presented a technique to design materials for FGM linear elastic cylinders and spheres for a constant hoop stress or a constant plane shear stress.

Analytical elastic solutions for pressurized hollow cylinders with internal functionally graded coatings were obtained by Sburlati [25]. In the study, the researcher derived analytical solutions for thick-walled cylinders subjected to internal and external pressure and assumed that the materials were isotropic with a constant Poisson's ratio.

An elasticity solution for functionally graded thick-walled tube subjected to internal pressure was obtained by Xin et al. [26]. They derived the hypergeometric differential equation of the radial displacement and their proposed method is valid for the materials with different Poisson's ratios. To reduce the stress concentration in the FGM tube, the difference between the circumferential and radial stresses was evaluated and the optimal ratio of two Young's moduli was presented in their study.

In the study of Akis [27], the yielding of FGM tubes with fixed ends under thermal loading was investigated analytically. Considering non-uniform heat generation in a long tube, the effect of grading parameters on the yielding behavior of the tube was presented. The thermal conductivity and the modulus of elasticity of the tube material

was assumed to vary radially in nonlinear forms, and it is found that the plastic flow may commence at the inner or outer surface or inside tube depending on the functionally grading parameters.

Elastic–plastic stress analysis in a long FGM solid cylinder with fixed ends subjected to uniform heat generation was studied by Ozturk and Gulgec [28]. The deformations of the assembly were investigated using Tresca's yield criterion and it was assumed that four of the material properties vary radially. These material properties are modulus of elasticity, yield strength, coefficients of thermal conduction and thermal expansion.

Analytical solutions considering the yielding behavior of FGM thick-walled cylindrical tubes undergoing thermomechanical loads were presented by Sadrabadi et al. [29]. In their study, they investigated a cylindrical thick-walled tube made of FGM and the tube material properties were assumed to be isotropic and vary as a power function of the radius. A yield variable parameter was defined according to von Mises criterion for internal pressure with heat generation.

Numerical solutions to multilayer composite tube problem under different loading conditions were also obtained by a number of researchers in the past. Different algorithms were developed for pressurized multilayer cylindrical composite tubes with or without temperature loading. The stress and displacement expressions were obtained in elastic stress state with plane or generalized plane strain assumptions. In a closely related study, Sollund, Vedeld and Hellesland [30] derived two independent sets of analytical solutions to calculate the displacements and stresses in elastic multi-layer cylinders subjected to pressure or thermal loading or both. The obtained solutions were used to find the stress response of a pipeline with a corrosion-resistant liner and a multi-layered thermal insulation coating. In a similar study by the same research group [31], an analytical solution for the displacement field and corresponding stress state in multi-layer cylinders subjected to pressure and thermal loading was developed. Their solutions were used for axially loaded and spring-mounted cylinders and the analytical solutions are verified by means of detailed three-dimensional finite element analyses.

Yeo et al. [32] found exact solutions for stresses and displacements in multilayered hollow cylinders under thermo-mechanical loading by using an approach named recursive method. The results for temperature, stresses and displacements obtained by using these solutions seems to be in a good agreement with the pressurized functionally graded material (FGM) results. In addition, they used their proposed method in the solution of a six-layer composite cylinder with different materials subjected to temperature, internal pressure and external pressure.

In this study, different form the studies mentioned above, an efficient and easy computational procedure is developed for the stress analysis of multilayer and functionally graded tubes under thermal and mechanical loading. With the proposed algorithm, by considering the uncoupled theory of thermoelasticity, thermal stress can be obtained for steady state and heat generation problems with different boundary conditions, including thermal insulation at the inner or outer surfaces. Internally or externally pressurized multilayer cylinder problems can also be handled by using this method. MATHEMATICA [33] software is used in the derivations and in the implementation of the numerical procedure.

The study is organized as follows: In Chapter 2, the analytical derivations for a single layer tube under thermal loading and/or pressure is presented for different boundary conditions. The computational procedure developed for the solution of multilayer tube problems is also given in that chapter. In Chapter 3, the problems solved with the proposed procedure are presented. In addition, the comparison of the results of some problems obtained by using the proposed method with the corresponding results given in previous studies are made in that chapter. Finally, in Chapter 4, the results are discussed and some conclusions are made.

CHAPTER 2

FORMULATION

2.1 General

In this study, polar cylinder coordinates (r, θ and z) are considered in all derivations and a state of plane strain and infinitely small deformations are presumed. In addition, the uncoupled theory of elasticity is considered throughout the study. At first, the temperature distributions for constant heat generation and for steady state conditions are derived for a single layer tube. Then, the stress and displacement expressions for the tube under both temperature load and pressure are presented. By reducing these derived expressions, the stress response of the single layer tube under internal, external or both internal and external pressures are obtained without considering the thermal loading. In addition, the formulation and the procedure used in the numerical analysis of the multilayer tube assemblies under thermal and mechanical loads is presented at the end of this chapter. In all derivations MATHEMATICA [33] software is used.

2.2 Single layer tube

In this part, the energy equation is solved first for the single layer tube under heat generation. Then, this solution is reduced to steady state solution, for which heat generation is not considered. Using all possible boundary condition, the temperature distributions are obtained for both cases. Then, the expressions for thermally loaded single layer tube under internal, external and both internal and external pressures are obtained. Finally, in the last part, the stress and displacement expressions for only mechanical loads (internal pressure, external pressure, and both internal and external pressure) are presented which are obtained by reducing the expressions derived for the temperature loading and pressure.

The geometry of the single layer tube is given in Figure 2.1. In this figure, a is the inner radius, b is the outer radius, and r is the radial coordinate.

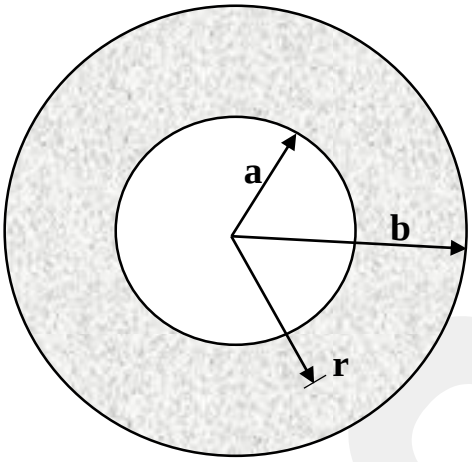

Figure 2.1. Cross-section of a single layer tube

2.2.1 Temperature distribution

Energy equation for an infinitely long cylindrical tube with axial symmetry producing internal heat is given as [5]

$$\frac{\mathrm{d}}{\mathrm{dr}}\left[\mathrm{r\,k}\frac{\mathrm{dT}}{\mathrm{dr}}\right]+\mathrm{rq}=0 \tag{1}$$

Here r is the radial coordinate, T is the temperature and k is the thermal conductivity. In addition, q is the constant heat generation. The solution of this equation for temperature T is obtained as

$$\mathrm{T}=\mathrm{A_1}+\mathrm{A_2}\ln(\mathrm{r})-\frac{\mathrm{q\,r^2}}{4\mathrm{k}} \tag{2}$$

where A_1 and A_2 are the integration constants. For the tube in steady state, where q = 0, Eq. (2) becomes

$$\frac{\mathrm{d}}{\mathrm{dr}}\left[\mathrm{r\,k}\frac{\mathrm{dT}}{\mathrm{dr}}\right]=0 \tag{3}$$

The solution of this equation for T is

$$\mathrm{T}=\mathrm{A_3}+\mathrm{A_4}\ln(r) \tag{4}$$

In order to find the integration constants, one must use the boundary conditions of the problem. In case of prescribed temperatures at the inner and outer surfaces, the boundary conditions are

$$T(a) = T_a \tag{5}$$

$$T(b) = T_b \tag{6}$$

The constants of integration for heat generation case are obtained as

$$A_1 = -\frac{-b^2 q \ln(a) + a^2 q \ln(b) + 4k \ln(b)\, T_a - 4\, k \ln(a)\, T_b}{4k\ \ln(a/b)} \tag{7}$$

$$A_2 = -\frac{b^2 q - a^2 q - 4k\, T_a + 4kT_b}{4k \ln(a/b)} \tag{8}$$

For steady state condition (*q = 0)*, the constants of integration are

$$A_3 = -\frac{\ln(b)\, T_a - \ln(a)\, T_b}{\ln(a/b)} \tag{9}$$

$$A_4 = -\frac{T_b - T_a}{\ln(a/b)} \tag{10}$$

For the case of thermally insulated outer surface, the boundary conditions become

$$T(a) = T_a \tag{11}$$

$$\frac{dT}{dr}\Big|_{r=b} = 0 \tag{12}$$

The integration constants for the heat generation case is

$$A_1 = \frac{q(a^2 - 2b^2 \ln(a))}{4\, k} + T_a \tag{13}$$

$$A_2 = \frac{b^2 q}{2k} \tag{14}$$

For steady case (*q = 0*), they are obtained as

$$A_3 = T_a \tag{15}$$

$$A_4 = 0 \tag{16}$$

Finally, for thermally insulated inner surface, the boundary conditions become

$$\left.\frac{dT}{dr}\right|_{r=a} = 0 \tag{17}$$

$$T(b) = T_b \tag{18}$$

A_1 and A_2 can be obtained for heat generation as

$$A_1 = \frac{1}{4}\left(b^2 kq - 2\,a^2 k\,q\,\ln(b) + 4\,T_b\right) \tag{19}$$

$$A_2 = \frac{1}{2k}\,a^2\,q \tag{20}$$

and for steady state case where $q=0$, the integrations constants are

$$A_3 = T_b \tag{21}$$

$$A_4 = 0 \tag{22}$$

2.2.2 Elastic solution for a single layer tube under thermal loading and pressure

In order to obtain the elastic solution, we use Hooke's law for cylindrical coordinate system [1]. The equations are

$$\epsilon_r = \frac{1}{E}\left(\sigma_r - \nu(\sigma_\theta + \sigma_z)\right) + \alpha\Delta T \tag{23}$$

$$\epsilon_\theta = \frac{1}{E}\left(\sigma_\theta - \nu(\sigma_r + \sigma_z)\right) + \alpha\Delta T \tag{24}$$

$$\epsilon_z = \frac{1}{E}\left(\sigma_z - \nu(\sigma_r + \sigma_\theta)\right) + \alpha\Delta T \tag{25}$$

where $\Delta T = T - T_i$. Here T_i is the reference temperature and in this study and it is taken as zero. For tubes with fixed ends, $\epsilon_z = 0$. The axial stress becomes

$$\sigma_z = -E\alpha T + \nu\sigma_r + \nu\sigma_\theta \tag{26}$$

Inserting Eq. (26) into equation (23) and (24) and by using the strain-displacement relations

$$\epsilon_r = \frac{du}{dr} \tag{27}$$

$$\epsilon_\theta = \frac{u}{r} \tag{28}$$

the following stress-displacement relations can be obtained

$$\sigma_r = \frac{E(r\,\alpha(1+\nu)T - \nu u + r(-1+\nu)u')}{r(1+\nu)(-1+2\nu)} \tag{29}$$

$$\sigma_\theta = \frac{E(r\,\alpha(1+\nu)T + (-1+\nu)u - r\nu u')}{r\,(1+\nu)(-1+2\nu)} \tag{30}$$

Putting these expressions into the equation of equilibrium in radial direction, which is

$$\frac{d\sigma_r}{dr} + \frac{\sigma_r - \sigma_\theta}{r} = 0 \tag{31}$$

the governing differential equation is obtained as

$$\frac{d^2u}{dr^2} + \frac{du}{dr}\frac{1}{r} - \frac{u}{r^2} = \frac{\alpha(1+\nu)}{1-\nu}\frac{dT}{dr} \tag{32}$$

The solution of this differential equation for *u* with heat generation is

$$u = C_1\, r + \frac{C_2}{r} + \frac{r\,\alpha(1+\nu)(4\,A_2 + k\,q\,r^2 - 8\,A_2\ln(r))}{16(-1+\nu)} \tag{33}$$

and the stresses become

$$\sigma_r = \frac{A_2\, E\, \alpha \ln(r)}{2(\nu-1)} - \frac{E\, C_2}{r^2(1+\nu)} - \frac{E\, C_1}{(1+\nu)(-1+2\nu)} - \frac{E(4\, A_2 + k\, q\, r^2)\alpha}{16(-1+\nu)} + \frac{A_1\, E\, \alpha}{2\nu-1} \tag{34}$$

$$\sigma_\theta = \frac{A_2\alpha}{4-4\nu} + \frac{3\, k\, q\, r^2\alpha}{16(\nu-1)} - \frac{A_1\alpha(1+\nu) - C_1}{(1-2\nu)(1+\nu)} - \frac{C_2}{r^2(1+\nu)} + \frac{A_2\, E\, \alpha \ln(r)}{2(-1+\nu)} \tag{35}$$

$$\sigma_z = -\frac{A_2\, E\, \alpha \ln(r)}{1-\nu} - \frac{2\, E\, \nu\, C_1}{(1+\nu)(-1+2\nu)} + E\, \alpha \left(\frac{k\, q\, r^2}{4(1-\nu)} - \frac{A_1}{1-2\nu} \right) \tag{36}$$

In case of steady state where q=0, the solution of Eq. (32) for *u* is

$$u = C_1 r + \frac{C_2}{r} - \frac{A_4\, r\, \alpha(1+\nu)(-1+2\ln(r))}{4(\nu-1)} \tag{37}$$

and the corresponding stresses are obtained as

$$\sigma_r = \frac{A_4\, E\, \alpha}{4-4\nu} - \frac{A_4\, E\, \alpha \ln(r)}{2(1-\nu)} - \frac{A_3\, E\, \alpha}{1-2\nu} + \frac{E\, C_1}{(1-2\nu)(1+\nu)} - \frac{E\, C_2}{r^2(1+\nu)} \tag{38}$$

$$\sigma_\theta = \frac{E\, C_2}{r^2(1+\nu)} + \frac{A_4\, E\, \alpha}{4(-1+\nu)} + \frac{E\, C_1}{(1-2\nu)(1+\nu)} - \frac{A_3\, E\, \alpha}{1-2\nu} - \frac{A_4\, E\, \alpha \ln(r)}{2(1-\nu)} \tag{39}$$

$$\sigma_z = -\frac{A_4\, E\, \alpha \ln(r)}{1-\nu} - \frac{E(A_3\, \alpha(1+\nu) - 2\, \nu\, C_1)}{(1-2\nu)(1+\nu)} \tag{40}$$

To complete the solution, one must find the integration constants C_1 and C_2 using boundary conditions. Possible boundary conditions and corresponding evaluated integration constants are listed below:

a) For a heat generating tube without pressure load, the boundary conditions are

$$\sigma_r(a) = 0 \tag{41}$$

$$\sigma_r(b) = 0 \tag{42}$$

The corresponding integration constants are

$$C_1 = \frac{a^2\ b^2\ \alpha\ (1+\nu)[(a-b)(a+b)q + 8\ A_2\ k\ (-\ln(b/a)]}{16\ (a-b)(a+b)\ k\ (-1+\nu)} \quad (43)$$

$$C_2 = \frac{A_2\ \alpha\ (-1+\nu+2\ \nu^2)(a^2\ \ln(a) - b^2 \ln(b))}{2(a-b)(a+b)(-1+\nu)} - \frac{A_2\ \alpha\ (-1+\nu+2\nu^2)}{4(-1+\nu)}$$

$$+ A_1\ \alpha\ (1+\nu) - \frac{(a^2+b^2)\ q\ \alpha\ (-1+\nu+2\nu^2)}{16\ k\ (-1+\nu)} \quad (44)$$

b) For a heat generating tube under internal pressure, the boundary conditions are

$$\sigma_r(a) = -P_{int} \quad (45)$$

$$\sigma_r(b) = 0 \quad (46)$$

The corresponding integration constants are

$$C_1 = \frac{a^2 b^2 (1+\nu)(16\ k\ P_{int} + a^2 E\ q\ \alpha - b^2\ E\ q\ \alpha - 16\ k\ P_{int}\ \nu - 8\ A_2\ E\ k\ \alpha \ln(a))}{16\ (a-b)(a+b)\ E\ k\ (-1+\nu)}$$

$$+ \frac{a^2\ A_2\ b^2\ \alpha\ (1+\nu)\ln(b)}{2\ (a-b)(a+b)(-1+\nu)} \quad (47)$$

$$C_2 = -\frac{a^4 q\ \alpha(1+\nu)(-1+2\nu)}{16(a-b)(a+b)\ k\ (-1+\nu)}$$

$$+ \frac{A_2\ \alpha\ (-1+\nu+2\nu^2)(a^2\ \ln(a) - b^2\ \ln(b))}{2(a-b)(a+b)(-1+\nu)}$$

$$+ \frac{b^2 \alpha(1+\nu)(-4\ A_2\ k + 16\ A_1\ k - b^2 q + 8\ A_2\ k\ \nu - 16\ A_1\ k\ \nu + 2b^2 q\ \nu)}{16(a-b)(a+b)\ k\ (-1+\nu)}$$

$$+ \frac{a^2(1+\nu)(4P_{int} + A_2\ E\alpha - 4A_1\ E\alpha - 12P_{int}\ \nu - 2A_2 E\alpha\nu + 4A_1\ E\alpha\nu + 8P_{int}\nu^2)}{4(a-b)(a+b)E(-1+\nu)}$$

(48)

c) For a heat generation tube under external pressure, the boundary conditions are

$$\sigma_r(a) = 0 \quad (49)$$

$$\sigma_r(b) = -P_{ext} \tag{50}$$

and the integration constants are obtained as

$$C_1 = \frac{a^2\, A_2\, b^2\, \alpha(1+\nu)\ln(b)}{2\,(a-b)(a+b)(-1+\nu)}$$

$$+\frac{a^2 b^2(1+\nu)(-16\,k\,P_{ext} + a^2 E\,q\,\alpha - b^2\,E\,q\,\alpha + 16\,k\,P_{ext}\,\nu - 8\,A_2\,E\,k\,\alpha\ln(a))}{16\,(a-b)(a+b)\,E\,k\,(-1+\nu)} \tag{51}$$

$$C_2 = \frac{b^4 q\,\alpha(1+\nu)(-1+2\nu)}{16(a-b)(a+b)\,k\,(-1+\nu)} + \frac{A_2\,\alpha\,(-1+\nu+2\nu^2)(a^2\ln(a) - b^2\ln(b))}{2(a-b)(a+b)(-1+\nu)}$$

$$-\frac{a^2\alpha(1+\nu)(-4\,A_2\,k + 16\,A_1\,k - a^2 q + 8\,A_2\,k\,\nu - 16\,A_1\,k\,\nu + 2a^2 q\,\nu)}{16(a-b)(a+b)\,k\,(-1+\nu)}$$

$$+\frac{b^2(1+\nu)(-4P_{ext} - A_2\,E\alpha + 4A_1\,E\alpha + 12P_{ext}\,\nu + 2A_2 E\alpha\nu - 4A_1\,E\alpha\nu - 8P_{ext}\nu^2)}{4(a-b)(a+b)E(-1+\nu)} \tag{52}$$

d) For a heat generating tube under both internal and external pressure, the boundary conditions become

$$\sigma_r(a) = -P_{int} \tag{53}$$

$$\sigma_r(b) = -P_{ext} \tag{54}$$

and the integration constants are obtained as

$$C_1 = -\frac{a^2 A_2 b^2\alpha(1+\nu)(\ln(a/b))}{2(a-b)(a+b)(-1+\nu)} - \frac{a^2 b^2 P_{int}(1+\nu)}{(a-b)(a+b)E} + \frac{a^2 b^2 P_{ext}(1+\nu)}{(a-b)(a+b)E}$$

$$+\frac{a^2 b^2\,q\,\alpha(1+\nu)}{16\,k(-1+\nu)} \tag{55}$$

$$C_2 = -\frac{a^4 q\,\alpha(1+\nu)(-1+2\nu)}{16(a-b)(a+b)k(-1+\nu)} + \frac{b^4 q\,\alpha(1+\nu)(-1+2\nu)}{16(a-b)(a+b)k\,(-1+\nu)}$$

$$-\frac{a^2(1+\nu)(-4\mathrm{P}_{int}-\mathrm{A}_2 e\alpha+4\mathrm{A}_1\,E\,\alpha+12\,\mathrm{P}_{int}\,\nu+2\,\mathrm{A}_2\,E\,\alpha\,\nu-4\,\mathrm{A}_1\,E\,\alpha\,\nu-8\mathrm{P}_{int}\,\nu^2)}{4(a-b)(a+b)E(-1+\nu)}$$

$$+\frac{b^2(1+\nu)(-4\mathrm{P}_{ext}-\mathrm{A}_2\,E\,\alpha+4\mathrm{A}_1\,E\,\alpha+12\mathrm{P}_{ext}\,\nu+2\,\mathrm{A}_2 E\,\alpha\,\nu-4\mathrm{A}_1\,E\,\alpha\,\nu-8\mathrm{P}_{ext}\,\nu^2)}{4(a-b)(a+b)E(-1+\nu)}$$

$$+\frac{a^2\mathrm{A}_2\alpha(1+\nu)(-1+2\nu)\ln(a)}{2(a-b)(a+b)(-1+\nu)}-\frac{\mathrm{A}_2\,b^2\alpha(1+\nu)(-1+2\nu)\ln(b)}{2(a-b)(a+b)(-1+\nu)} \tag{56}$$

e) For a tube without heat generation (*q=0*), prescribed temperatures at the inner and outer surfaces, and no pressure load, the following boundary conditions are valid:

$$\sigma_{\mathrm{r}}(\mathrm{a})=0 \tag{57}$$

$$\sigma_{\mathrm{r}}(\mathrm{b})=0 \tag{58}$$

and the integration constants are evaluated as

$$\mathrm{C}_1=\frac{\mathrm{a}^2\mathrm{A}_4\mathrm{E}\,\alpha(1+\nu)(-1+2\nu)\ln(\mathrm{a})}{2\mathrm{E}\,(\mathrm{a}^2-\mathrm{b}^2)(-1+\nu)}-\frac{\mathrm{A}_4\mathrm{E}\,\alpha\,(1+\nu)(-1+2\nu)}{4\,\mathrm{E}\,(-1+\nu)}+\frac{\mathrm{A}_3\,\mathrm{E}\,\alpha(1+\nu)}{\mathrm{E}}$$

$$-\frac{\mathrm{A}_4\,\mathrm{b}^2\mathrm{E}\alpha(1+\nu)(-1+2\nu)\ln(\mathrm{b})}{2\mathrm{E}(\mathrm{a}^2-\mathrm{b}^2)(-1+\nu)} \tag{59}$$

$$\mathrm{C}_2=-\frac{\mathrm{a}^2\mathrm{A}_4\,\mathrm{b}^2\,\alpha\,(1+\nu)\big(\ln(a/b)\big)}{2(\mathrm{a}^2-\mathrm{b}^2)(-1+\nu)} \tag{60}$$

f) For an internally pressurized tube with no heat generation and with prescribed temperatures at the inner and outer surfaces, the boundary conditions are

$$\sigma_{\mathrm{r}}(\mathrm{a})=-\mathrm{P}_{int} \tag{61}$$

$$\sigma_{\mathrm{r}}(\mathrm{b})=0 \tag{62}$$

By using these conditions, integration constants can be obtained as

$$C_1 = \frac{A_4\alpha(1+\nu)(-1+2\nu)(a^2\ln(a) - b^2\ln(b))}{2(a^2-b^2)(-1+\nu)} + \frac{a^2 P_{int}(1+\nu)(-1+2\nu)}{(a^2-b^2)E}$$

$$+ A_3\,\alpha(1+\nu) - \frac{A_4\alpha(1+\nu)(-1+2\nu)}{4(-1+\nu)} \tag{63}$$

$$C_2 = -\frac{a^2\,b^2\,(1+\nu)\left(2\,P_{int}(-1+\nu) + A_4\,E\,\alpha\left(\ln(a/b)\right)\right)}{2(a^2-b^2)\,E\,(-1+\nu)} \tag{64}$$

g) For an externally pressurized tube without heat generation and with prescribed temperatures at the inner and outer surfaces, the boundary conditions are

$$\sigma_r(a) = 0 \tag{65}$$

$$\sigma_r(b) = -P_{ext} \tag{66}$$

and the integration constants are

$$C_1 = -\frac{a^2\alpha(1+\nu)(-A_4 + 4\,A_3 + 2\,A_4\nu - 4\,A_3\,\nu)}{4(a^2-b^2)(-1+\nu)}$$

$$-\frac{A_4\,b^2\,\alpha(1+\nu)(-1+2\nu)\ln(b)}{2\,(a^2-b^2)\,(-1+\nu)} + \frac{a^2 A_4\alpha(1+\nu)(-1+2\nu)\ln(a)}{2\,(a^2-b^2)\,(-1+\nu)}$$

$$+\frac{b^2(1+\nu)(-4\,P_{ext} - A_4\,E\,\alpha + 4\;A_3\,E\,\alpha + 12\,P_{ext}\,\nu + 2\,A_4 E\,\alpha\,\nu - 4\,A_3\,E\,\alpha\,\nu - 8\,P_{ext}\,\nu^2)}{4(a^2-b^2)\,E\,(-1+\nu)} \tag{67}$$

$$C_2 = \frac{a^2 b^2(1+\nu)(2\,P_{ext}(-1+\nu) + A_4\,E\,\alpha(\ln(b/a)))}{2E\,(a^2-b^2)\;(-1+\nu)} \tag{68}$$

h) For an externally and internally pressurized tube under steady state temperature distribution, with prescribed temperatures at the inner and outer surfaces, the boundary conditions are

$$\sigma_r(a) = -P_{int} \tag{69}$$

$$\sigma_r(b) = -P_{ext} \tag{70}$$

Using these boundary conditions, the integration constants can be evaluated as

$$C_1 = -\frac{b^2 P_{ext}(1+\nu)(-1+2\nu)}{(a-b)(a+b)E} - \frac{A_3\, b^2 \alpha(1+\nu)(-1+2\nu)\ln(b)}{2(a-b)(a+b)(-1+\nu)}$$

$$-\frac{a^2(1+\nu)(-4P_{int} - A_3\, E\alpha + 4\, A_4\, E\alpha + 12\, P_{int}\,\nu + 2A_3\, E\alpha\nu - 4\, A_3\, E\alpha\nu - 8\, P_{int}\nu^2)}{4(a-b)(a+b)E(-1+\nu)}$$

$$+\frac{a^2 A_3 \alpha(1+\nu)(-1+2\nu)\ln(a)}{2(a-b)(a+b)(-1+\nu)} + \frac{b^2\alpha(1+\nu)(-A_3 + 4\, A_4 + 2A_3\nu - 4A_4\,\nu)}{4(a-b)(a+b)(-1+\nu)} \tag{71}$$

$$C_2 = -\frac{a^2 b^2(1+\nu)\big(2(P_{int} - P_{ext})(-1+\nu) + A_3 E\alpha\,\ln(a) - A_3\, E\,\alpha\ln(b)\big)}{2(a^2-b^2)E(-1+\nu)} \tag{72}$$

2.2.3 Elastic solution for a single layer tube under pressure

The generalized Hooke's law in cylindrical coordinates can be written without temperature term as

$$\epsilon_r = \frac{1}{E}\big(\sigma_r - \nu(\sigma_\theta + \sigma_z)\big) \tag{73}$$

$$\epsilon_\theta = \frac{1}{E}\big(\sigma_\theta - \nu(\sigma_r + \sigma_z)\big) \tag{74}$$

$$\epsilon_z = \frac{1}{E}\big(\sigma_z - \nu(\sigma_r + \sigma_\theta)\big) \tag{75}$$

For the fixed ends tubes $\epsilon_z = 0$. The stress in axial direction can be written as

$$\sigma_z = \nu(\sigma_r + \sigma_\theta) \tag{76}$$

Inserting Eq. (76) into equation (73) and (74) and by using the strain-displacement relations given in Eq. (27) and (28), the following stress-displacement relations can be obtained

$$\sigma_r = \frac{E(\nu\, u + r\, u'(1-\nu))}{r(1+\nu)(1-2\nu)} \tag{77}$$

$$\sigma_\theta = \frac{E(u\,(1-\nu) + r\,\nu\,u')}{r(1+\nu)(1-2\nu)} \tag{78}$$

Putting these expressions into the equation of equilibrium in radial direction (Eq. 31), the governing differential equation is obtained as

$$\frac{d^2u}{dr^2} + \frac{du}{dr}\frac{1}{r} - \frac{u}{r^2} = 0 \tag{79}$$

The solution of this differential equation for *u* is

$$u = C_1\,r + \frac{C_2}{r} \tag{80}$$

Then, the stress relations are evaluated as

$$\sigma_r = \frac{E}{1+\nu}\left(\frac{C_1}{1-2\nu} - \frac{C_2}{r^2}\right) \tag{81}$$

$$\sigma_\theta = \frac{E}{1+\nu}\left(\frac{C_1}{1+2\nu} + \frac{C_2}{r^2}\right) \tag{82}$$

$$\sigma_z = \frac{2\,\nu\,E\,C_1}{(1+\nu)(1-2\nu)} \tag{83}$$

To complete solution, the integration constants C_1 and C_2 should be found. In the next part, the integration constants obtained for different boundary conditions are presented.

a) For a tube with internal pressure, the boundary conditions are

$$\sigma_r(a) = -P_{int} \tag{84}$$

$$\sigma_r(b) = 0 \tag{85}$$

and the integration constants can be obtained as

$$C_1 = \frac{a^2 P_{int}(1+\nu)(1+2\nu)}{(b^2 - a^2)E} \tag{86}$$

$$C_2 = \frac{a^2\,b^2\,P_{int}(1+\nu)}{(b^2 - a^2)E} \tag{87}$$

b) For an externally pressurized tube, the boundary conditions are

$$\sigma_r(a) = 0 \tag{88}$$

$$\sigma_r(b) = -P_{ext} \tag{89}$$

and the integration constants can be obtained as

$$C_1 = -\frac{b^2\, P_{ext}(1+\nu)(1-2\nu)}{(b^2-a^2)E} \tag{90}$$

$$C_2 = -\frac{a^2\, b^2\, P_{ext}(1+\nu)}{(b^2-a^2)E} \tag{91}$$

c) For tube with both internal and external pressures

$$\sigma_r(a) = -P_{int} \tag{92}$$

$$\sigma_r(b) = -P_{ext} \tag{93}$$

and the integration constants are obtained as

$$C_1 = -\frac{(1+\nu)(2\nu-1)(b^2P_{ext} - a^2P_{int})}{(b^2-a^2)E} \tag{94}$$

$$C_2 = -\frac{a^2b^2(1+\nu)(P_{ext} - P_{int})}{(b^2-a^2)E} \tag{95}$$

2.3 Multilayer tubes

The cross-section of a typical multilayer tube is shown in Fig. 2.2. In this figure *a* is the inner radius and *b* is the outer radius. It is assumed that the multilayer tube consists of *n* layers. In the formulations, r_i is the interface radius between *i-th* and *(i+1)-th* layers. In the next part, the temperature distribution, displacement and stress expressions derived for the solution of multilayer tube problems are presented. In addition, the numerical procedure under thermal loads and pressure are also given.

2.3.1 Temperature distribution

For a constant heat generating tube layer, the temperature distribution is

$$T_i(r) = (A_1)_i + (A_2)_i \ln(r) - \frac{q_i\, r^2}{4\, k_i} \tag{96}$$

Here, T_i is the temperature distribution for the *i-th* layer. Similarly, $(A_1)_i$ and $(A_2)_i$ are the integration constants for that layer. On the other hand, q_i is the constant heat generation term, and k_i is the thermal conductivity of the *i-th* layer. For steady state, the temperature distribution for any *i-th* layer is defined as

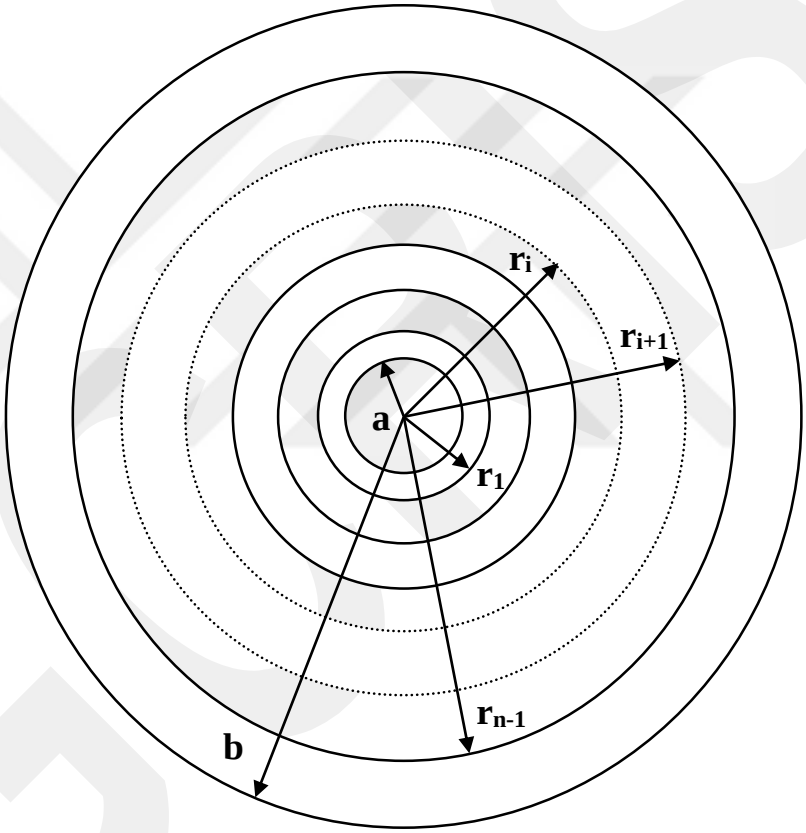

Figure 2.2. Cross-section of a multilayer tube

$$T_i(r) = (A_3)_i + (A_4)_i \ln(r) \tag{97}$$

For finding the corresponding integration constants, the following boundary condition are used:

a) In case of prescribed temperature for inner and outer surfaces, the boundary conditions are

$$T_1(\mathrm{a}) = \mathrm{T_a} \tag{98}$$

$$T_n(\mathrm{b}) = \mathrm{T_b} \tag{99}$$

where T_1 is the temperature distribution of the first layer and T_n is the temperature distribution of the *n-th* layer (the outer layer).

b) For the thermally insulated inner surface, the boundary conditions are

$$\frac{dT_1}{\mathrm{dr}}\Big|_{\mathrm{r=a}} = 0 \tag{100}$$

$$\mathrm{T_n(b) = T_b} \tag{101}$$

c) For the thermally insulated outer surface, the boundary conditions are

$$\mathrm{T_1(a) = T_a} \tag{102}$$

$$\frac{dT_n}{\mathrm{dr}}\Big|_{\mathrm{r=b}} = 0 \tag{103}$$

Finally, the following interface conditions between *i-th* and *(i+1)-th* layers are used in the solutions:

$$T_i(r_i) = T_{i+1}(r_i) \tag{104}$$

$$k_i \left.\frac{dT_i}{dr}\right|_{r=r_i} = k_{i+1} \left.\frac{dT_{i+1}}{dr}\right|_{r=r_i} \tag{105}$$

The temperature distribution of multilayer tubes under heat loads can be evaluated by the simultaneous solution of the nonlinear equations obtained by using the boundary and interface conditions defined above. It should be noted that, if there is heat generation at all layers, the temperature distribution given Eq. (96) should be used for all layers. On the other hand, if the is heat generation at only one layer, one should use the temperature distribution given in Eq. (96) for that layer, and use the temperature

distribution given in Eq. (97) for the other layers (together with the corresponding boundary and interface conditions). For the steady state case, the temperature distribution given in Eq. (97) should be used for each layer.

This method can also be used for finding the temperature distribution of FGM tubes under temperature loading. To do this, the tube should be divided into n-layers first. Then, the average thermal properties for each layer should be obtained by using the FGM properties. The boundary and interface conditions should be defined next. Then, similar to multilayer tubes, the temperature distribution can be obtained by simultaneous solution of the predefined equations.

The simultaneous solution of the nonlinear equations for each layer of the tube assembly is obtained by the using the command "NSolve" in MATHEMATICA [33]. After defining the temperature distribution for each layer, using interface and boundary conditions 2xn equations are obtained. These equations are then solved simultaneously by NSolve comment. MATHEMATICA software has several build-in numerical methods for the solution of system of nonlinear equations. NSolve comment has an automatic selection option for choosing the most convenient numerical method for the solution.

The flowchart of the computational method for finding the temperature distribution of the multilayer and FGM tubes under thermal loads is shown in Figure 2.3.

2.3.2 Elastic solution for multilayer tubes under thermal loading and pressure

In the elastic solution, using the derived expressions for the single layer tube, the displacement and stresses for the *i-th* tube in a multilayer tube assembly can be determined. For the case $q \neq 0$ (heat generation case), the displacement expression can be written as

$$u_i = (C_1)_i\, r + \frac{(C_2)_i}{r} - \frac{r\,\alpha_i(1+\nu_i)\left(4\,(A_2)_i + k_i\,q_i\,r^2 - 8\,(A_2)_i \ln(r)\right)}{16(1-\nu_i)} \qquad (106)$$

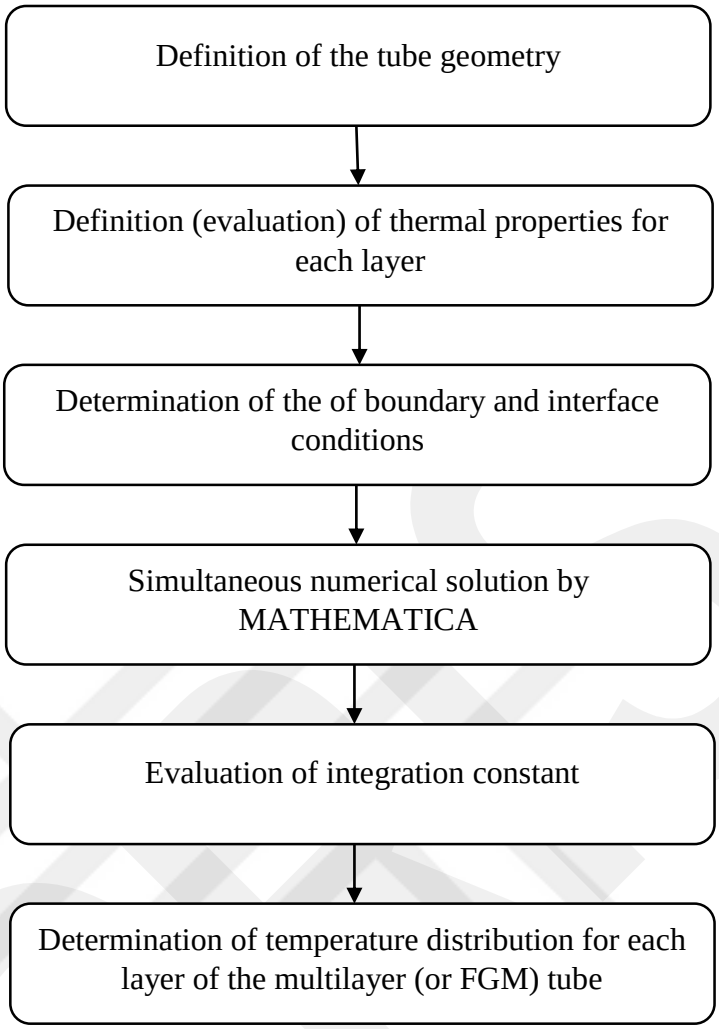

Figure 2.3 The flowchart of the computational procedure for finding the temperature distribution in multilayer and FGM tube problems

The corresponding stresses in radial, circumferential and axial directions become

$$\sigma_{ri} = -\frac{(A_2)_i\, E_i\, \alpha_i \ln(r)}{2(1-\nu_i)} - \frac{E_i\, (C_2)_i}{r^2(1+\nu_i)} + \frac{E_i\, (C_1)_i}{(1+\nu_i)(1-2\nu_i)} - \frac{(A_1)_i\, E_i\, \alpha_i}{1-2\nu_i}$$

$$+\frac{E_i(4\,(A_2)_i + k_i\, q_i\, r^2)\alpha_i}{16(1-\nu_i)} \qquad (107)$$

$$\sigma_{\theta i} = \frac{(A_2)_i \alpha_i}{4(1-\nu_i)} - \frac{3\, k_i\, q_i\, r^2 \alpha_i}{16(1-\nu_i)} - \frac{(A_1)_i \alpha_i\,(1+\nu_i) - (C_1)_i}{(1-2\nu_i)(1+\nu_i)} - \frac{(C_2)_i}{r^2(1+\nu_i)} - \frac{(A_2)_i\, E_i\, \alpha_i \ln(r)}{2(1-\nu_i)} \quad (108)$$

$$\sigma_{zi}(r) = -\frac{(A_2)_i\, E_i\, \alpha_i \ln(r)}{1-\nu_i} + \frac{2\, E_i\, \nu_i (C_1)_i}{(1+\nu_i)(1-2\nu_i)} + E_i\, \alpha_i \left(\frac{k_i\, q_i\, r^2}{4(1-\nu_i)} - \frac{(A_1)_i}{1-2\nu_i}\right) \quad (109)$$

Here *i* is number of the tube layer starting from the first layer. On the other hand, the displacement and the stresses for the steady state case can be determined as

$$u_i = (C_1)_i\, r + \frac{(C_2)_i}{r} - \frac{(A_2)_i\, r\, \alpha_i (1+\nu_i)(1-2\ln(r))}{4(1-\nu_i)} \quad (110)$$

$$\sigma_{ri} = \frac{(A_2)_i\, E_i\, \alpha_i}{4-4\nu_i} - \frac{(A_2)_i\, E_i\, \alpha_i \ln(r)}{2(1-\nu_i)} - \frac{(A_1)_i\, E_i\, \alpha_i}{1-2\nu_i} + \frac{E_i\, (C_1)_i}{(1-2\nu_i)(1+\nu_i)} - \frac{E_i\, (C_2)_i}{r^2(1+\nu_i)} \quad (111)$$

$$\sigma_{\theta i} = \frac{E_i\, (C_2)_i}{r^2(1+\nu_i)} + \frac{(A_2)_i\, E_i\, \alpha_i}{4(1-\nu_i)} + \frac{E_i\, (C_1)_i}{(1-2\nu_i)(1+\nu_i)} - \frac{(A_1)_i\, E_i\, \alpha_i}{1-2\nu_i} - \frac{(A_2)_i\, E_i\, \alpha_i \ln(r)}{2(1-\nu_i)} \quad (112)$$

$$\sigma_{zi} = -\frac{(A_2)_i\, E_i\, \alpha_i \ln(r)}{1-\nu_i} - \frac{E_i(\,(A_1)_i\, \alpha_i (1+\nu_i) - 2\,\nu_i\,(C_2)_i)}{(1-2\nu_i)(1+\nu_i)} \quad (113)$$

The integration constants $(C_1)_i$ and $(C_2)_i$ are determined by the use of boundary and interface conditions. The following possible boundary and interface conditions can be considered in the computations:

a) Heat generation or steady state cases without pressure:

$$\sigma_{r1}\,(a) = 0 \quad (114)$$

$$\sigma_{rn}(b) = 0 \quad (115)$$

$$\sigma_{ri}(r_i) = \sigma_{r(i+1)}(r_i) \quad (116)$$

$$u_i(r_i) = u_{i+1}(r_i) \quad (117)$$

b) Heat generation or steady state cases with internal pressure:

$$\sigma_{r1}(a) = -P_{int} \quad (118)$$

$$\sigma_{rn}(b) = 0 \quad (119)$$

$$\sigma_{ri}(r_i) = \sigma_{r(i+1)}(r_i) \quad (120)$$

$$u_i(r_i) = u_{i+1}(r_i) \quad (121)$$

c) Heat generation or steady state cases with external pressure:

$$\sigma_{r1}(a) = 0 \quad (122)$$

$$\sigma_{rn}(b) = -P_{ext} \quad (123)$$

$$\sigma_{i}(r_i) = \sigma_{r(i+1)}(r_i) \quad (124)$$

$$u_i(r_i) = u_{i+1}(r_i) \quad (125)$$

d) Heat generation or steady state cases with both internal and external pressure:

$$\sigma_{r1}(a) - P_{int} \quad (126)$$

$$\sigma_{rn}(b) = -P_{ext} \quad (127)$$

$$\sigma_{ri}(r_i) = \sigma_{r(i+1)}(r_i) \quad (128)$$

$$u_i(r_i) = u_{i+1}(r_i) \quad (129)$$

2.3.3 Elastic solution for multilayer tubes under pressure

Using the derived expressions for the single layer tube under only pressure, the displacement and stresses for the *i-th* tube in a multilayer tube assembly can determined. The displacement expression can be written as

$$u_i = (C_1)_i\, r + \frac{(C_2)_i}{r} \tag{130}$$

and the corresponding stress component become

$$\sigma_{ri} = \frac{E_i}{1+\nu_i}\left(\frac{(C_1)_i}{1-2\nu_i} - \frac{(C_2)_i}{r^2}\right) \tag{131}$$

$$\sigma_{\theta i} = \frac{E_i}{1+\nu_i}\left(\frac{(C_1)_i}{1+2\nu_i} + \frac{(C_2)_i}{r^2}\right) \tag{132}$$

$$\sigma_{zi} = \frac{2\,\nu_i\, E_i (C_1)_i}{(1+\nu_i)(1-2\nu_i)} \tag{133}$$

To complete solution, the integration constants $(C_1)_i$ and $(C_2)_i$ must be evaluated. The following boundary and interface conditions can be used for different loading cases.

a) Tube under internal pressure:

$$\sigma_{r1}(a) = -P_{int} \tag{134}$$

$$\sigma_{rn}(b) = 0 \tag{135}$$

$$\sigma_{ri}(r_i) = \sigma_{r(i+1)}(r_i) \tag{136}$$

$$u_i(r_i) = u_{i+1}(r_i) \tag{137}$$

b) Tube under external pressure:

$$\sigma_{r1}(a) = 0 \tag{138}$$

$$\sigma_{rn}(b) = -P_{ext} \tag{139}$$

$$\sigma_{i}(r_i) = \sigma_{r(i+1)}(r_i) \tag{140}$$

$$u_i(r_i) = u_{i+1}(r_i) \tag{141}$$

c) Tube under both internal and external pressure:

$$\sigma_{r1}(a) - P_{int} \tag{142}$$

$$\sigma_{rn}(b) = -P_{ext} \tag{143}$$

$$\sigma_{ri}(r_i) = \sigma_{r(i+1)}(r_i) \tag{144}$$

$$u_i(r_i) = u_{i+1}(r_i) \tag{145}$$

Similar to the solution method for the temperature distribution in the multilayer tube problems, the elastic solutions can be obtained for both multilayer and FGM tubes for different loading and boundary conditions. The flowchart which shows the algorithm for the elastic solution is shown in Fig. 2.4.

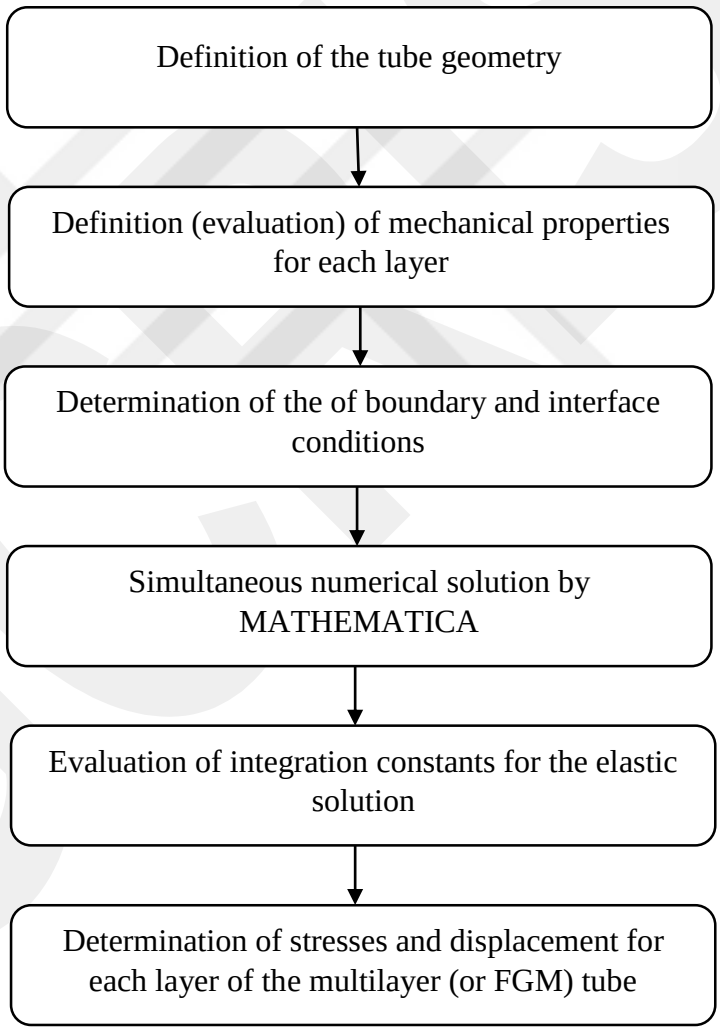

Figure 2.4 The flowchart of the computational procedure of the elastic solution for the multilayer and FGM tube problems

CHAPTER 3

NUMERICAL RESULTS

3.1. General

In Chapter 2, the basic expressions are derived for single and multilayer tubes under thermal loading with different boundary conditions. The expressions of stress components and radial displacement for one layer and multilayer tubes are also obtained for pressure load in that chapter. In this chapter, some numerical results for single and multilayer layer tubes under different loading and boundary conditions are given first. Then, some example problems solved in different studies is handled in order to validate the proposed numerical method. The material properties used in the analyses presented at the first part are given in Table 3.1.

Table 3.1. Material properties used in the numerical results

	E (GPa)	ν	σ_0 (MPa)	α ($^0C^{-1}x10^{-6}$)	k ($Wm^{-1}\ ^0K^{-1}$)
Steel	200	0.30	430	11.7	45
Copper	120	0.365	265	16.9	380
Brass	105	0.35	410	20.9	104
Aluminum	70	0.35	100	23.6	200

3.2 Single layer tube results

3.2.1 Single layer tube under thermal loading

The deformation behavior of a fixed-ended single steel layer tube ($a = 0.4\,m$, $b = 0.7\,m$) under steady state condition is presented in this section. The inner surface temperature of the tube is $T_a = 100$ ℃ and the outer surface temperature is $T_b = 0$ ℃. Fig 3.1 shows the distribution of the temperature throughout the tube. On the other hand, the distributions of stresses and radial displacement are given in Fig 3.2. The

nondimensional stress components are obtained by $\bar{\sigma}_i = \sigma_i/\sigma_0$ and the dimensionless radial displacement is defined as $\bar{u} = uE/(\sigma_0 b)$. The corresponding integration constants are found as $A_1 = -63.735$, $A_2 = -178.694$, $\overline{C_1} = C_1/b^2 = 10.5 \times 10^{-4}$, and $\overline{C_2} = C_2 = 2.581 \times 10^{-4}$.

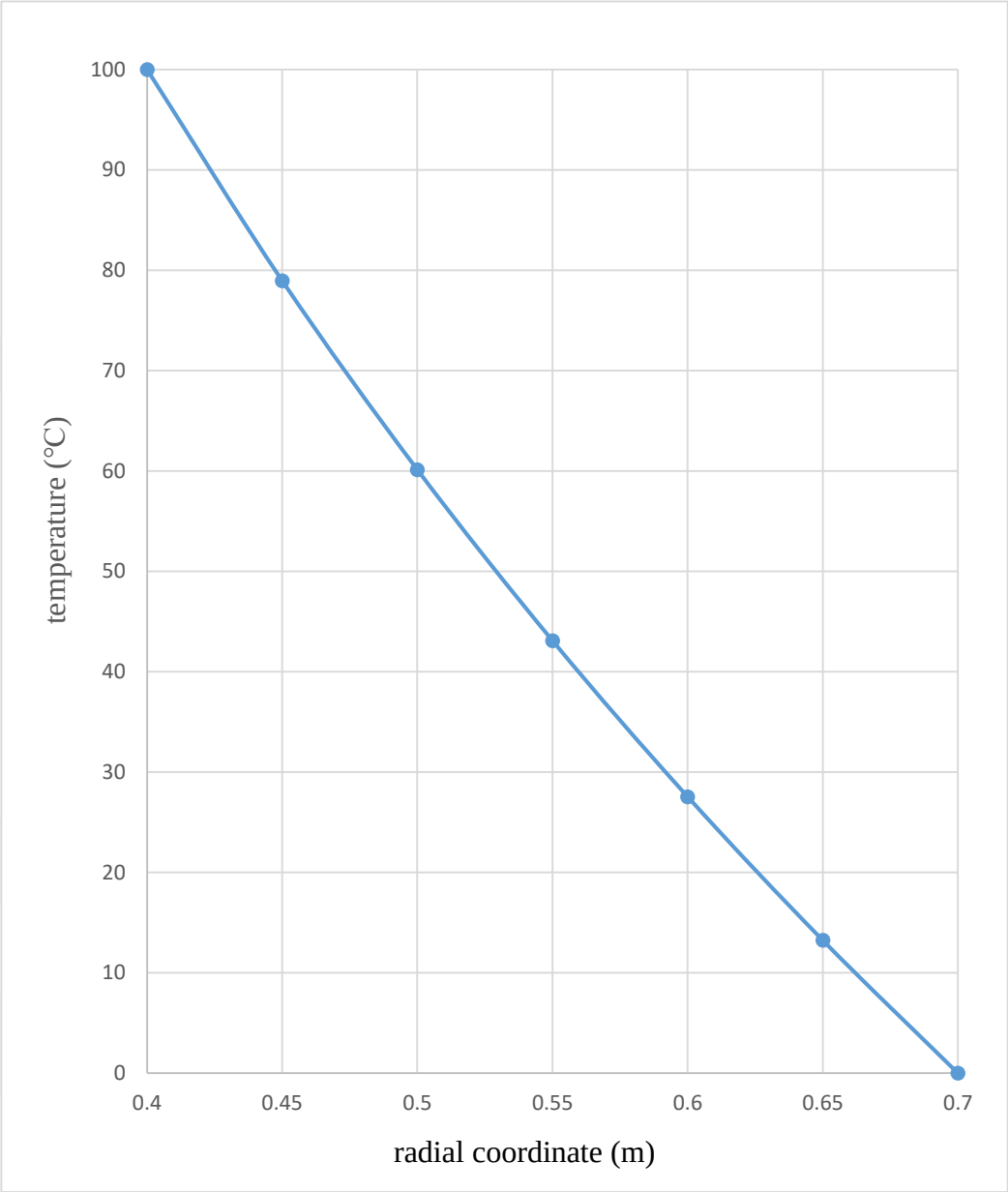

Figure 3.1. Distribution of temperature for the single layer steel tube ($a = 0.4\ m, b = 0.7\ m$) for $T_a = 100\ ^0$C and $T_b = 0\ ^0$C

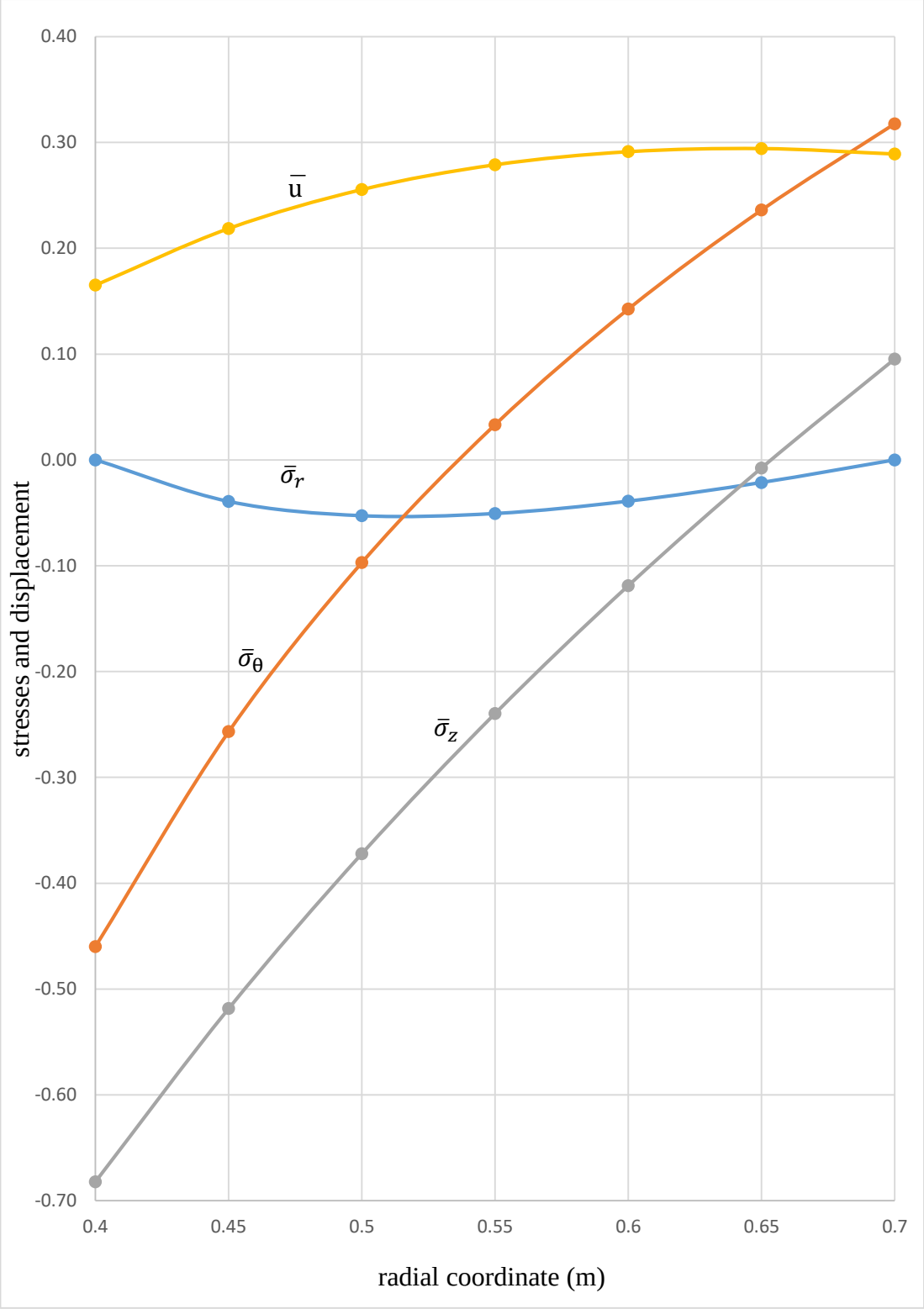

Figure 3.2. Distributions of stresses and radial displacement for a single layer steel tube ($a = 0.4$ m, $b = 0.7$ m) for $T_a = 100\ ^0$C and $T_b = 0\ ^0$C

3.2.2 Single layer tube under pressure

For a fixed-ended single layer steel tube with inner radius $a = 0.4\ m$ and outer radius $b = 0.7\ m$, the stress and radial displacement distributions are given in Fig 3.3 for the internal pressure value of $\overline{P}_{int} = P_{int}/\sigma_0 = 0.387$. The corresponding dimensionless integration constants are found as $\overline{C}_1 = C_1/b^2 = 4.281 \times 10^{-4}$ and $\overline{C}_2 = C_2 = 2.5746 \times 10^{-4}$.

For the external pressure value of $\overline{P}_{ext} = P_{ext}/\sigma_0 = 0.3788$, the distributions of stresses and radial displacement are shown in Fig 3.4 for the steel tube. The inner radius is $a = 0.4\ m$ and the outer radius is $b = 0.7\ m$. The integration constants are found as $\overline{C}_1 = C_1/b^2 = 0.1283 \times 10^{-4}$, and $\overline{C}_2 = C_2 = 2.517 \times 10^{-4}$.

The stresses and radial displacements of a steel tube ($a = 0.4\ m$ and $b = 0.7\ m$) under both external and internal pressure ($\overline{P}_{int} = 0.3$, and $\overline{P}_{ext} = 0.66$) are given in Fig 3.5. The corresponding integration constants are calculated as $\overline{C}_1 = C_1/b^2 = 19.0 \times 10^{-4}$, and $\overline{C}_2 = C_2 = 2.43 \times 10^{-4}$.

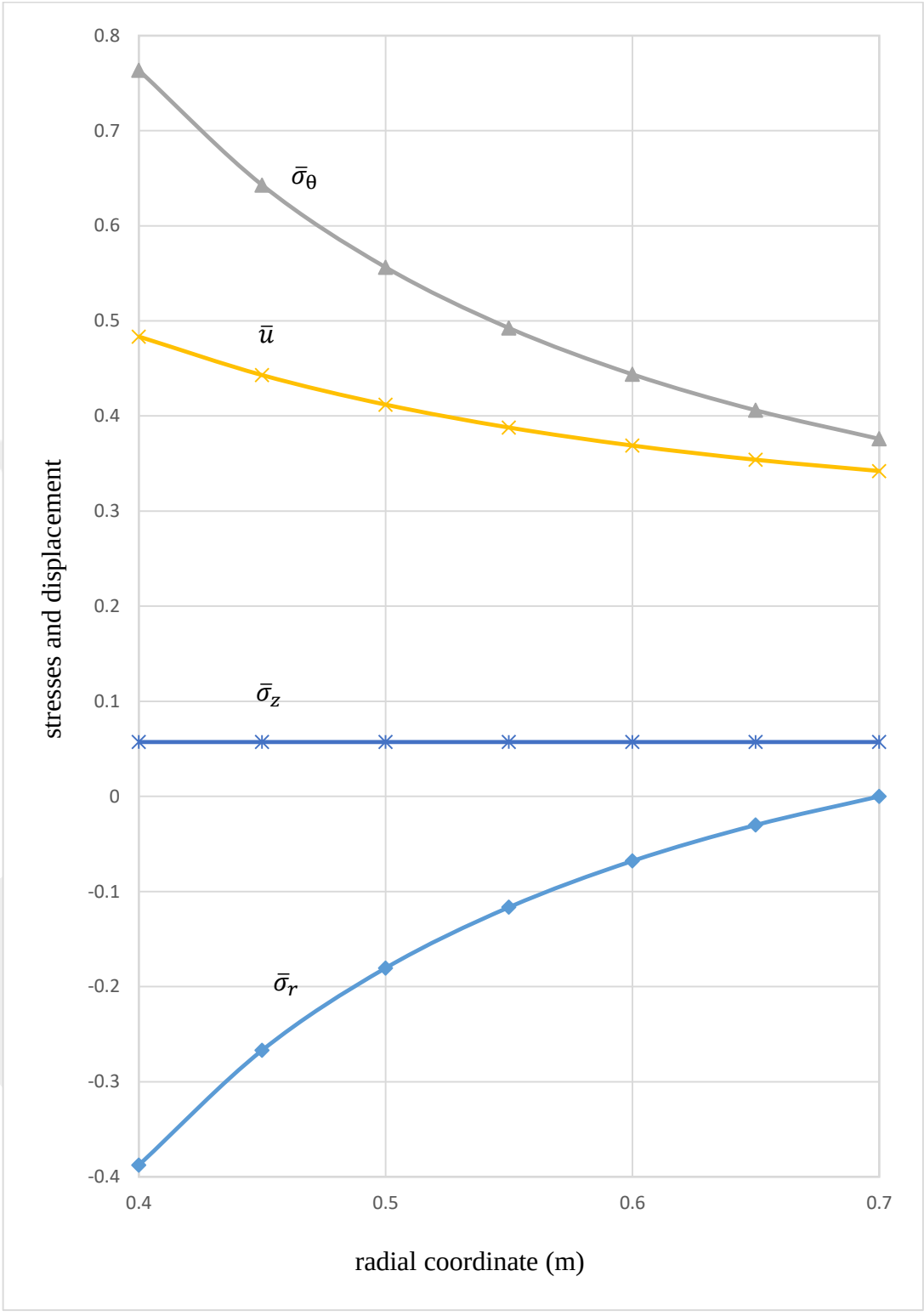

Figure 3.3. Distributions of stresses and radial displacement for a single layer steel tube ($a = 0.4\,m, b = 0.7\,m$) under internal pressure $\overline{P}_{int} = 0.387$

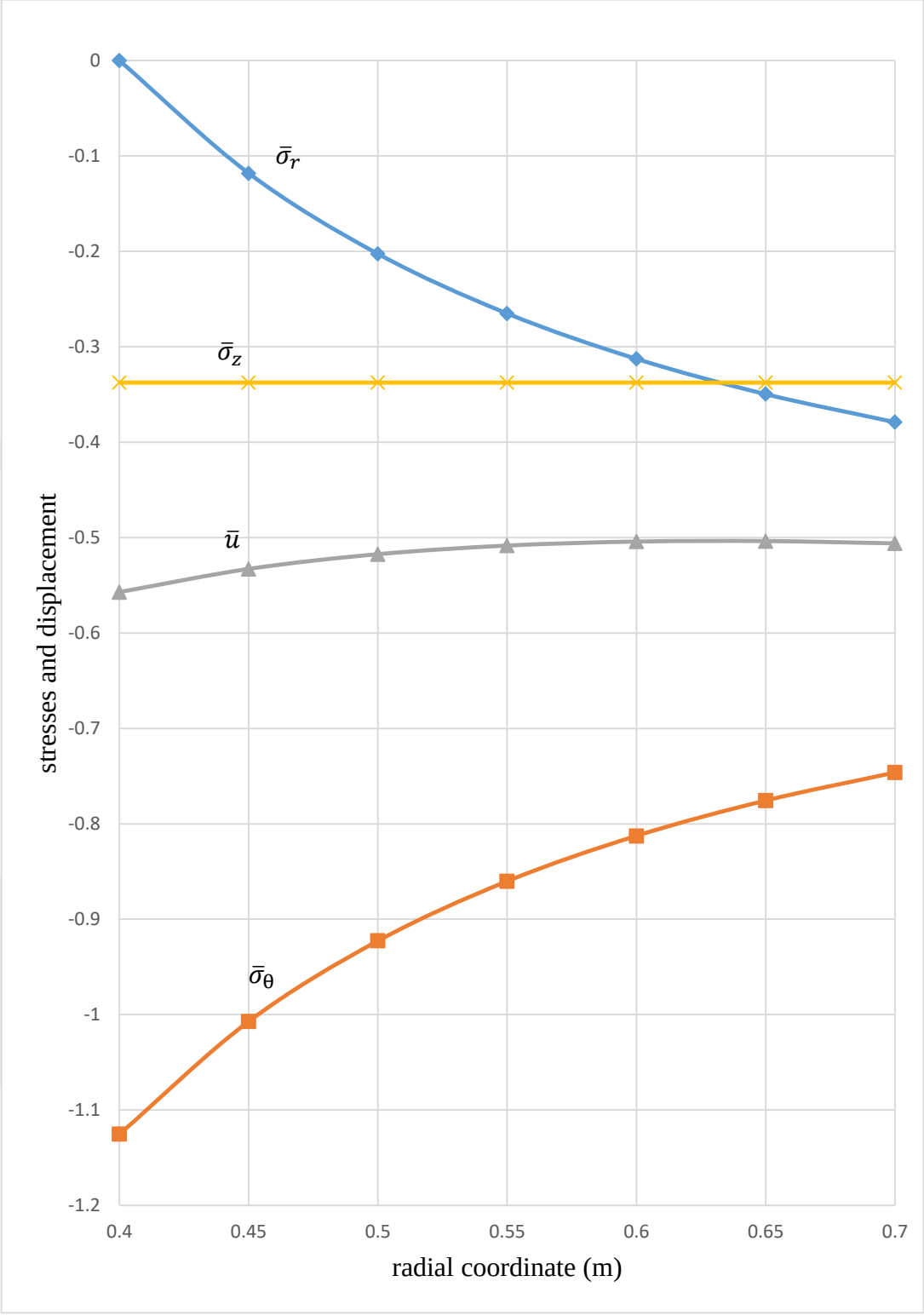

Figure 3.4. Distributions of stresses and radial displacement for a single layer steel tube ($a = 0.4\ m, b = 0.7\ m$) under external pressure $\overline{P}_{ext} = 0.3788$

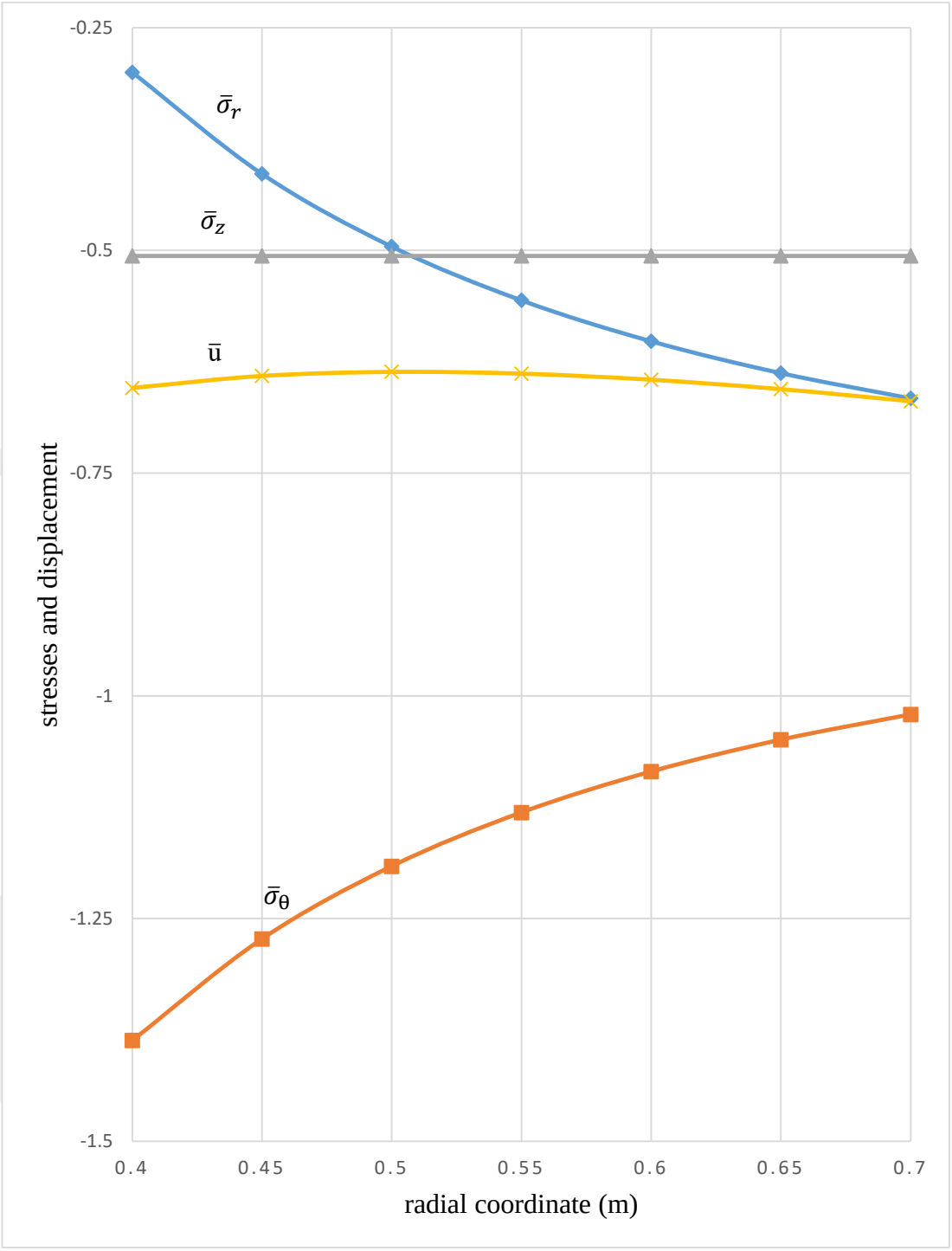

Figure 3.5. Distributions of stresses and radial displacement for a single layer steel tube ($a = 0.4\,m\,, b = 0.7m$) under internal pressure $\overline{P}_{int} = 0.3$ and external pressure $\overline{P}_{ext} = 0.66$.

3.3 Two-layer tube result

In two-layer tubes, the layers consist of different materials. In the examples, it is assumed that the inner layer is steel and the outer layer is aluminum. The material properties of steel and aluminum are given in Table 3.1. The first tube is between *a* to r_1 and the second tube is between r_1 to b. The dimensionless form of the stress components is defined as $\bar{\sigma}_i = \sigma_i/\sigma_{01}$, and dimensionless radial displacement is $\bar{u} = uE_1/(\sigma_{01}b)$. Here the subscript 1 denotes the material properties of the inner tube. For example, σ_{01} is the yield stress of steel.

3.3.1 Two-layer tube under thermal loading and pressure

For the two-layer steel-aluminum composite tube ($a = 0.4\,m$, $r_1 = 0.55\,m$ and $b = 0.7\,m$), it is assumed that the inner and outer surfaces have constant temperatures ($T_a = 100$ ℃, $T_b = 0$ ℃). In addition, an internal pressure of $\overline{P}_{int} = P_{int}/\sigma_{01} = 0.3$ is applied at the inner surface. Using the expressions derived in Chapter 2, the temperature distribution given in Fig. 3.6 is obtained. On the other hand, the distributions of stresses and radial displacement is presented in Fig. 3.7. The corresponding integration constants are calculated as $A_1 = -145.842$, $A_2 = -268.301$, $A_3 = -21.531$, $A_4 = -60.367$ $\overline{C}_1 = C_1/b^2 = 22.93 \times 10^{-4}$, $\overline{C}_2 = C_2 = 0.88 \times 10^{-4}$, $\overline{C}_3 = C_3/b^2 = 4.75 \times 10^{-4}$ and $\overline{C}_4 = C_4 = 1.18 \times 10^{-4}$.

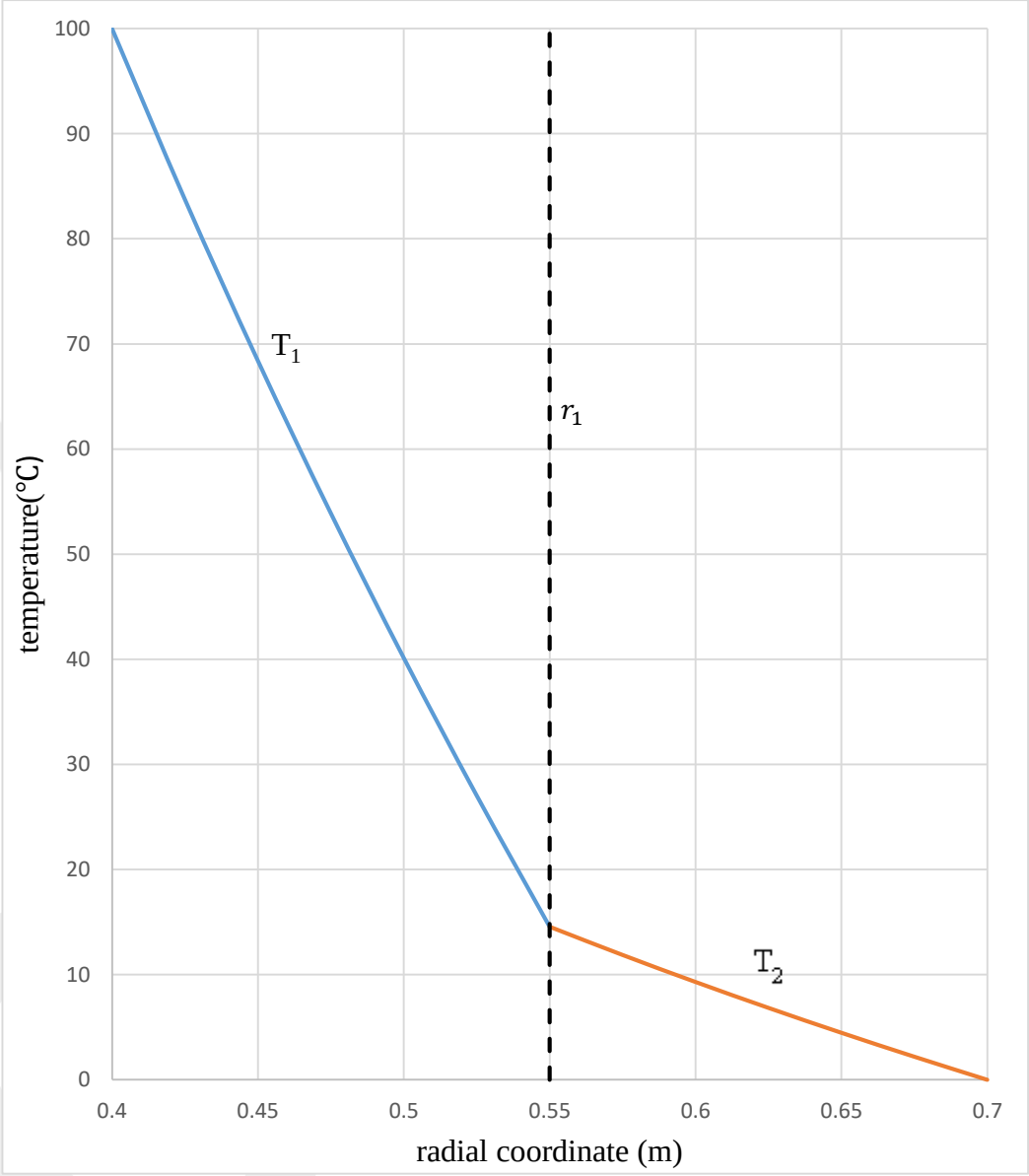

Figure 3.6. Distribution of temperature for the two-layer steel-aluminum tube ($a = 0.4\,m,\ r_1 = 0.55$ m, $b = 0.7\,m$) for $T_a = 100$ ℃ , $T_b = 0$ ℃ and $\overline{P}_{int} = 0.3$

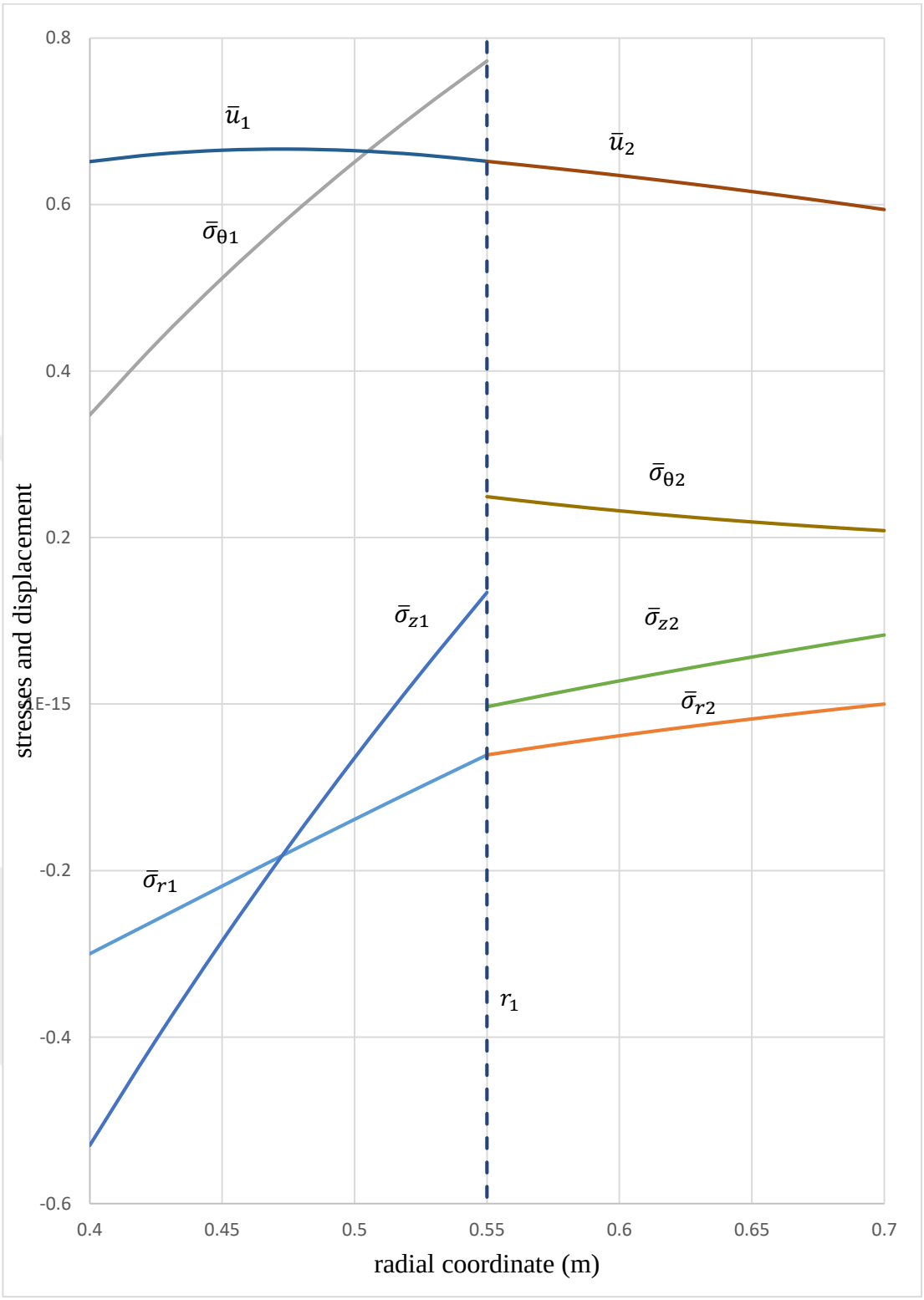

Figure 3.7. Distributions of stresses and radial displacement for the two-layer steel-aluminum tube ($a = 0.4\ m$, $r_1 = 0.55$ m, $b = 0.7\ m$) for $T_a = 100$ ℃ , $T_b = 0$ ℃ and $\overline{P}_{int} = 0.3$.

3.3.2 Two-layer tube under pressure

Using the expressions derived before, the stress response of a two-layer steel-aluminum tube is investigated. The inner radius, interface radius and outer radius are taken as $a = 0.4\,m$, $r_1 = 0.55\,m$, and $b = 0.7\,m$, respectively. For the internal pressure $\overline{P}_{int} =$ 0.3 the distributions of stresses and radial displacement are shown in Fig 3.8. The dimensionless integration constants are calculated as $\overline{C}_1 = C_1/b^2 = 5.6391 \times 10^{-4}$, $\overline{C}_2 = C_2 = 2.44 \times 10^{-4}$, $\overline{C}_3 = C_3/b^2 = 3.4607 \times 10^{-4}$ and $\overline{C}_4 = C_4 = 2.76 \times 10^{-4}$.

In Fig 3.9, the distributions of stresses and radial displacement for the same tube assembly under external pressure of $\overline{P}_{ext} =$ 0.3 is presented. The dimensionless integration constants are found as $\overline{C}_1 = C_1/b^2 = 13.12 \times 10^{-4}$, $\overline{C}_2 = C_2 = 2.57 \times 10^{-4}$, $\overline{C}_3 = C_3/b^2 = 17.61 \times 10^{-4}$ and $\overline{C}_4 = C_4 = 1.90 \times 10^{-4}$.

Finally, in Fig. 3.10, the stress response and radial displacement of the tube assembly under both internal pressure of $\overline{P}_{int} =$ 0.3 and external pressure is $\overline{P}_{ext} =$ 0.3 are shown. The corresponding integration constants are computed as $\overline{C}_1 = C_1/b^2 = 7.4829 \times 10^{-4}$, and $\overline{C}_2 = C_2 = 0.12 \times 10^{-4}$, $\overline{C}_3 = C_3/b^2 = 14.152 \times 10^{-4}$ and $\overline{C}_4 = C_4 = 0.86 \times 10^{-4}$.

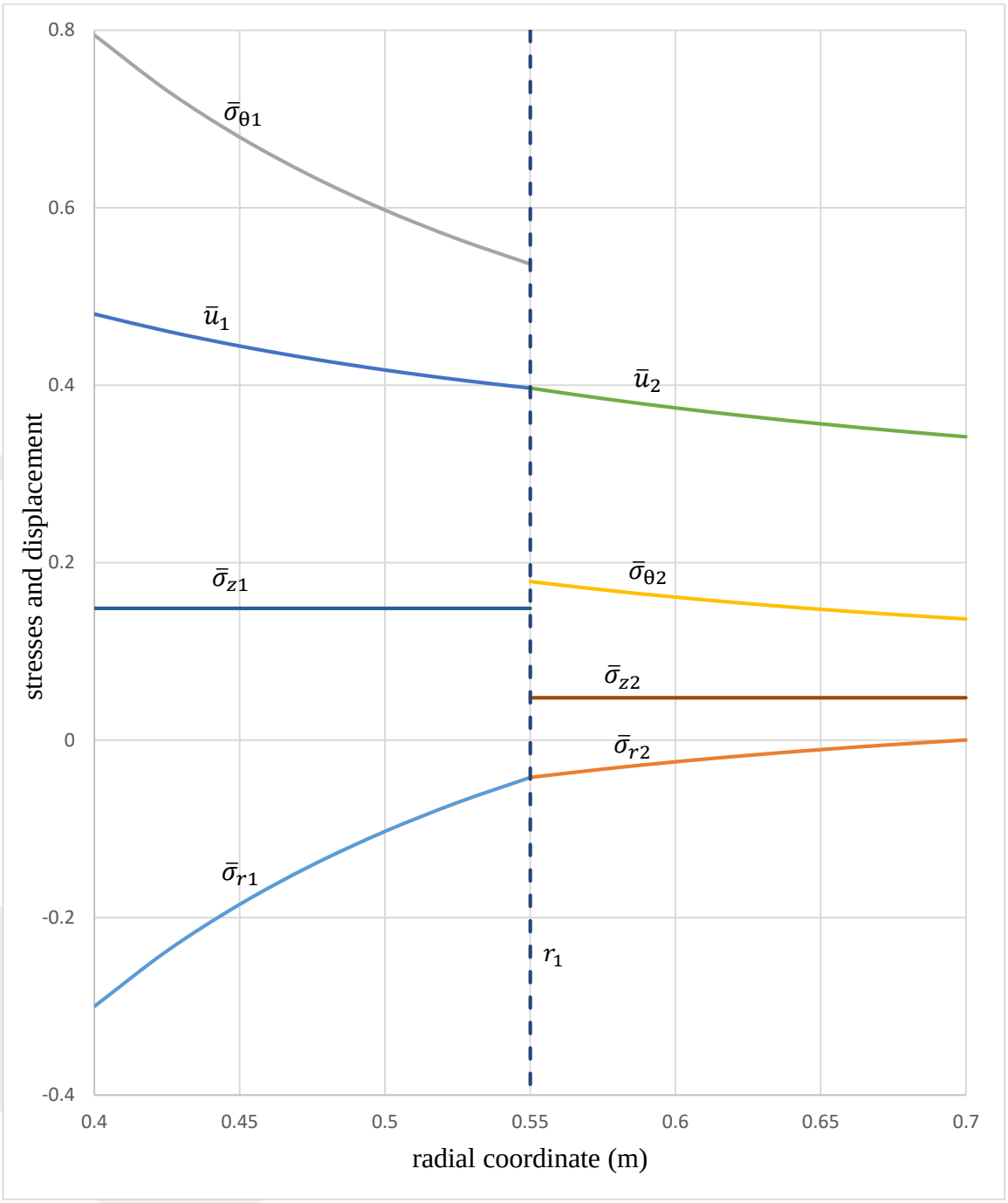

Figure 3.8. Distributions of stresses and radial displacement for the two-layer steel-aluminum tube ($a = 0.4\ m$, $b = 0.7\ m$, $r_1 = 0.55$ m) under internal pressure $\overline{P}_{int} = 0.3$.

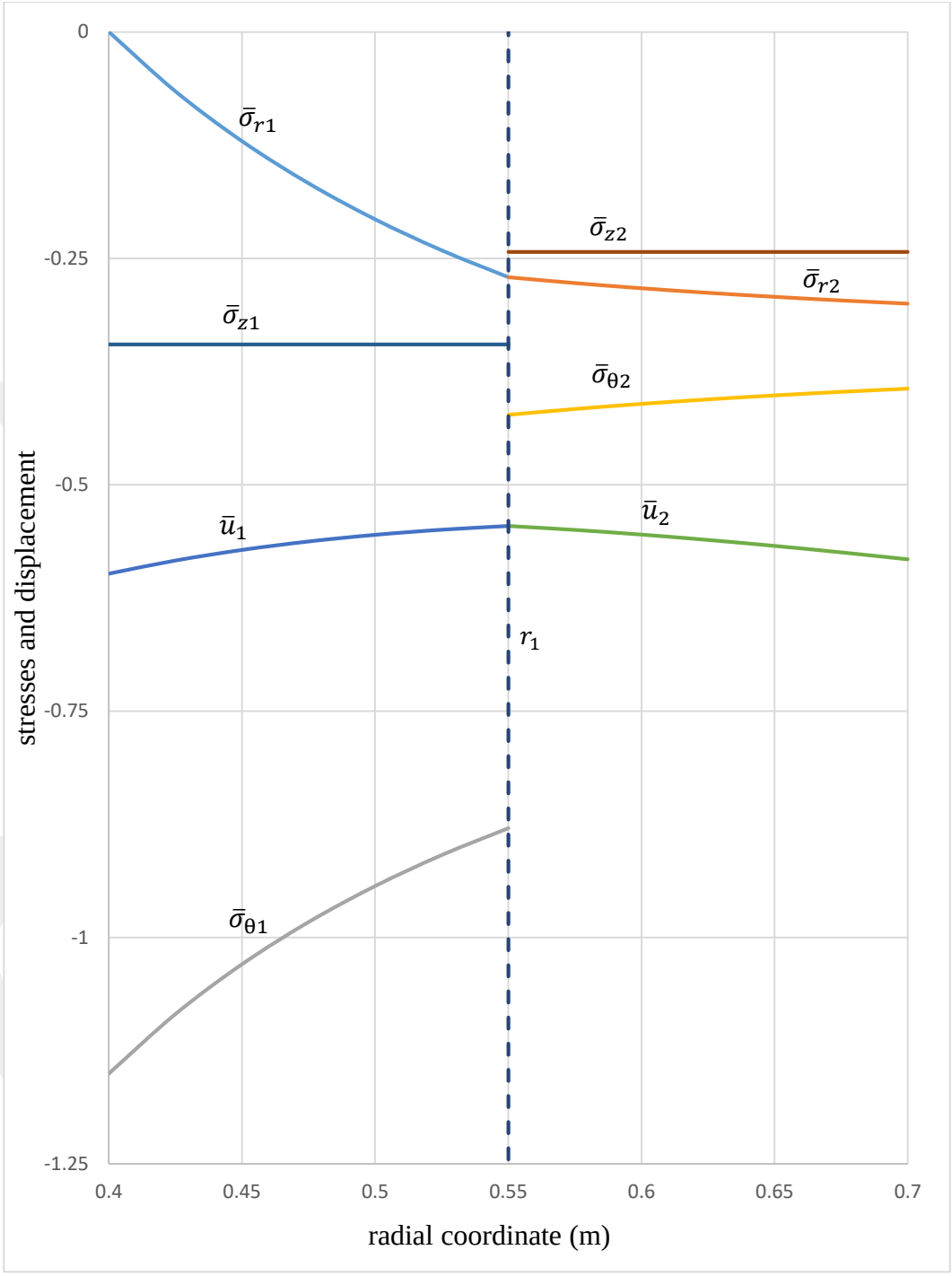

Figure 3.9. Distributions of stresses and radial displacement for the two-layer steel-aluminum tube ($a = 0.4\ m, b = 0.7\ m, r_1 = 0.55\ m$) under external pressure $\overline{P}_{ext} = 0.3$.

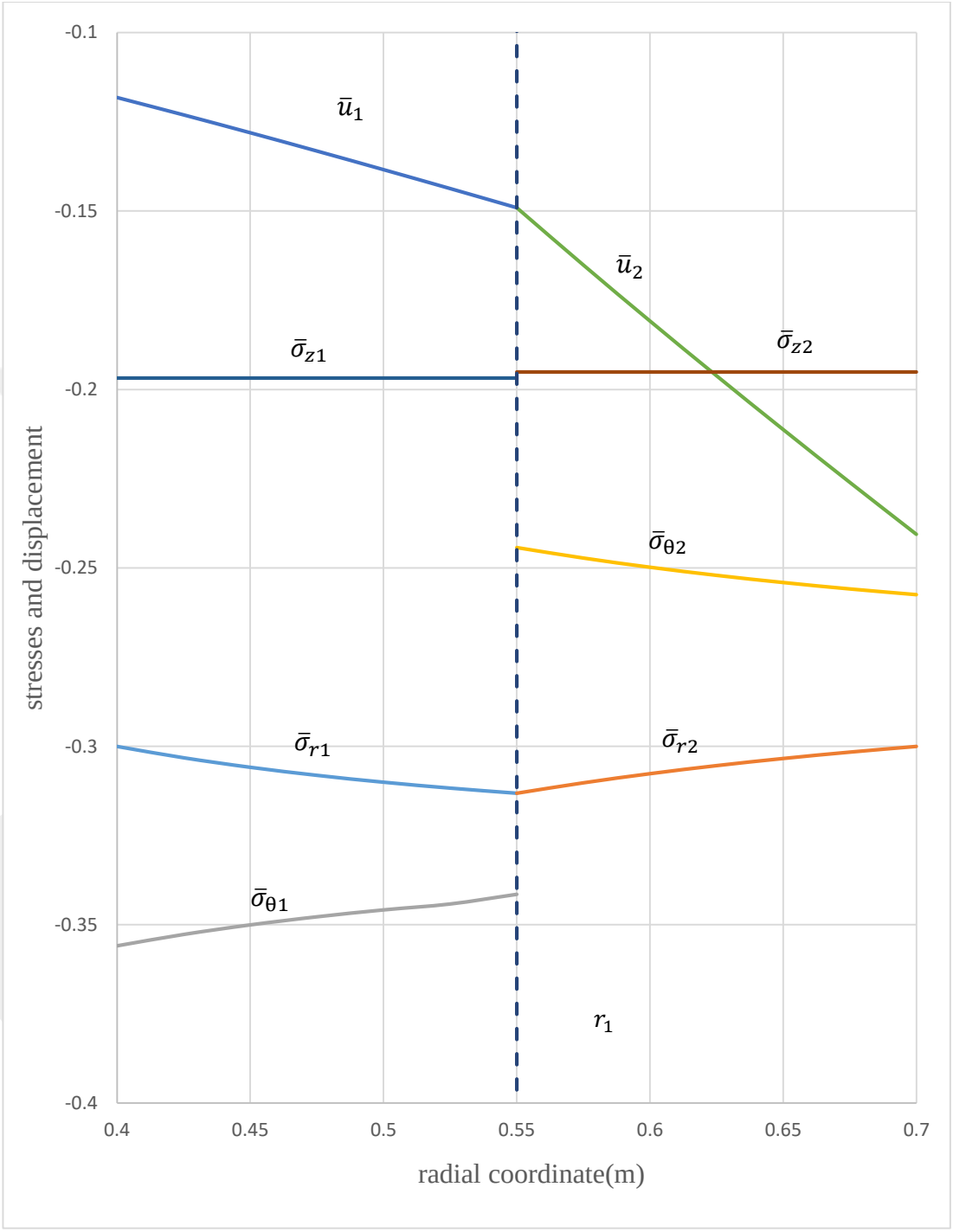

Figure 3.10. Distributions of stresses and radial displacement for the two-layer steel-aluminum tube ($a = 0.4\ m, b = 0.7\ m, r_1 = 0.55\ m$) under internal pressure $\overline{P}_{int} = 0.3$ and external pressure $\overline{P}_{ext} = 0.3$

3.4 Five-layer tube results

As a last example, a five-layer tube is considered. In the first part, the assembly is subjected to thermal loading and pressure. The distributions of temperature, stresses and radial displacement are obtained for that case. Then, for the same tube assembly, different cases of pressure loading is considered: Internal pressure, external pressure and both internal and external pressures. The stresses and radial displacement are also drawn for these three cases. The nondimensional values of stresses and displacements are used in plotting all those graphs.

The layers of the assembly consist of different materials. The first layer is steel, the second one is aluminum, the third one is steel, the fourth one is brass and the outer layer is copper. The properties of these materials are given in Table 3.1. The locations of the tubes are defined as follows: First tube: *a* to r_1, second tube: r_1 to r_2, third tube: r_2 to r_3, fourth tube: r_3 to r_4, *and* fifth tube: r_4 to *b*. The dimensionless form of the stress components is defined as $\bar{\sigma}_i = \sigma_i/\sigma_{01}$, and dimensionless radial displacement is $\bar{u} = uE_1/(\sigma_{01}b)$.

3.4.1 Five-layer tube under thermal loading and pressure

The inner surface of the five-layer tube assembly ($a = 0.4\,m,\ r_1 = 0.55\,m,\ r_2 = 0.7\,m,\ r_3 = 0.85\,m,\ r_4 = 1.00\,m,\ b = 1.15\,m$) is assumed to have the temperature of $T_a = 100$ ℃, while the outer surface has a temperature of $T_b = 0$ ℃. The internal pressure is assumed to be $\overline{P}_{int} = 0.3$. The integration constants are evaluated as $A_1 = -40.160$, $A_2 = -152.965$, $A_3 = 30.711$, $A_4 = -152.965$, $A_5 = -11.571$, $A_6 = -152.965$, $A_7 = 2.531$, $A_8 = -66.187$, $A_9 = 2.531$, $A_{10} = -18.114$, $\overline{C}_1 = C_1/b^2 = 2.4 \times 10^{-4}$, $\overline{C}_2 = C_2 = 1.25 \times 10^{-4}$, $\overline{C}_3 = C_3/b^2 = 4.08 \times 10^{-4}$, $\overline{C}_4 = C_4 = 1.13 \times 10^{-4}$, $\overline{C}_5 = C_5/b^2 = 0.14 \times 10^{-4}$, $\overline{C}_6 = C_6 = 1.82 \times 10^{-4}$, $\overline{C}_7 = C_7/b^2 = 1.45 \times 10^{-4}$, $\overline{C}_8 = C_8 = 2.28 \times 10^{-4}$, $\overline{C}_9 = C_9/b^2 = 1.23 \times 10^{-4}$, $\overline{C}_{10} = C_{10} = 3.55 \times 10^{-4}$. Fig 3.11 shows the distribution of temperature. On the other hand, Fig 3.12 gives the radial displacement of the assembly. Finally, Fig 3.13 shows the distributions stresses throughout the tube assembly.

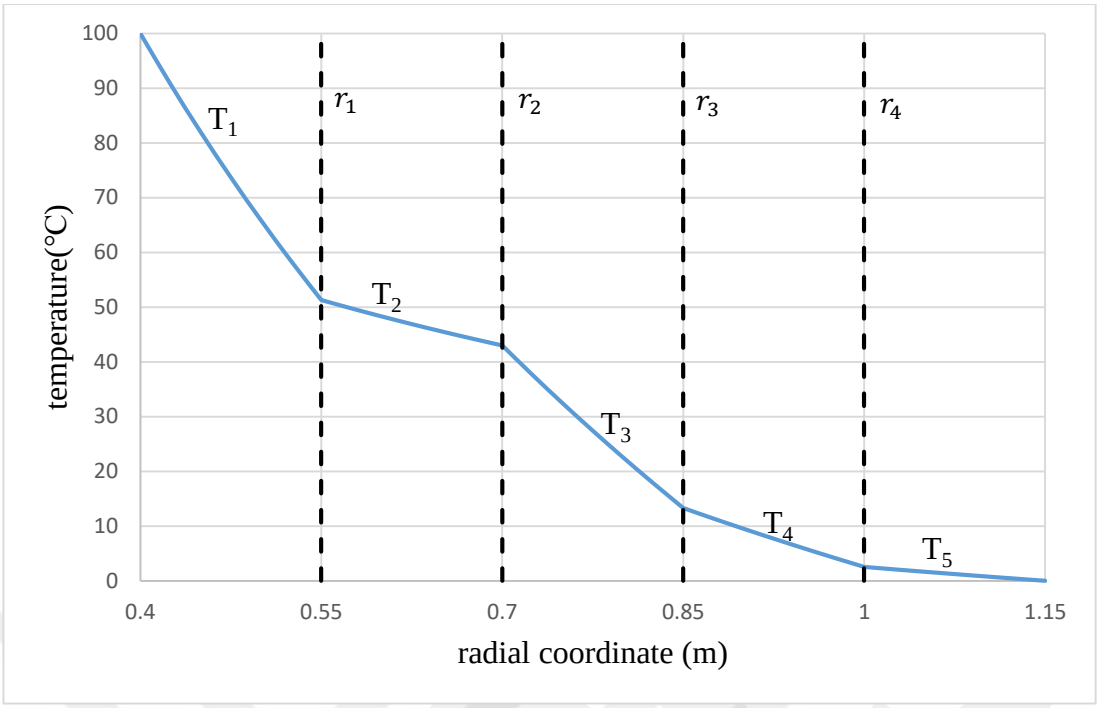

Figure 3.11. Distribution of temperature for the five-layer tube ($a = 0.4\,m, r_1 = 0.55\,m,\ r_2 = 0.7\,m,\ r_3 = 0.85\,m,\ r_4 = 1.00\,m,\ b = 1.15\,m$) for $T_a = 100$ ℃ , $T_b = 0$ ℃ and $\overline{P}_{int} = 0.3$.

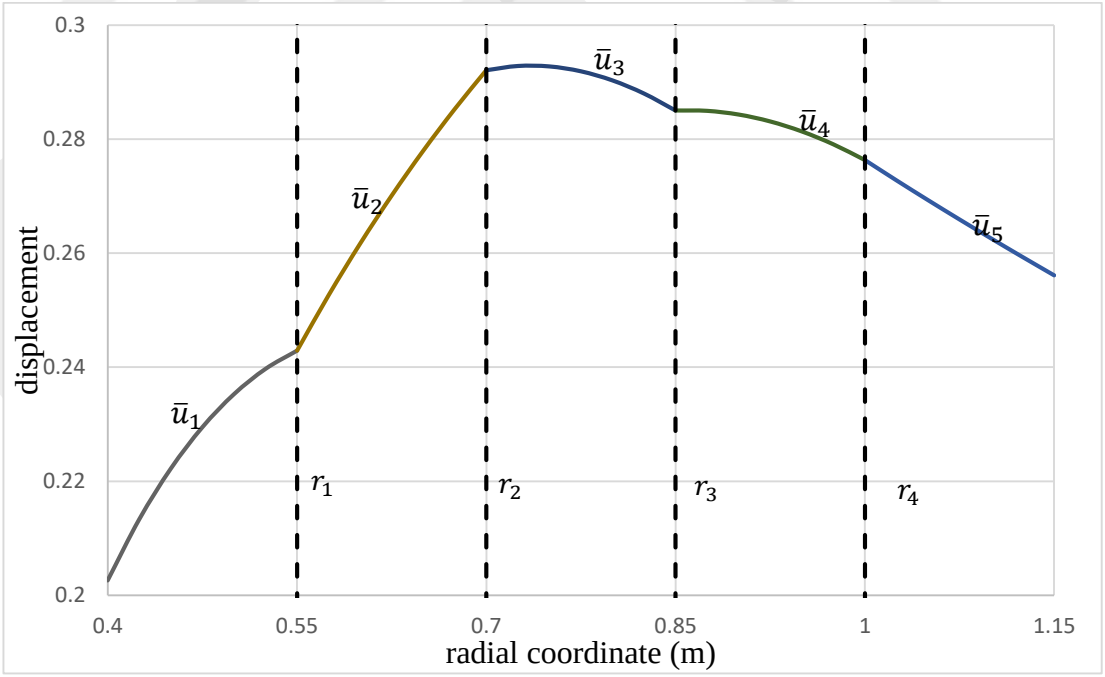

Figure 3.12. Distribution of radial displacement of the five-layer tube ($a = 0.4\,m$, $r_1 = 0.55\,m,\ r_2 = 0.7\,m,\ r_3 = 0.85\,m,\ r_4 = 1.00\,m,\ b = 1.15\,m$) for $T_a = 100$ ℃ , $T_b = 0$ ℃ and $\overline{P}_{int} = 0.3$.

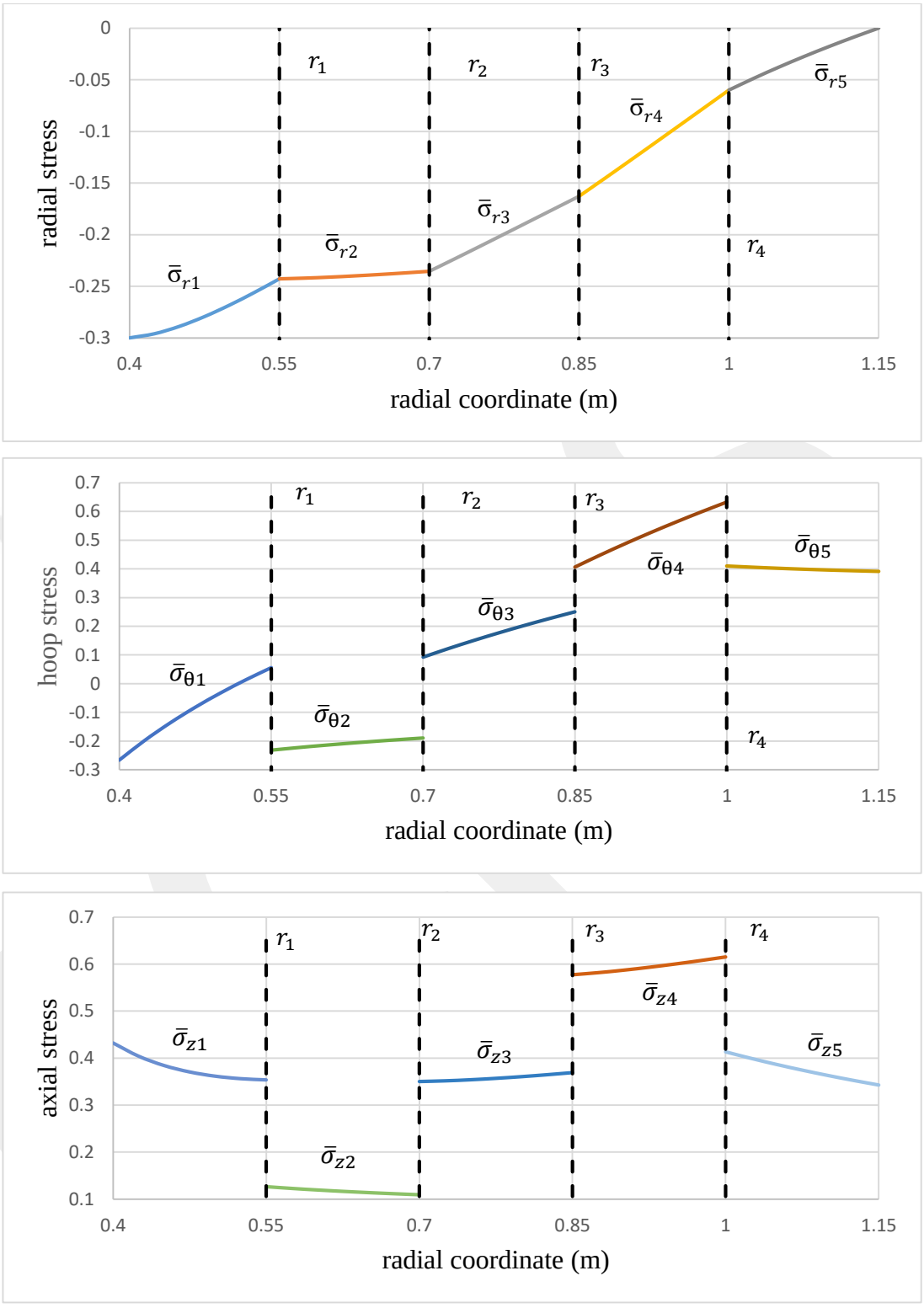

Figure 3.13. Distributions of stresses for the five-layer tube ($a = 0.4\ m, r_1 = 0.55\ m,\ r_2 = 0.7\ m,\ r_3 = 0.85\ m,\ r_4 = 1.00\ m,\ b = 1.15\ m$) for $T_a = 100\ ℃$, $T_b = 0\ ℃$ and $\overline{P}_{int} = 0.3$

3.4.2 Five-layer tube under pressure

For the same tube assembly ($a = 0.4\,m,\ r_1 = 0.55\,m,\ r_2 = 0.7\,m,\ r_3 = 0.85\,m,\ r_4 = 1.00\,m,\ b = 1.15\,m$) considered in the previous section, the stresses and displacement are obtained first for an internal pressure of $\overline{P}_{int} = 0.3$. The distributions of stresses are shown in Fig 3.14 and distribution of radial displacement is given in 3.15. The integration constants are calculated as $\overline{C}_1 = C_1/b^2 = 5.71 \times 10^{-4}$, $\overline{C}_2 = C_2 = 1.64 \times 10^{-4}$, $\overline{C}_3 = C_3/b^2 = 7.55 \times 10^{-4}$, $\overline{C}_4 = C_4 = 2.17 \times 10^{-4}$, $\overline{C}_5 = C_5/b^2 = 0.17 \times 10^{-4}$, $\overline{C}_6 = C_6 = 1.57 \times 10^{-4}$, $\overline{C}_7 = C_7/b^2 = 0.27 \times 10^{-4}$, $\overline{C}_8 = C_8 = 1.47 \times 10^{-4}$, $\overline{C_9} = C_9/b^2 = 0.23 \times 10^{-4}$, $\overline{C_{10}} = C_{10} = 1.52 \times 10^{-4}$.

For the external pressure of $\overline{P}_{ext} = 0.3$, the dimensionless integration constants are found as $\overline{C}_1 = C_1/b^2 = 2.62 \times 10^{-4}$, $\overline{C}_2 = C_2 = 1.38 \times 10^{-4}$, $\overline{C}_3 = C_3/b^2 = 3.52 \times 10^{-4}$, $\overline{C}_4 = C_4 = 1.02 \times 10^{-4}$, $\overline{C}_5 = C_5/b^2 = 2.44 \times 10^{-4}$, $\overline{C}_6 = C_6 = 1.73 \times 10^{-4}$, $\overline{C}_7 = C_7/b^2 = 1.48 \times 10^{-4}$, $\overline{C}_8 = C_8 = 2.64 \times 10^{-4}$, $\overline{C}_9 = C_9/b^2 = 1.72 \times 10^{-4}$, $\overline{C}_{10} = C_{10} = 2.32 \times 10^{-4}$. The distributions of radial displacement and stresses are shown in Figs. 3.16 and 3.17, respectively.

Finally, for the internal pressure $\overline{P}_{int} = 0.3$ and the external pressure of $\overline{P}_{ext} = 0.3$, the distributions of stress components are shown in Fig. 3.18. On the other hand, Fig 3.19 shows the radial displacement of the tube assembly. The dimensionless integration constants are found as $\overline{C}_1 = C_1/b^2 = 2.05 \times 10^{-4}$,$\overline{C}_2 = C_2 = 0.25 \times 10^{-4}$, $\overline{C}_3 = C_3/b^2 = 4.27 \times 10^{-4}$, $\overline{C}_4 = C_4 = 1.14 \times 10^{-4}$, $\overline{C}_5 = C_5/b^2 = 2.26 \times 10^{-4}$, $\overline{C}_6 = C_6 = 0.16 \times 10^{-4}$, $\overline{C}_7 = C_7/b^2 = 1.20 \times 10^{-4}$, $\overline{C}_8 = C_8 = 1.17 \times 10^{-4}$, $\overline{C}_9 = C_9/b^2 = 1.48 \times 10^{-4}$, $\overline{C}_{10} = C_{10} = 0.79 \times 10^{-4}$.

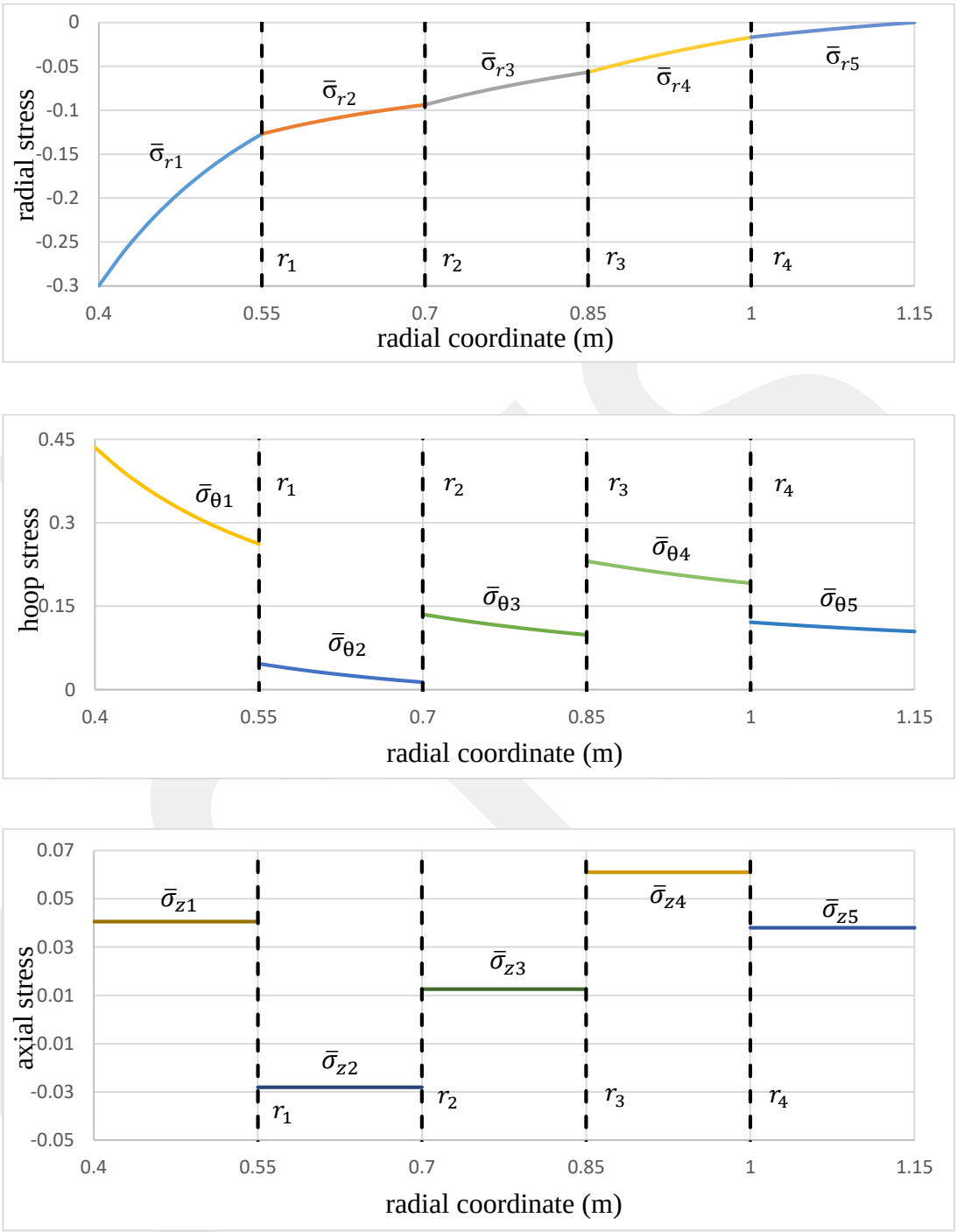

Figure 3.14. Distributions of stresses for the five-layer tube ($a = 0.4\ m, r_1 = 0.55\ m,\ r_2 = 0.7\ m,\ r_3 = 0.85\ m,\ r_4 = 1.00\ m,\ b = 1.15\ m$) for $\overline{P}_{int} = 0.3$.

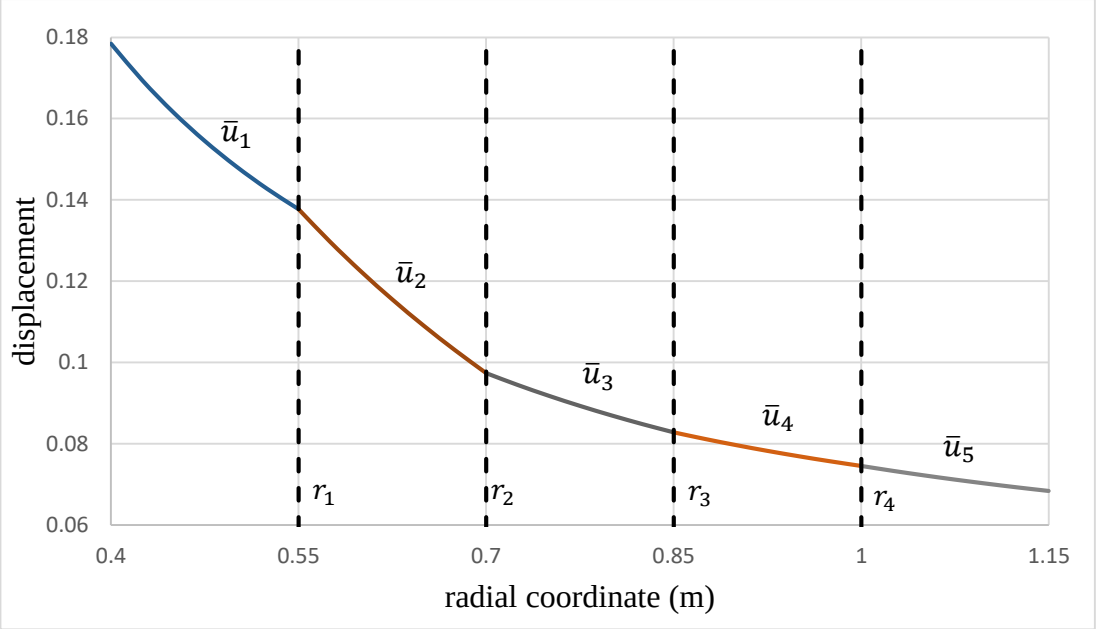

Figure 3.15. Distribution of radial displacement for the five-layer tube ($a = 0.4\ m,\ r_1 = 0.55\ m,\ r_2 = 0.7\ m,\ r_3 = 0.85\ m,\ r_4 = 1.00\ m,\ b = 1.15\ m$) under internal pressure $\overline{P}_{int} = 0.3$.

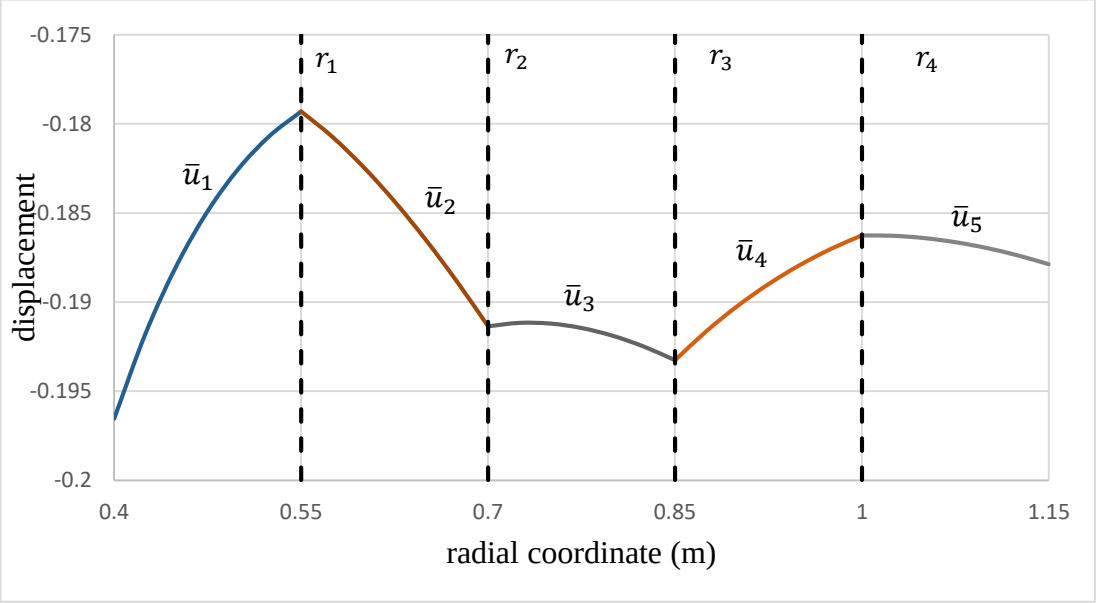

Figure 3.16. Distribution of radial displacement for the five-layer tube ($a = 0.4\ m,\ r_1 = 0.55\ m,\ r_2 = 0.7\ m,\ r_3 = 0.85\ m,\ r_4 = 1.00\ m,\ b = 1.15\ m$) under external pressure $\overline{P}_{ext} = 0.3$.

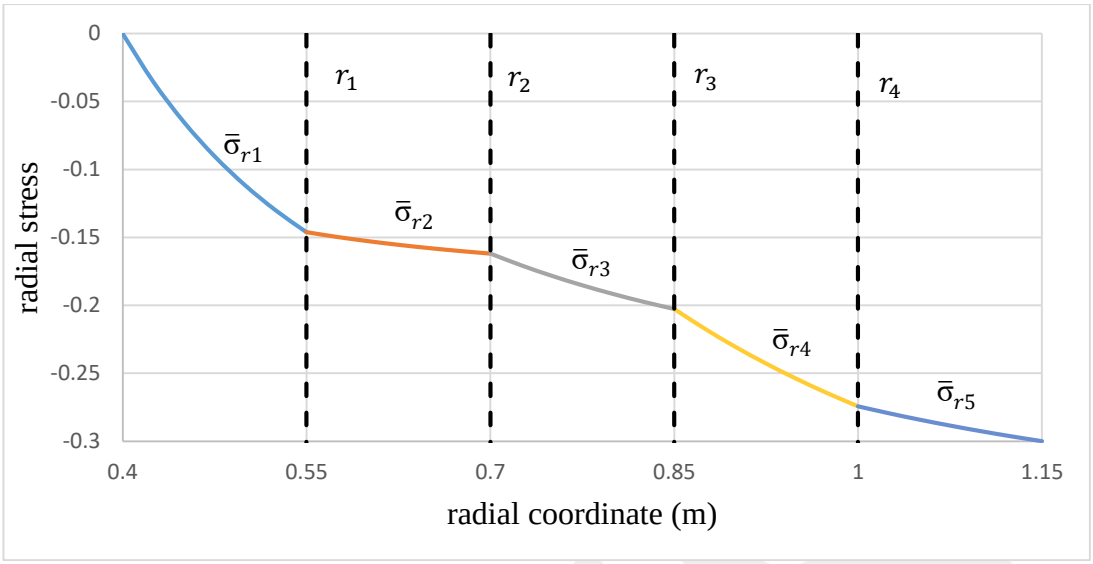

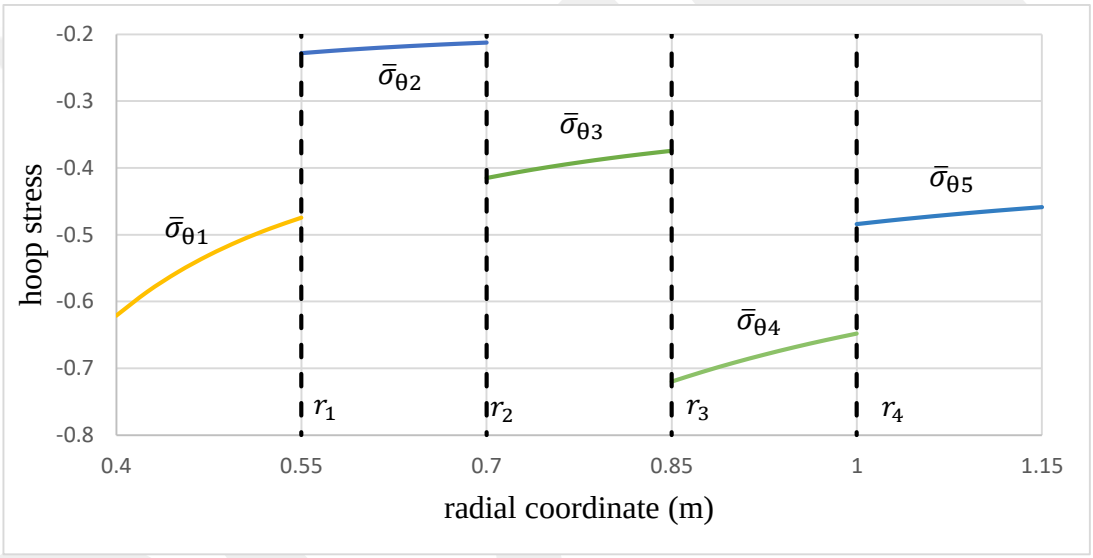

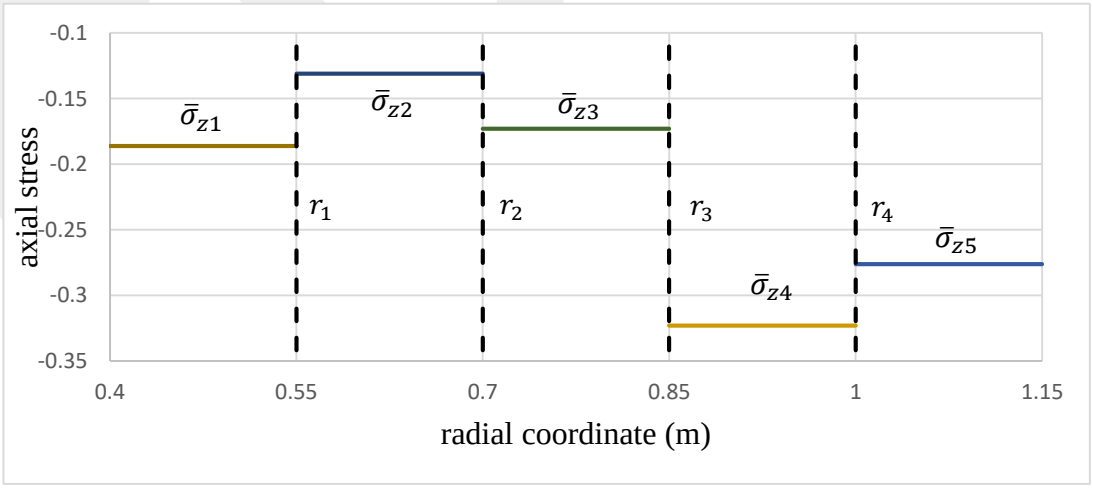

Figure 3.17. Distributions of stresses for the five-layer tube ($a = 0.4\ m, r_1 = 0.55\ m,\ r_2 = 0.7\ m,\ r_3 = 0.85\ m,\ r_4 = 1.00\ m,\ b = 1.15\ m$) under external pressure $\overline{P}_{ext} = 0.3$.

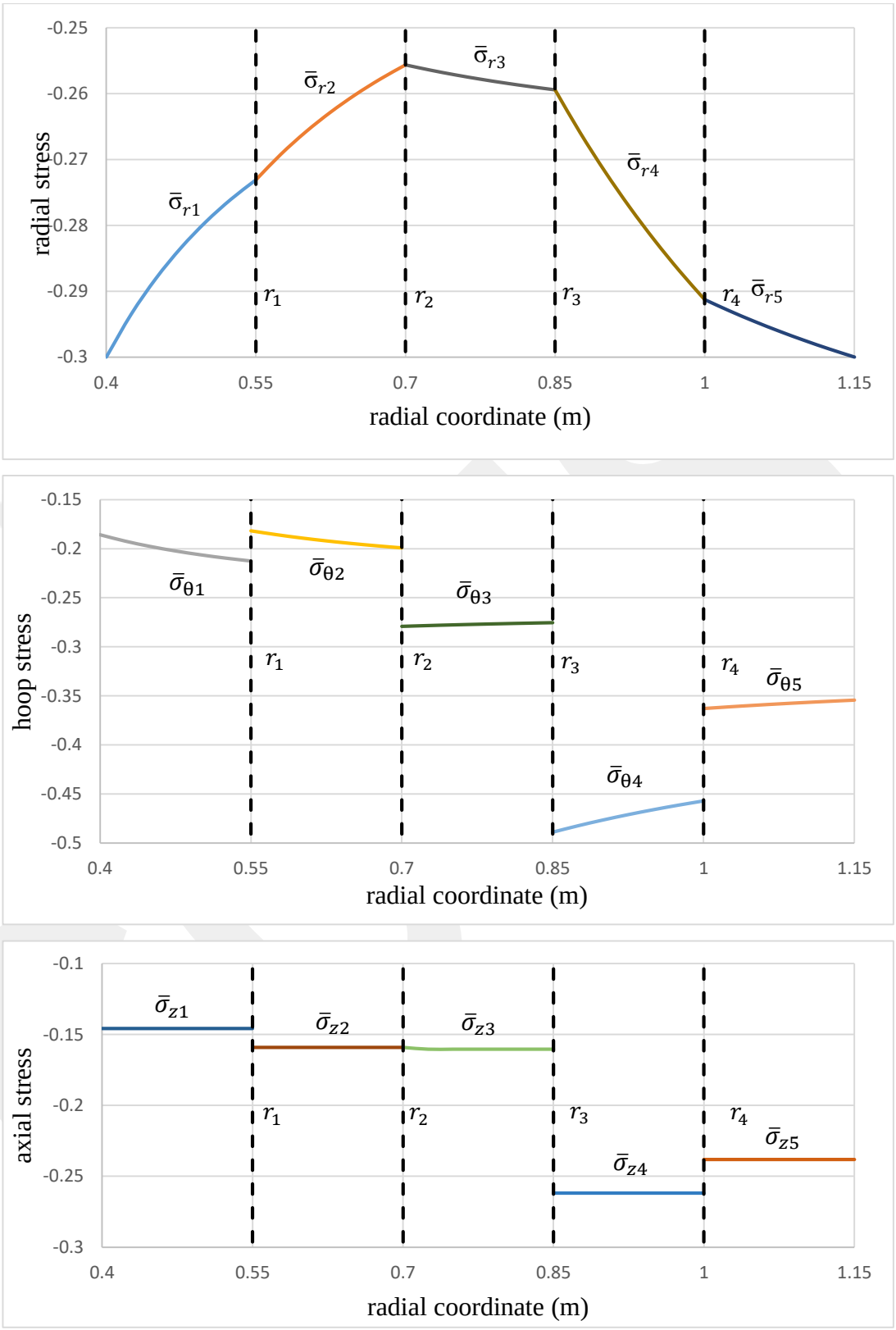

Figure 3.18. Distributions of stresses for five-layer tube ($a = 0.4\ m, r_1 = 0.55\ m, r_2 = 0.7\ m, r_3 = 0.85\ m, r_4 = 1.00\ m, b = 1.15\ m$), under internal pressure $\overline{P}_{int} = 0.3$ and external pressure $\overline{P}_{ext} = 0.3$.

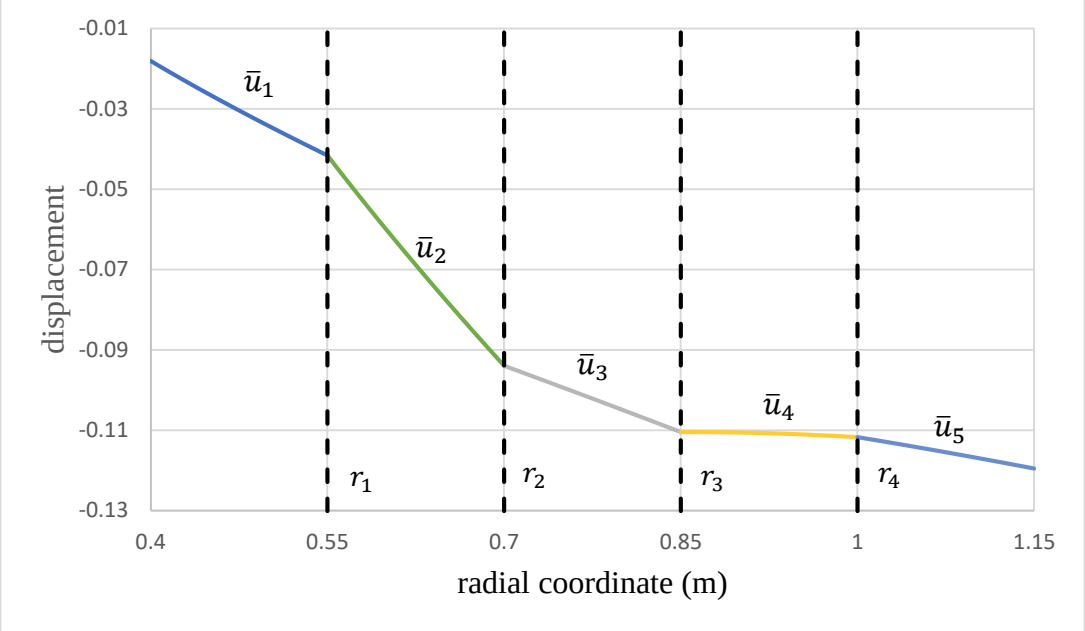

Fig. 3.19. Distribution of radial displacement of the five-layers tube ($a = 0.4\ m,\ r_1 = 0.55\ m,\ r_2 = 0.7\ m,\ r_3 = 0.85\ m,\ r_4 = 1.00\ m,\ b = 1.15\ m$) under internal pressure $\overline{P}_{int} = 0.3$ and external pressure $\overline{P}_{ext} = 0.3$.

3.5 Example problems

In order to check the validity of the procedure, four example problems are handled. Those example problems are taken from the works of Eraslan and Akis [22], Yeo et al. [32], Akis [27] and Vedeld and Sollund [31]. The tubes with the same dimensions, same material properties and same loading and boundary conditions are considered in the verification studies. In the next part, these comparison studies are presented. It should be noted that in all graphs, dotted results belong to the previous studies, while solid lines belong to the results obtained by the proposed method.

3.5.1 FGM tube under pressure by Eraslan and Akis [22]

In the study of Eraslan and Akis [18], an FGM tube (inner radius $\bar{a} = a/b = 0.7$ and the outer radius $\bar{b} = 1$) under internal pressure of $\overline{P}_{int} = 0.269$ was considered, where the stresses were obtained analytically in elastic stress state. The same problem is handled by considering two, five, and ten homogenous layers using the proposed method. Using MATHEMATICA, the nonlinear equations are solved and the integration constants are obtained. Then, using the integration constants, the distributions of stresses and radial displacements are obtained for each layer. Finally,

the results are compared with the analytical results given by Eraslan and Akis [18]. Firstly, a two-layer tube is considered. The geometry and the calculated material properties are given in Table 3.2. The dimensionless integration constants are found as $\overline{C}_1 = C_1/b^2 = 0.124178$, $\overline{C}_2 = C_2 = 0.31688$, $\overline{C}_3 = C_3/b^2 = 0.12617$ and $\overline{C}_4 = C_4 = 0.31543$. The radial stress distribution for this case is shown in Fig 3.20(a), the hoop stress distribution is shown in Fig 3.21(a), and the axial stress distributions is shown in Fig 3.22(a).

Table 3.2 Geometrical and materials properties of two-layer composite tube

Layer	$\overline{r}_{i-1}$	$\overline{r}_i$	E_i /E(a)	ν_i
1	0.70	0.85	1.0399	0.3
2	0.85	1.00	1.1082	0.3

For the five-layer solution, the geometry and the calculated material properties are given in Table 3.3. The dimensionless integration constants are found as $\overline{C}_1 = C_1/b^2 = 8.22 \times 10^{-4}$, $\overline{C}_2 = C_2 = 21.45 \times 10^{-4}$, $\overline{C}_3 = C_3/b^2 = 8.37 \times 10^{-4}$, $\overline{C}_4 = C_4 = 21.36 \times 10^{-4}$, $\overline{C}_5 = C_5/b^2 = 8.46 \times 10^{-4}$,$\overline{C}_6 = C_6 = 21.31 \times 10^{-4}$, $\overline{C}_7 = C_7/b^2 = 8.50 \times 10^{-4}$, $\overline{C}_8 = C_8 = 21.28 \times 10^{-4}$, $\overline{C}_9 = C_9/b^2 = 8.50 \times 10^{-4}$, and $\overline{C}_{10} = C_{10} = 21.27 \times 10^{-4}$. The radial stress distribution for this case is shown in Fig 3.20(b), while the hoop stress distribution is shown in Fig 3.21(b). The axial stress distribution for this case is given in Fig. 3.22(b).

For the ten-layer solution, the data given in Table 3.4 is used. The dimensionless integration constants are found as $\overline{C}_1 = C_1/b^2 = 8.15 \times 10^{-4}$, $\overline{C}_2 = C_2 = 21.46 \times 10^{-4}$, $\overline{C}_3 = C_3/b^2 = 8.25 \times 10^{-4}$, $\overline{C}_4 = C_4 = 21.41 \times 10^{-4}$, $\overline{C}_5 = C_5/b^2 = 8.32 \times 10^{-4}$, $\overline{C}_6 = C_6 = 21.37 \times 10^{-4}$, $\overline{C}_7 = C_7/b^2 = 8.38 \times 10^{-4}$, $\overline{C}_8 = C_8 = 21.33 \times 10^{-4}$,$\overline{C}_9 = C_9/b^2 = 8.42 \times 10^{-4}$, $\overline{C}_{10} = C_{10} = 21.30 \times 10^{-4}$, $\overline{C}_{11} = C_{11}/b^2 = 8.45 \times 10^{-4}$, $\overline{C}_{12} = C_{12} = 21.28 \times 10^{-4}$, $\overline{C}_{13} = C_{13}/b^2 = 8.47 \times 10^{-4}$,

$\overline{C}_{14} = C_{14} = 21.27 \times 10^{-4}$, $\overline{C}_{15} = C_{15}/b^2 = 8.48 \times 10^{-4}$, $\overline{C}_{16} = C_{16} = 21.26 \times 10^{-4}$, $\overline{C}_{17} = C_{17}/b^2 = 8.49 \times 10^{-4}$, $\overline{C}_{18} = C_{18} = 21.2 \times 10^{-4}$, $\overline{C}_{19} = C_{19}/b^2 = 8.49 \times 10^{-4}$, $\overline{C}_{20} = C_{20} = 21.24 \times 10^{-4}$. The radial stress distribution is shown in Fig 3.20(c), the hoop stress distribution is shown in Fig 3.21(c), and the axial stress distribution is given in Fig 3.22(c).

Table 3.3 Geometrical and materials properties of five-layer composite tube

Layer	$\overline{r}_{i-1}$	$\overline{r}_i$	Ei /E(a)	ν_i
1	0.70	0.76	1.0177	0.3
2	0.76	0.82	1.0513	0.3
3	0.82	0.88	1.0799	0.3
4	0.88	0.94	1.1046	0.3
5	0.94	1.00	1.1260	0.3

Table 3.4 Geometrical and materials properties of ten-layer composite tube

Layer	$\overline{r}_{i-1}$	$\overline{r}_i$	E_i /Ea	ν_i
1	0.70	0.73	1.0090	0.3
2	0.73	0.76	1.0272	0.3
3	0.76	0.79	1.0439	0.3
4	0.79	0.82	1.0593	0.3
5	0.82	0.85	1.0736	0.3
6	0.85	0.88	1.0868	0.3
7	0.88	0.91	1.0990	0.3
8	0.91	0.94	1.1105	0.3
9	0.94	0.97	1.1212	0.3
10	0.97	1.00	1.1312	0.3

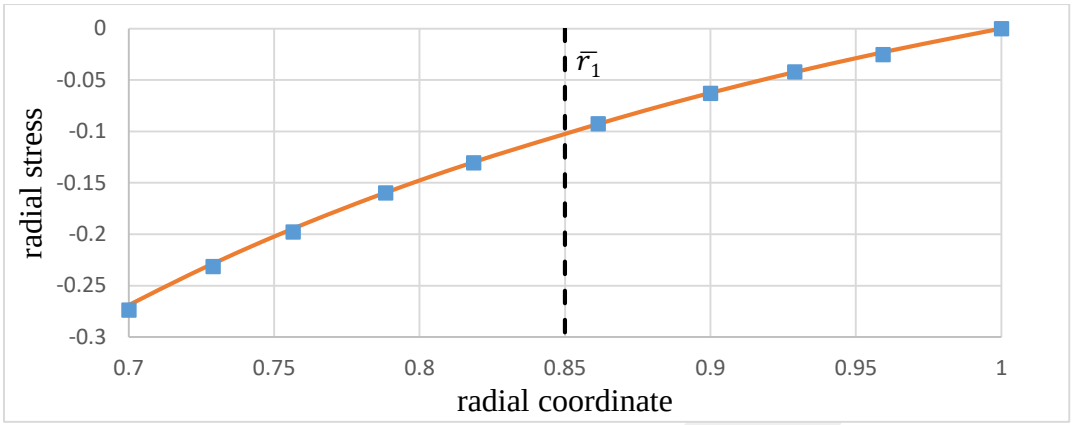

(a)Two-layer tube

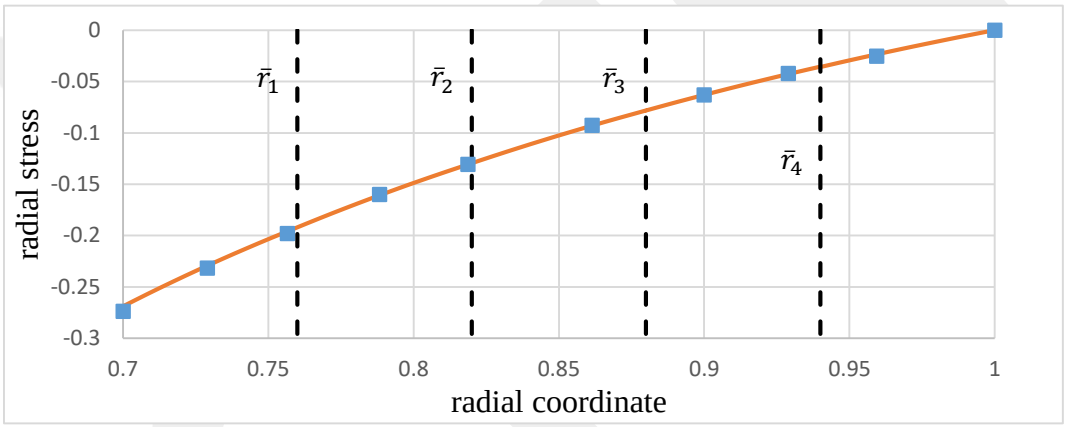

(b) Five-layer tube

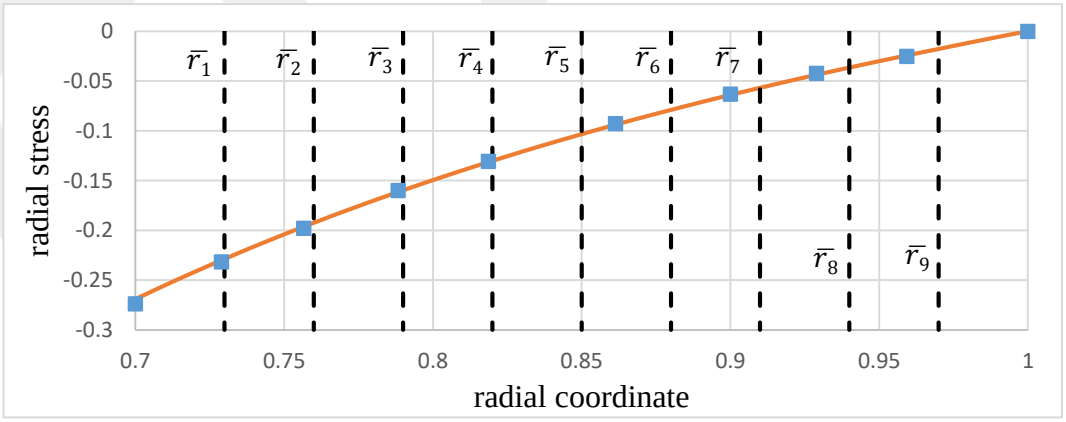

(c)Ten-layer tube

Figure 3.20. Comparison of radial stresses with (a) two, (b) five, and (c) ten-layer tubes ($\bar{a} = 0.7$, $\bar{b} = 1$) under the internal pressure $\overline{P}_{int} = 0.269$

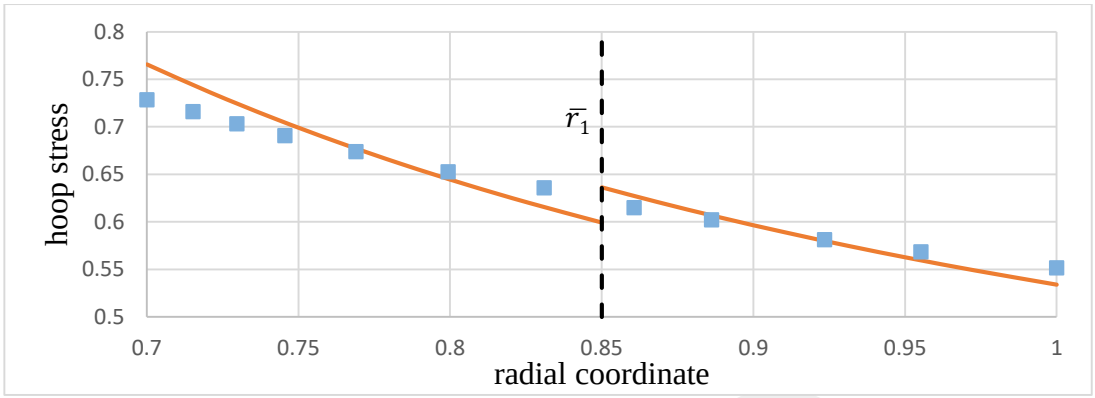

(a) Two-layer tube

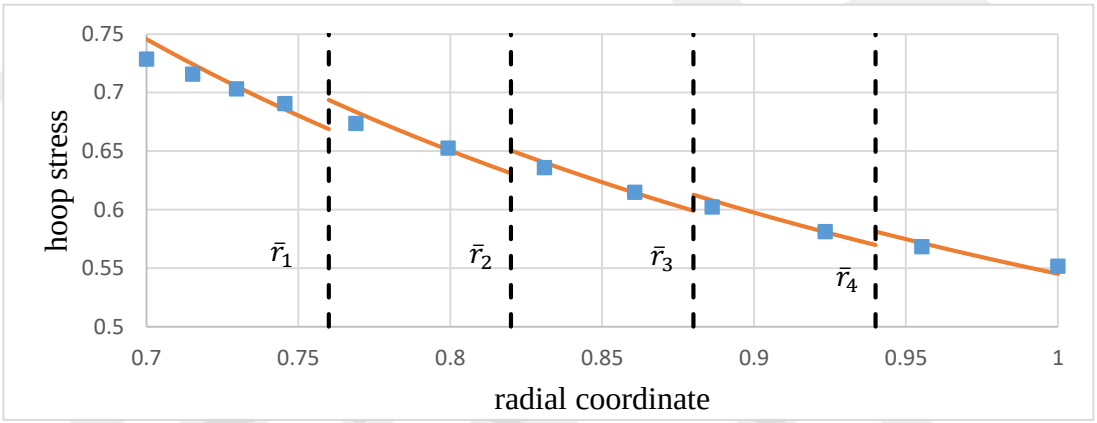

(b) Five-layer tube

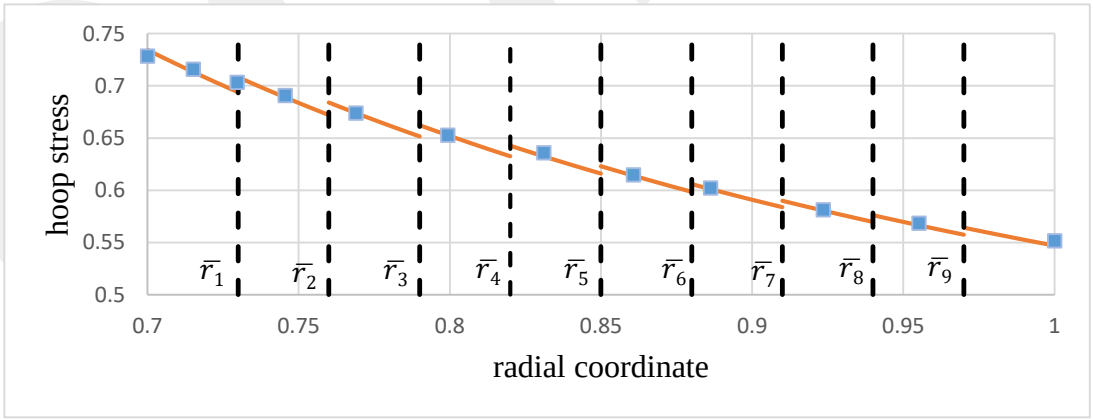

(c) Ten-layer tube

Figure 3.21. Comparison of tangential stresses with (a) two, (b) five, and (c) ten-layer tubes ($\bar{a} = 0.7,\ \bar{b} = 1$) the internal under internal pressure $\overline{P}_{int} = 0.269$

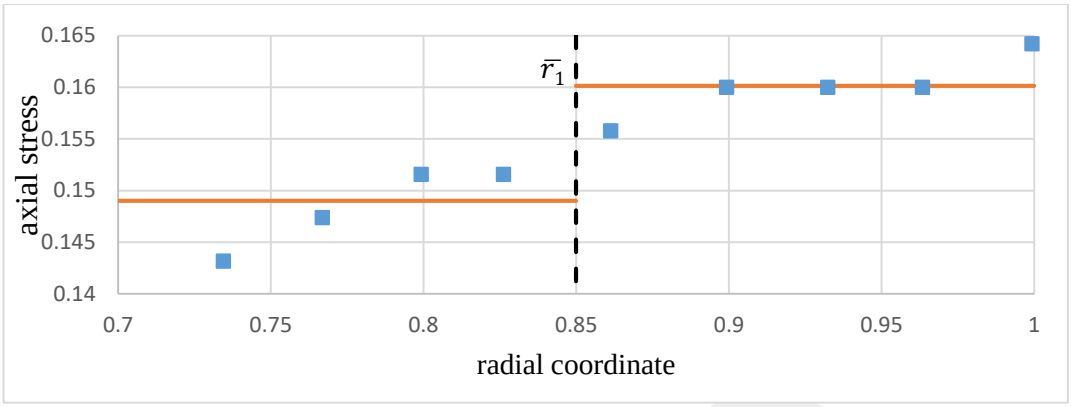

(a) Two-layer tube

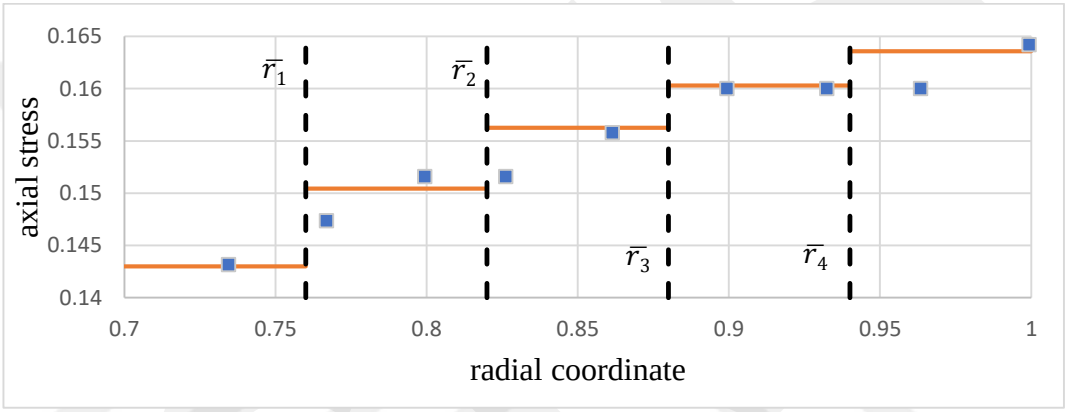

(b) Five-layer tube

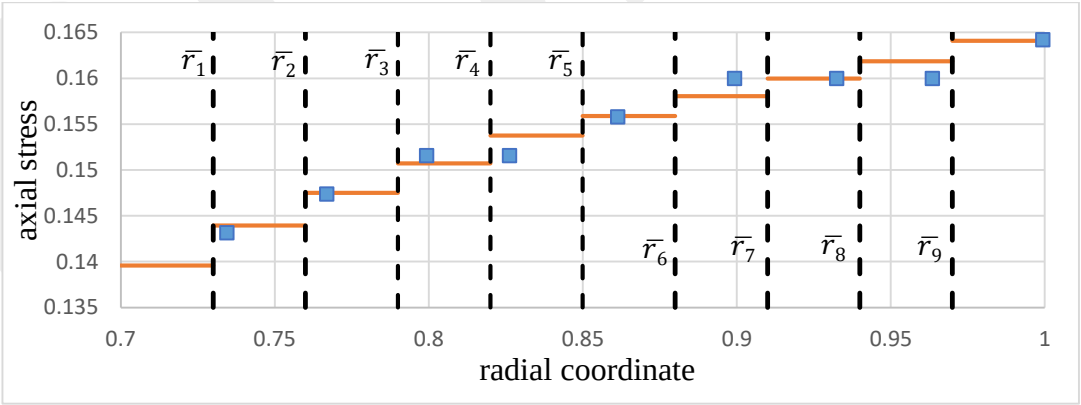

(c) Ten-layer tube

Figure 3.22. Comparison of axial stresses with (a) two, (b) five, and (c) ten-layer tubes ($\bar{a} = 0.7, \bar{b} = 1$) under the internal pressure $\overline{P}_{int} = 0.269$

3.5.2. Multilayer tube under thermal and mechanical loading by Yeo et al. [32]

The problem solved in the study of Yeo et al. [32] is taken into consideration in order to demonstrate the ability of the proposed method in evaluating temperatures and stresses. The problem is about a six-layer composite tube. The geometry and the materials properties are presented in Table 3.5. In the example, the internal pressure is defined as $P_{int} = 22$ MPa and the external pressure is $P_{ext} = 1.5$ MPa. In addition, the inner and outer surfaces of the multilayer tube have the temperatures of 200 ^{0}C and 150 ^{0}C, respectively. In the comparison studies, same material properties, same thicknesses and same loading conditions are taken into consideration. Fig 3.23 shows the comparison of temperature distribution obtained by the proposed method and the results at the study of Yeo et al. [32]. The comparison of stress distributions in radial, tangential and axial directions are given in Fig. 3.24. Finally, the comparison of the radial displacement is given in Fig. 3.25. The integration constants are computed as $A_1 = -238.742$, $A_2 = -632.972$, $A_3 = -121.284$, $A_4 = -485.531$, $A_5 = -56.502$, $A_6 = -359.465$, $A_7 = -15.956$, $A_8 = -295.601$, $A_9 = 11.255$, $A_{10} = -251.006$, $A_{11} = 31.193$, $A_{12} = -218.103$, $\overline{C}_1 = C_1/b^2 = -0.83 \times 10^{-4}$, $\overline{C}_2 = C_2 = -14.70 \times 10^{-4}$, $\overline{C}_3 = C_3/b^2 = -0.223 \times 10^{-4}$, $\overline{C}_4 = C_4 = -9.69 \times 10^{-4}$, $\overline{C}_5 = C_5/b^2 = 9.21 \times 10^{-4}$, $\overline{C}_6 = C_6 = -6.5 \times 10^{-4}$, $\overline{C}_7 = C_7/b^2 = -0.271 \times 10^{-4}$, $\overline{C}_8 = C_8 = -4.19 \times 10^{-4}$, $\overline{C}_9 = C_9/b^2 = 0.374 \times 10^{-4}$, $\overline{C}_{10} = C_{10} = -2.30 \times 10^{-4}$, $\overline{C}_{11} = C_{11}/b^2 = 0.416 \times 10^{-4}$, $\overline{C}_{12} = C_{12} = -0.98 \times 10^{-4}$. As seen from these figures, almost identical results are obtained with the proposed method.

Table 3.5 Geometrical and materials properties of six-layer composite tube

Layer	r_{i-1}(mm)	r_i(mm)	E_i (GPa)	ν_i	α_i($^0C^{-1}$) x10^{-6}	k_i (W m^{-1} $^0K^{-1}$)
1	500	510	190	0.28	18.7	18.4
2	510	520	194	0.28	17.4	25.4
3	520	530	198	0.28	16.1	32.4
4	530	540	202	0.28	14.8	39.4
5	540	550	206	0.28	13.5	46.4
6	550	580	210	0.30	12.2	53.4

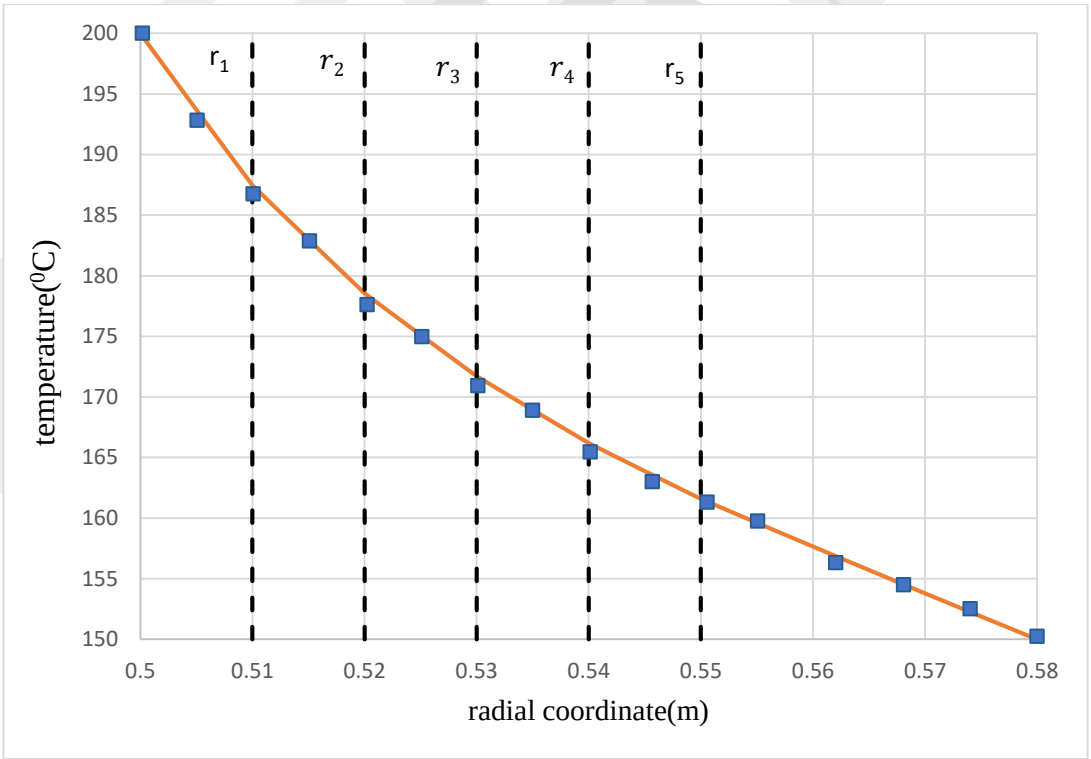

Figure 3.23. Comparison of temperature distribution for the six-layer tube for P_{int} = 22 MPa, P_{ext} = 1.5 MPa, T_{int} = 200 ^{0}C, and T_{ext} = 150 ^{0}C

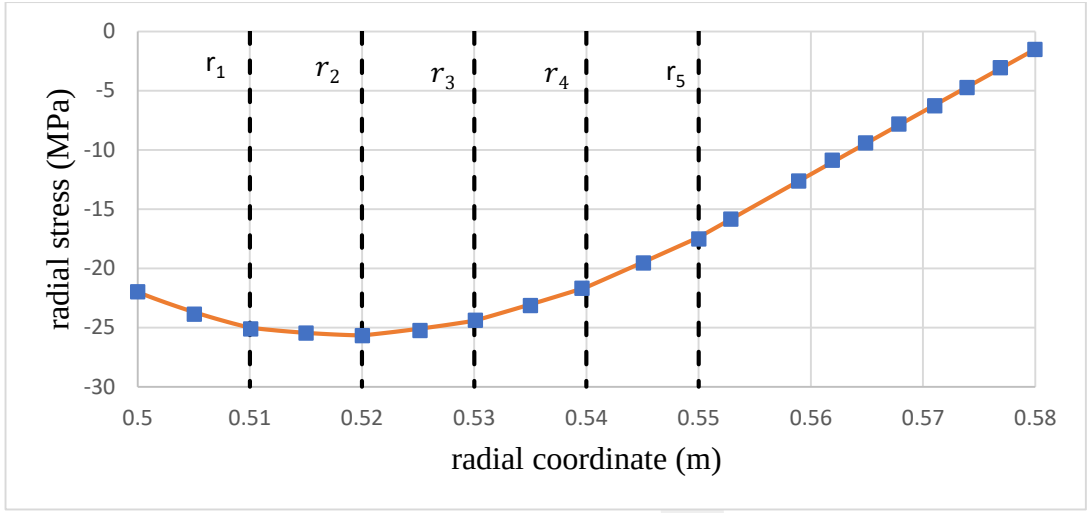

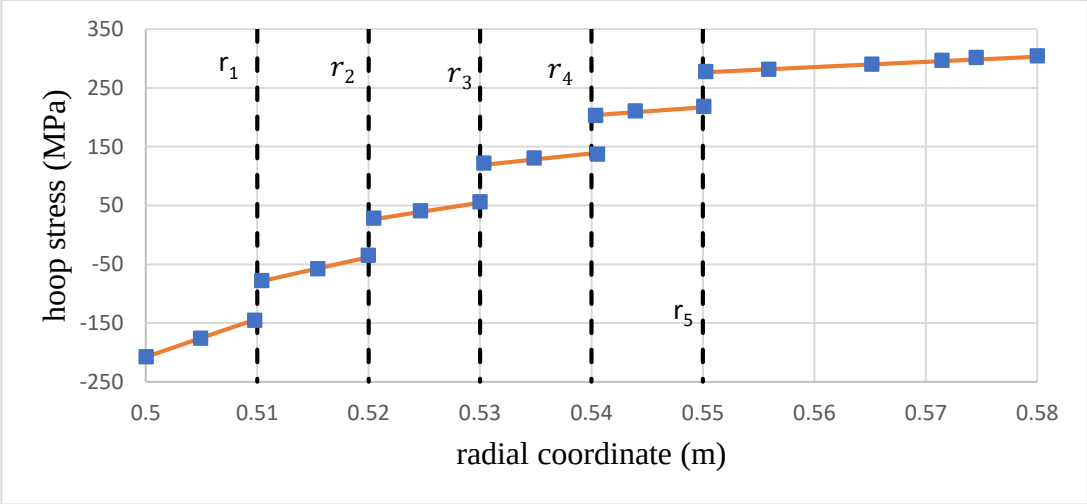

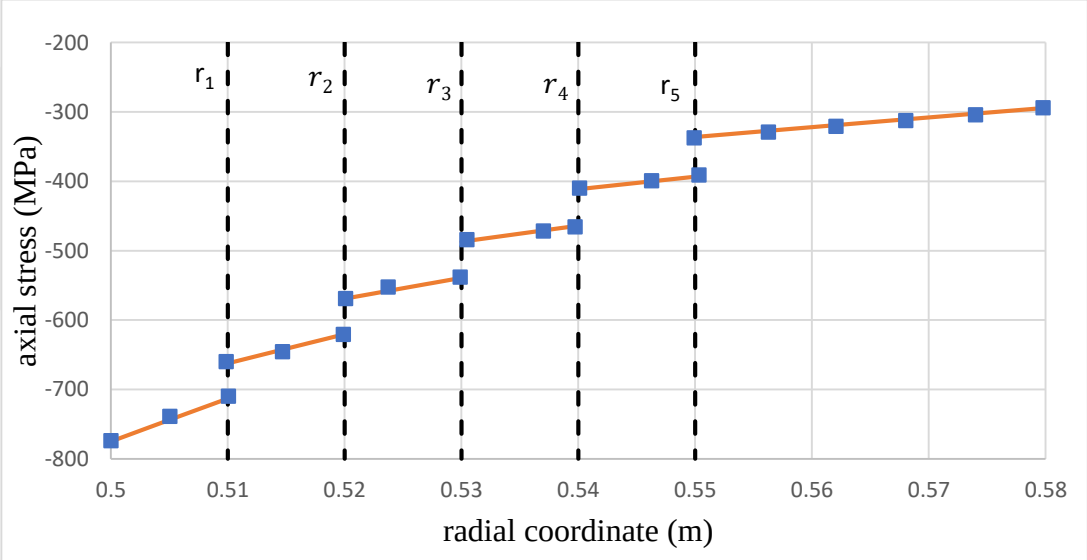

Figure 3.24. Comparison of the distributions of stresses for the six-layer tube for P_{int} = 22 MPa, P_{ext} = 1.5 MPa, T_{int} = 200 ^{0}C, and T_{ext} = 150 ^{0}C

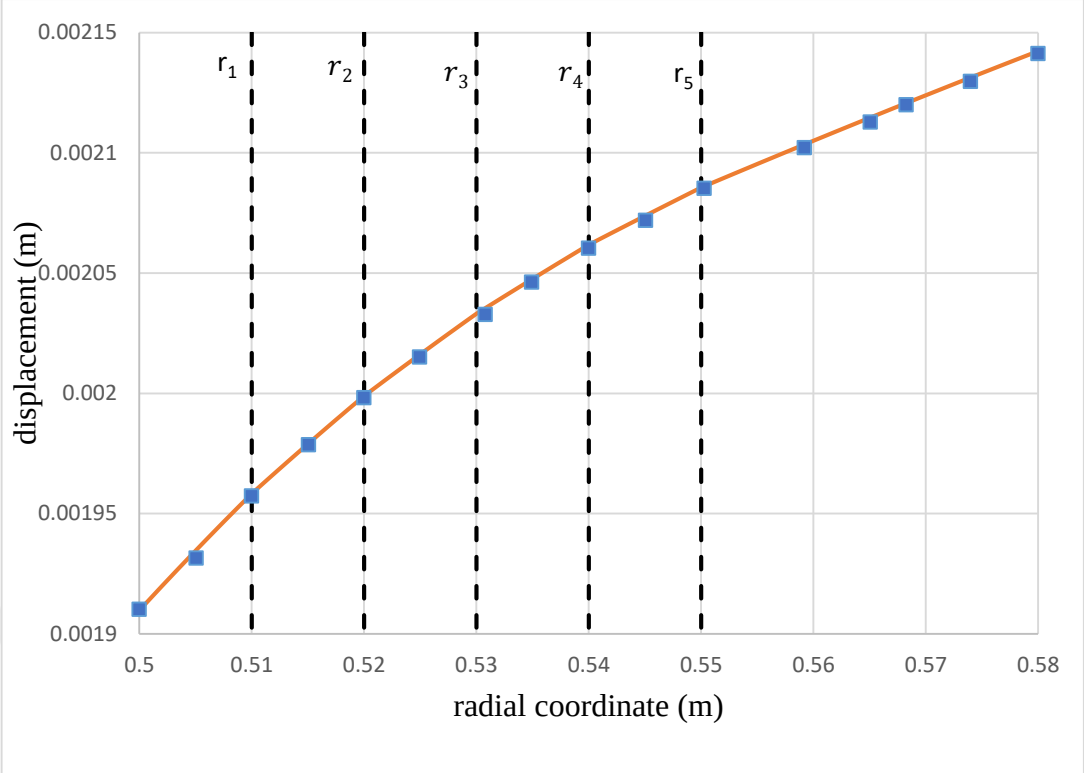

Figure 3.25. Comparison of distribution of radial displacement for the six-layer tube for $P_{int} = 22$ MPa, $P_{ext} = 1.5$ MPa, $T_{int} = 200\ ^0$C, and $T_{ext} = 150\ ^0$C.

3.5.3. Heat generating FGM tube by Akış [27]

In the example problem solved by Akış [27] a nonlinear heat generating FGM tube (inner radius $\bar{a} = a/b = 0.6$, outer radius $\bar{b} = 1$) is taken into consideration. In order to use the proposed method, the equations derived for constant heat generation are modified for nonlinear heat generation case. The heat generation term in the energy equation is considered as

$$q_1(r) = Q_1\,(r - a)(r_1 - r) \tag{146}$$

for the first inner layer. For the mid-layers the following equation is used:

$$q_i(r) = Q_i\,(r - r_i)(r_{i+1} - r) \tag{147}$$

Here *i* defines the layers of the tube assembly. Similarly, at the outer layer of the tube, the nonlinear heat generation term becomes

$$q_n(r) = Q_n (r - r_{n-1}) (b - r) \quad (148)$$

In the computations, the temperature distribution is obtained by using the expressions given above in the heat equation.

The thermal conductivity *k* and modulus of elasticity *E* in that study was not constant and varied with the following forms:

$$k = k_0(r/b)^m \quad (149)$$

$$E = E_0(r/b)^n \quad (150)$$

The boundary conditions for the problem was

$$T(a) = T_0 \quad (151)$$

$$\frac{dT}{dr}\Big|_{r=b} = 0 \quad (152)$$

In this study, two, five, and ten equal layers are considered for comparison studies. For the multilayer tubes, the material properties for each layer is calculated by considering an average value, which is obtained by the FGM tube properties at the layer boundaries. For the two-layer tube, the geometry and material properties are given in Table 3.6. Using these, the integration constants are found as $A_1 = -1534.57$, $A_2 = -793.95$, $A_3 = -1910.244$, $A_4 = -976.512$, $\overline{C}_1 = C_1/b^2 = 5.39 \times 10^{-4}$, $\overline{C}_2 = C_2 = -0.016285$, $\overline{C}_3 = C_3/b^2 = 6.96 \times 10^{-4}$ and $\overline{C}_4 = C_4 = -0.020359$. The comparison of the temperature distributions is shown in Fig. 3.26. On the other hand, the comparison of temperature gradients is given in Fig. 3.27. In Fig. 3.28 the dimensionless radial displacements are compared, while the comparison of distributions of dimensionless stress components is made in Fig. 3.29.

Table 3.6. Geometry and the materials properties of two-layer tube

Layer	$\bar{r}_{i-1}$	$\bar{r}_i$	E_i (GPa)	q (W/m^3)	k ($W\ m^{-1}\ {}^0K^{-1}$)
1	0.6	0.8	250.192	62762.89	64.80579
2	0.8	1.0	214.326	62762.89	52.69057

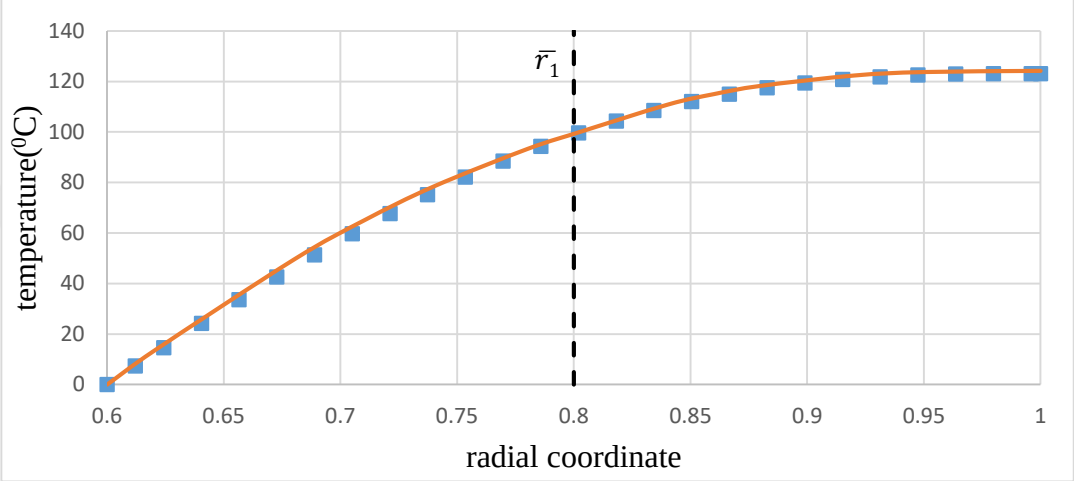

Figure 3.26. Comparison of temperature distributions of the two-layer solution with the analytical solution ($\bar{a}\ = 0.6,\ \bar{r}_1 = 0.8,\ \bar{b}\ = 1.0$).

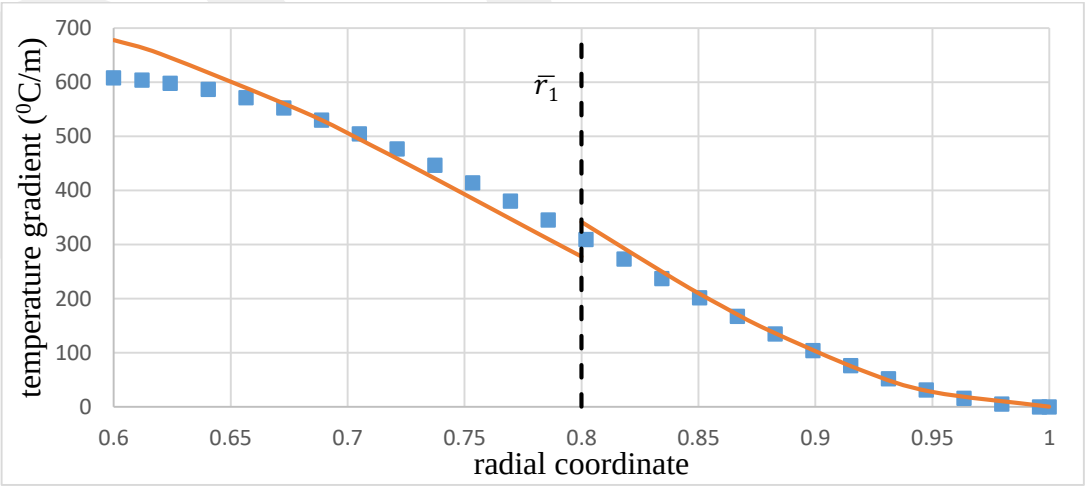

Figure 3.27. Comparison of temperature gradients of the two-layer solution and the analytical solution ($\bar{a}\ = 0.6,\ \bar{r}_1 = 0.8, \bar{b}\ = 1.0$)

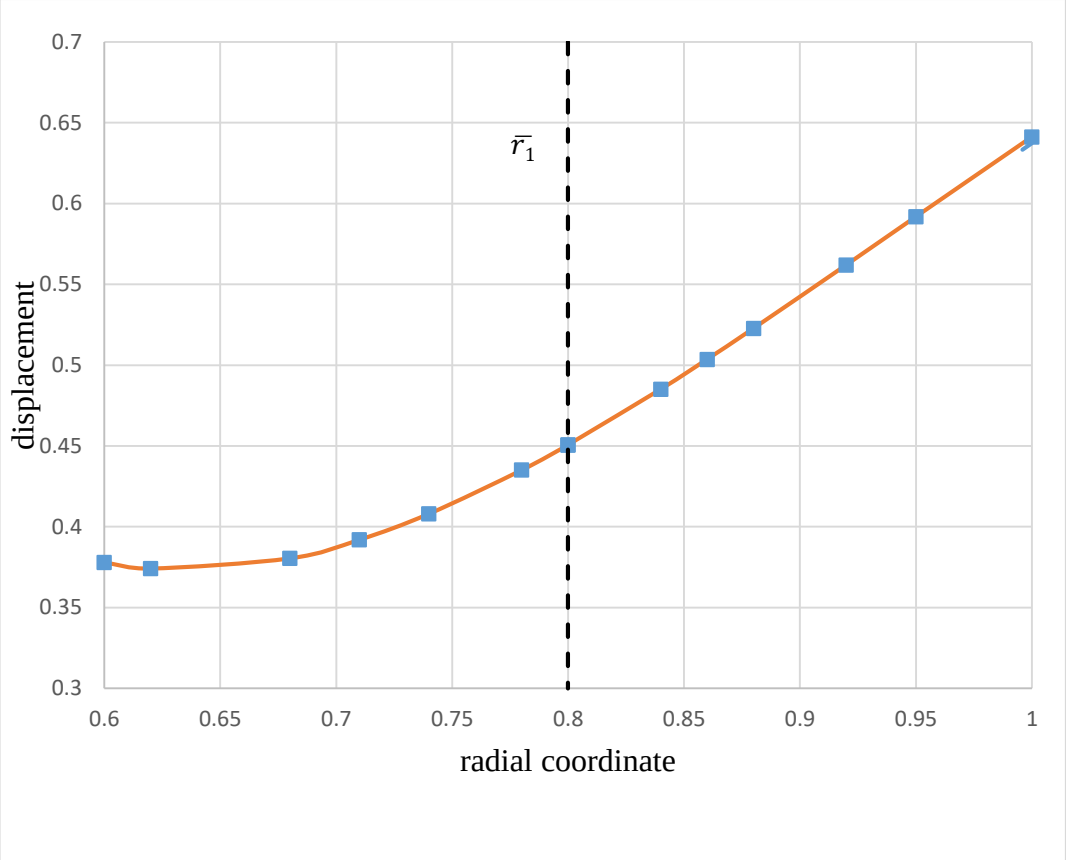

Figure 3.28. Comparison of radial displacements of the two-layer solution and the analytical solution ($\bar{a} = 0.6,\ \bar{r}_1 = 0.8,\ \bar{b} = 1.0$)

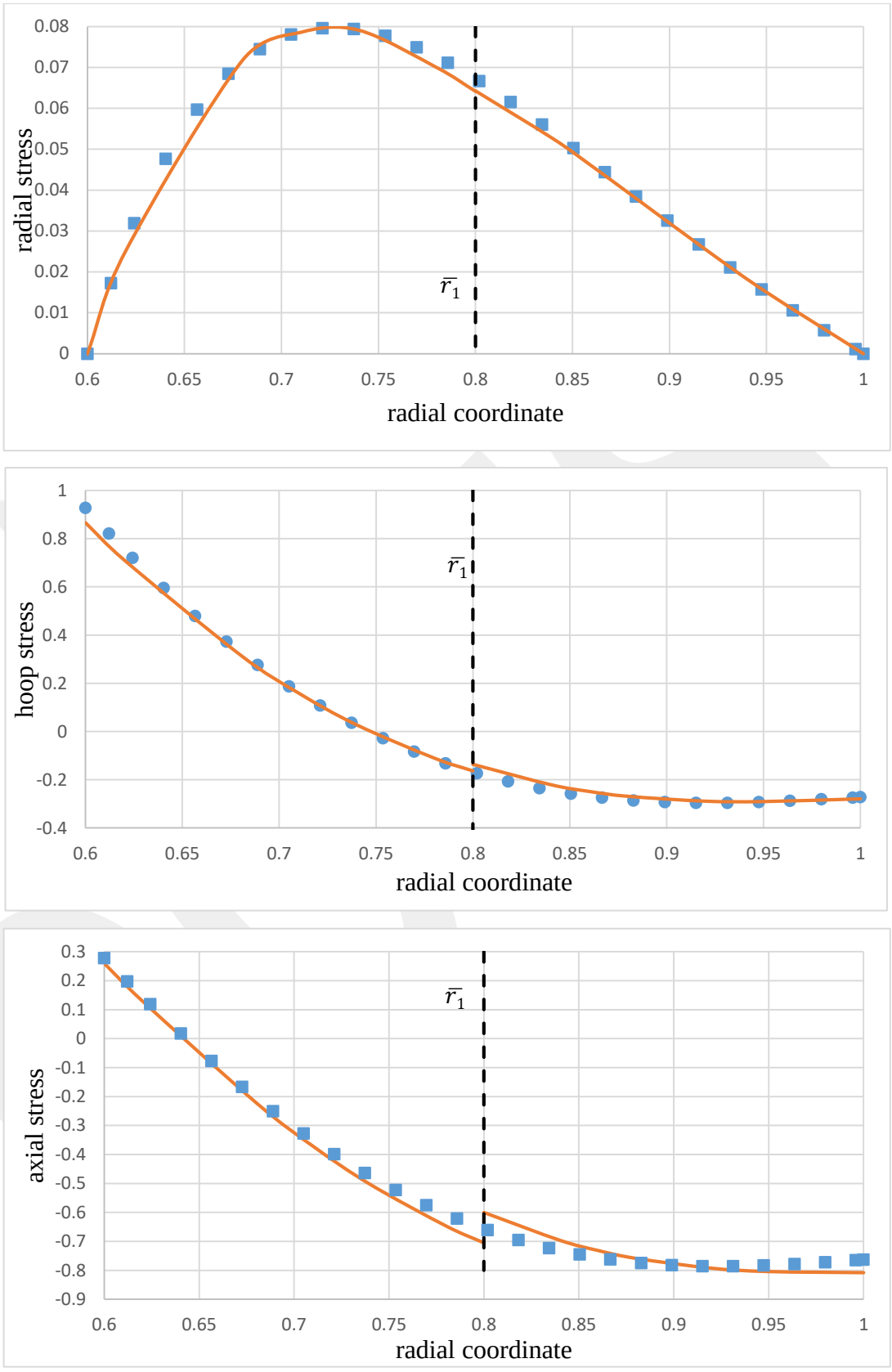

Figure 3.29. Comparison of stresses of the two-layer solution and the analytical solution ($\bar{a} = 0.6, \bar{r}_1 = 0.8, \bar{b} = 1.0$)

In the second part, the tube is divided into five equal layers. parts. The corresponding geometry and material properties are given in Table 3.7. The temperature and dimensionless integration constants are found as $A_1 = -1445.71$, $A_2 = -747.979$, $A_3 = -1594.14$, $A_4 = -822.373$, $A_5 = -1742.56$, $A_6 = -895.073$, $A_7 = -1889.95$, $A_8 = 966.293$, $A_9 = 2035.46$, $A_{10} = -1036.2$, $\overline{C}_1 = C_1/b^2 = 5.21 \times 10^{-4}$, $\overline{C}_2 = C_2 = -0.015327$, $\overline{C}_3 = C_3/b^2 = 5.58 \times 10^{-4}$, $\overline{C}_4 = C_4 = -0.016936$, $\overline{C}_5 = C_5/b^2 = 6.13 \times 10^{-4}$, $\overline{C}_6 = C_6 = -0.018546$, $\overline{C}_7 = C_7/b^2 = 0.681 \times 10^{-4}$, $\overline{C}_8 = C_8 = -0.020146$, $\overline{C}_9 = C_9/b^2 = 7.55 \times 10^{-4}$, $\overline{C}_{10} = C_{10} = -0.021726$. The corresponding comparison graphs are given in Figs. 3.30 to 3.33.

Table 3.7. Geometry and the materials properties of five-layer tube

Layer	$\overline{r}_{i-1}$	$\overline{r}_i$	E_i (GPa)	q (W/m^3)	k (W m^{-1} ^{0}K^{-1})
1	0.6	0.68	261.902	39515.89744	68.78935
2	0.68	0.76	243.935	98789.74359	62.56651
3	0.76	0.84	228.927	118547.6923	57.48467
4	0.84	0.92	216.158	98789.74359	53.24782
5	0.92	1.00	205.130	39515.89744	49.65553

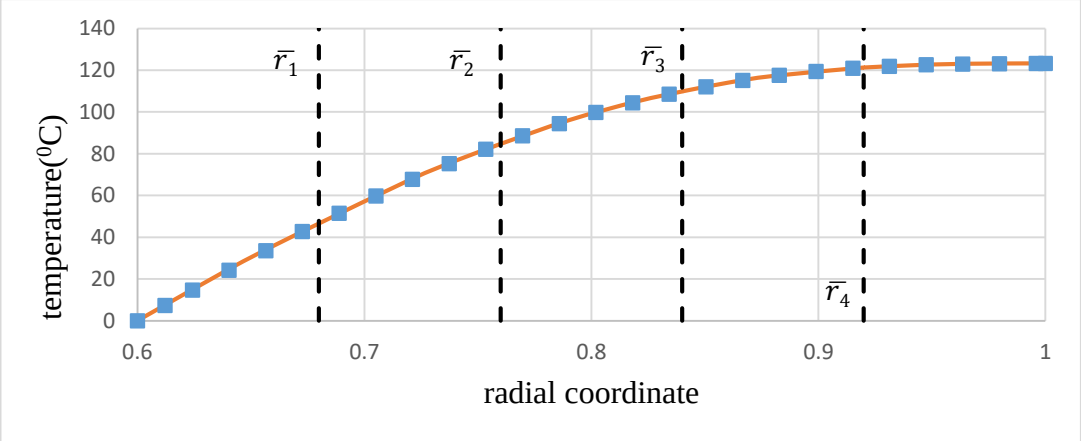

Figure 3.30. Comparison of temperature distributions of the five-layer solution and the analytical solution ($\bar{a} = 0.6$, , $\overline{r}_1 = 0.68$, $\overline{r}_2 = 0.76$, $\overline{r}_3 = 0.84$, $\overline{r}_4 = 0.92$, $\bar{b} = 1.0$)

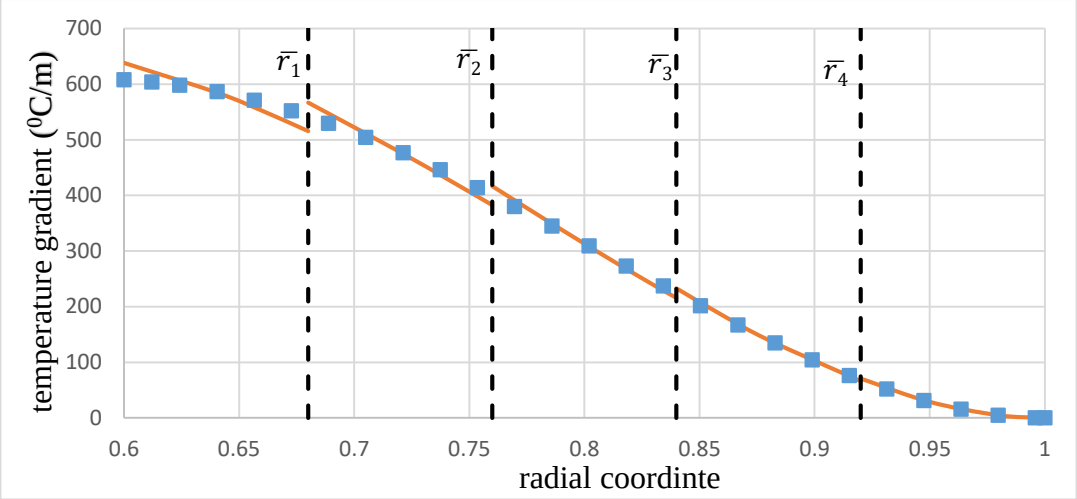

Figure 3.31. Comparison of temperature gradients of the five-layer solution and the analytical solution ($\bar{a} = 0.6,, \bar{r}_1 = 0.68, \bar{r}_2 = 0.76, \bar{r}_3 = 0.84, \bar{r}_4 = 0.92, \bar{b} = 1.0$)

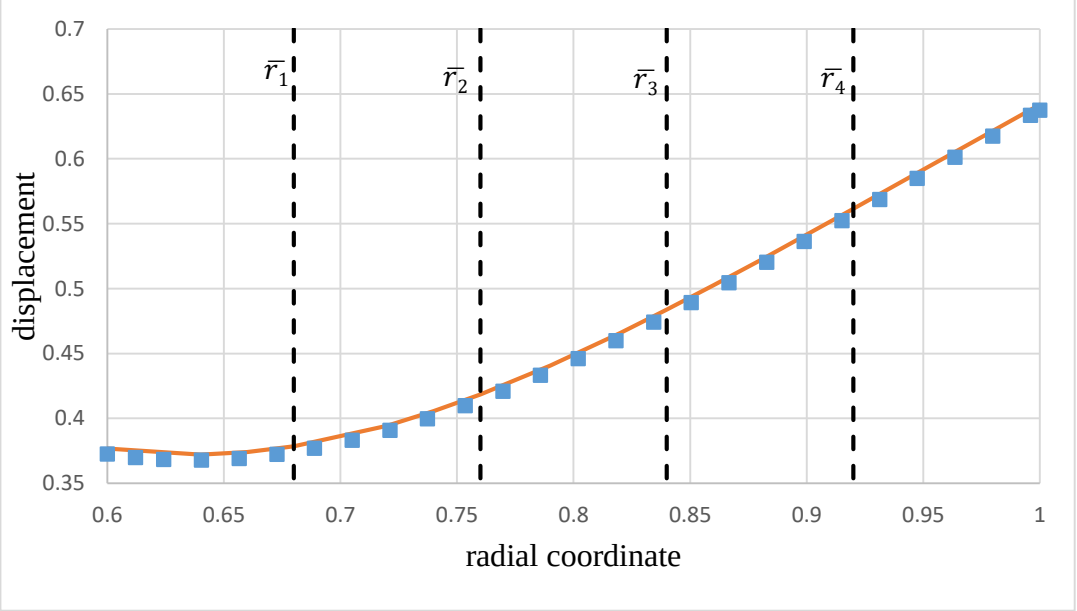

Figure 3.32. Comparison of radial displacements of the five-layer solution and the analytical solution ($\bar{a} = 0.6,, \bar{r}_1 = 0.68, \bar{r}_2 = 0.76, \bar{r}_3 = 0.84, \bar{r}_4 = 0.92, \bar{b} = 1.0$)

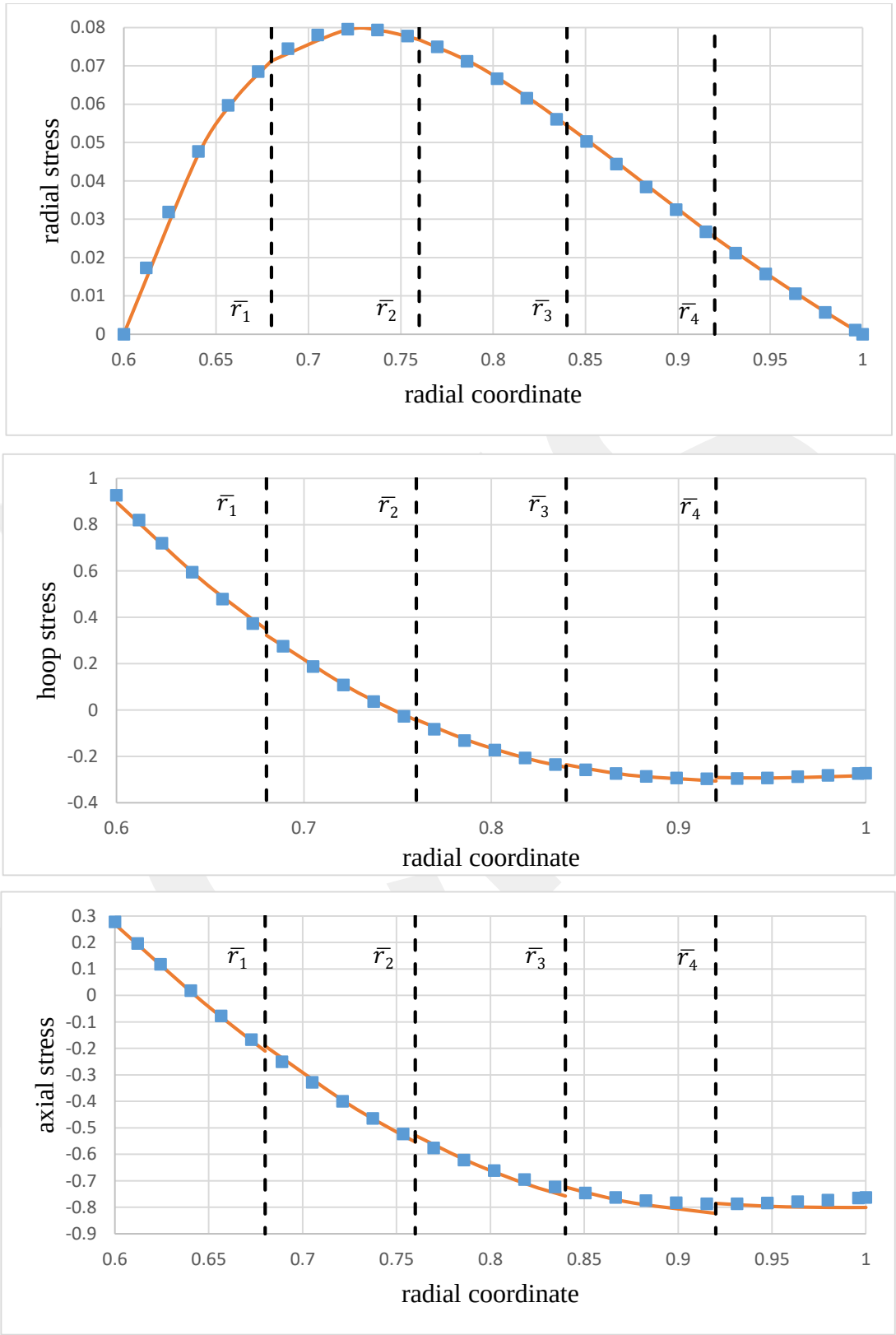

Figure 3.33. Comparison of stresses of the five-layer solution and the analytical solution ($\bar{a} = 0.6, , \bar{r}_1 = 0.68, \bar{r}_2 = 0.76, \bar{r}_3 = 0.84, \bar{r}_4 = 0.92, \bar{b} = 1.0$)

Finally, in the third part, the tube is divided into ten equal layers. The corresponding geometry and material properties are given in Table 3.8. The temperature and dimensionless integration constants are found as $A_1 = -1435.960$, $A_2 = -742.793$, $A_3 = -1510.70$, $A_4 = -780.959$, $A_5 = -1585.92$, $A_6 = -818.659$, $A_7 = -1661.23$, $A_8 = -855.92$, $A_9 = 1736.48$, $A_{10} = -892.79$, $A_{11} = 1811.56$, $A_{12} = -929.27$, $A_{13} = -1886.33$, $A_{14} = -965.40$, $A_{15} = -1960.68$, $A_{16} = -1001.19$, $A_{17} = -2034.525$, $A_{18} = -1036.37$, $A_{19} = -2107.78$, $A_{20} = -1071.84$, $\overline{C}_1 = C_1/b^2 = 5.22 \times 10^{-4}$, $\overline{C}_2 = C_2 = -0.015216$, $\overline{C}_3 = C_3/b^2 = 5.36 \times 10^{-4}$, $\overline{C}_4 = C_4 = -0.016029$, $\overline{C}_5 = C_5/b^2 = 5.55 \times 10^{-4}$, $\overline{C}_6 = C_6 = -0.016845$, $\overline{C}_7 = C_7/b^2 = 5.78 \times 10^{-4}$, $\overline{C}_8 = C_8 = -0.017661$, $\overline{C}_9 = C_9/b^2 = 6.06 \times 10^{-4}$, $\overline{C}_{10} = C_{10} = -0.018477$. as $\overline{C}_{11} = C_{11}/b^2 = 6.37 \times 10^{-4}$, $\overline{C}_{12} = C_{12} = -0.019292$, $\overline{C}_{13} = C_{13}/b^2 = 6.72 \times 10^{-4}$, $\overline{C}_{14} = C_{14} = -0.020103$, $\overline{C}_{15} = C_{15}/b^2 = 7.083 \times 10^{-4}$, $\overline{C}_{16} = C_{16} = -0.020910$, $\overline{C}_{17} = C_{17}/b^2 = 7.45 \times 10^{-4}$, $\overline{C}_{18} = C_{18} = -0.0217120$, $\overline{C}_{19} = C_{19}/b^2 = 7.83 \times 10^{-4}$, $\overline{C}_{20} = C_{20} = -0.022507$. The graphs that compare the ten-layer solution with the analytical solution are given in Figs. 3.34 to 3.37.

Table 3.8. Geometry and the materials properties of ten-layer tube

Layer	$\overline{r}_{i-1}$	$\overline{r}_i$	E_i (GPa)	q (W/m^3)	k (W m^{-1} ^{0}K^{-1})
1	0.6	0.64	266.570	22594.6397	70.4131
2	0.64	0.68	256.741	62762.8882	66.9720
3	0.68	0.72	247.823	92889.0745	63.8878
4	0.72	0.76	239.686	112973.1988	61.1061
5	0.76	0.80	232.226	123015.2609	58.5829
6	0.8	0.84	225.354	123015.2609	56.2829
7	0.84	0.88	219.000	112973.1988	54.1766
8	0.88	0.92	213.102	92889.0745	52.2398
9	0.92	0.96	207.610	62762.8882	50.4523
10	0.96	1.00	202.480	22594.6397	48.7967

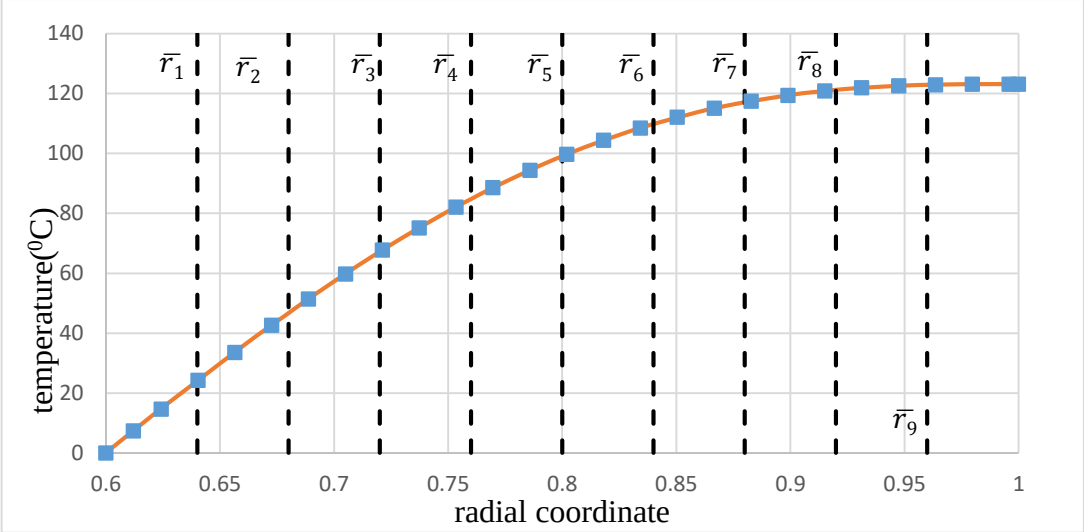

Figure 3.34. Comparison of temperature distributions of the ten-layer solution and the analytical solution ($\bar{a} = 0.6,$, $\bar{r}_1 = 0.64$, $\bar{r}_2 = 0.68$, $\bar{r}_3 = 0.72$, $\bar{r}_4 = 0.76$, $\bar{r}_5 = 0.80$, $\bar{r}_6 = 0.84$, $\bar{r}_7 = 0.88$, $\bar{r}_8 = 0.92$, $\bar{r}_9 = 0.96$, $\bar{b} = 1.0$)

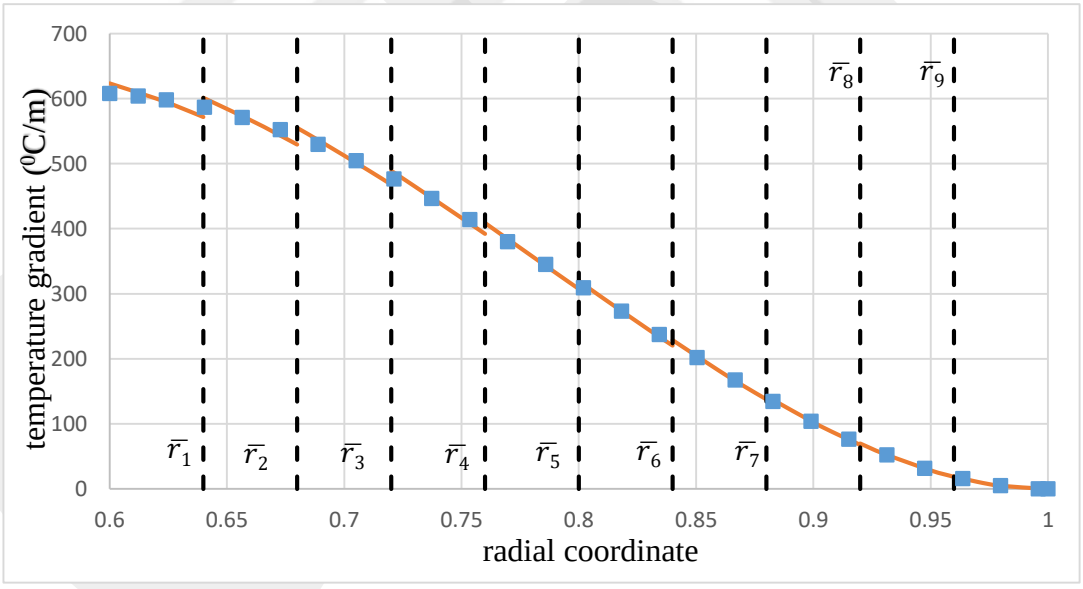

Figure 3.35. Comparison of temperature gradients of the ten-layer solution and the analytical solution

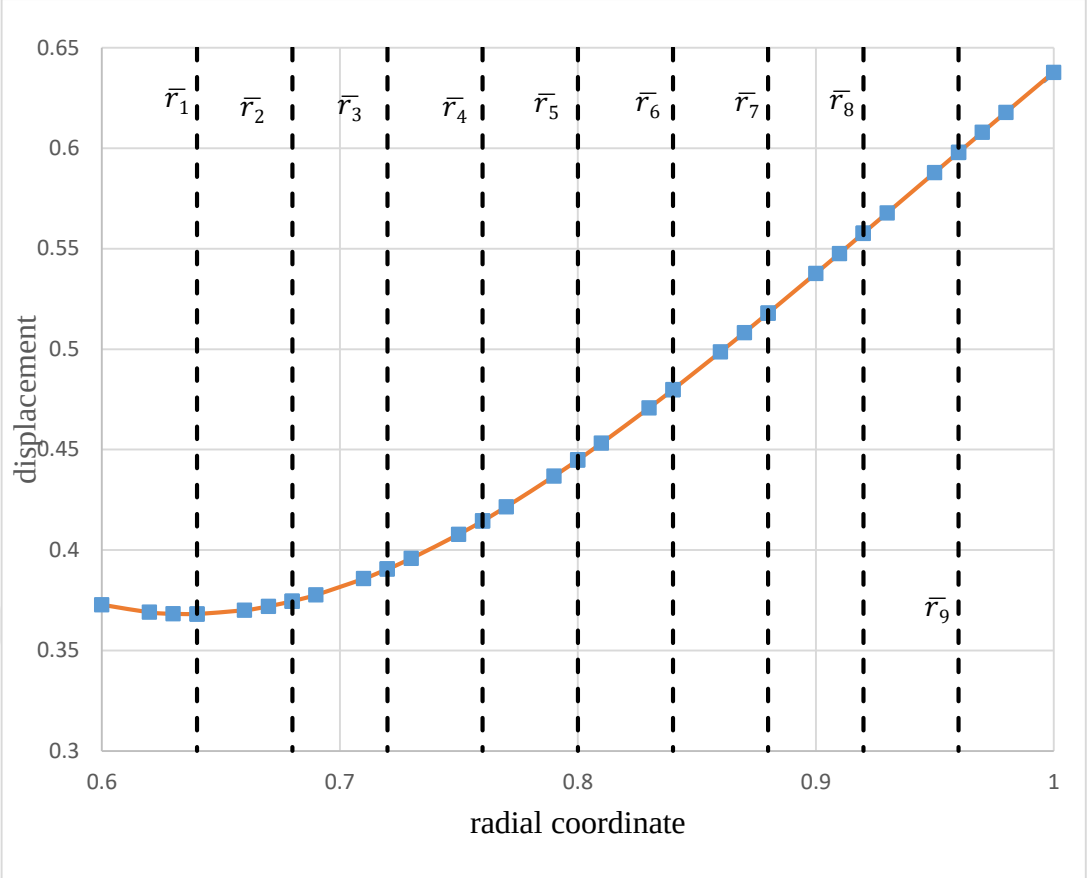

Figure 3.36. Comparison of radial displacements of the ten-layer solution and the analytical solution

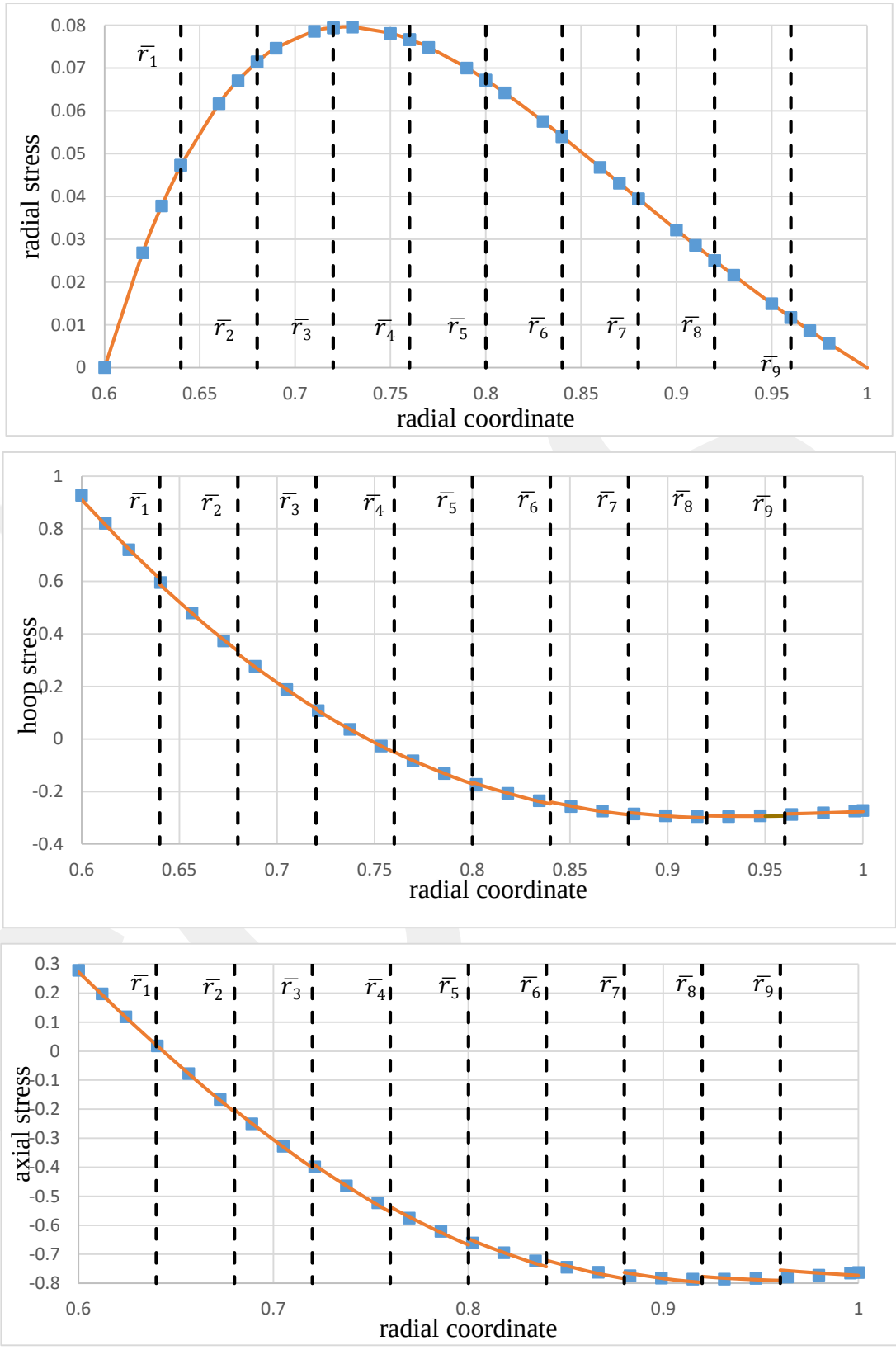

Figure 3.37. Comparison of stresses of the ten-layer solution and the analytical solution

3.5.4. Multilayer tube under thermal loading, internal and external pressure by Sollund et al. [31]

In the study of Sollund et al. [31], a 6-layer tube, which has a layer of corrosion resistant alloy and a thick thermal insulation coating, is considered. The geometry, layer thicknesses and material characteristics are presented below in Table 3.9. along with the applied temperature in each individual layer. The applied internal pressure is $P_{int} = 220$ bars and the external pressure is $P_{ext} = 15$ bars. In Fig 3.38. the comparison of radial, tangential and axial stresses are made. As seen in these graphs, a perfect agreement is obtained between the results of the proposed model and the results obtained by Sollund et al. [31].

Table 3.9. Geometry, material properties and applied temperatures for the six-layer tube

Description	Layer number (i)	r_{i-1} (mm)	r_i (mm)	E_i (GPa)	ν_i	α_i ($°C^{-1}$)	ΔT_i (°C)
CRA liner	1	172.1	175.1	191	0.29	1.7×10^{-5}	131.23
CMn steel	2	175.1	194.2	207	0.30	1.17×10^{-5}	129.02
Epoxy	3	194.2	194.5	3.0	0.40	5.4×10^{-5}	127.08
Adhesive PP	4	194.5	197.5	1.3	0.40	1.6×10^{-5}	126.75
Syntactic PP	5	197.5	252.5	1.1	0.32	5.0×10^{-5}	120.95
Adhesive PP	6	252.5	255.5	1.3	0.40	1.6×10^{-5}	29.84

As it was mentioned before, the aim for examining these example problems is to show the effectiveness of the proposed method. As seen in all comparisons, good agreement with the previous studies are obtained.

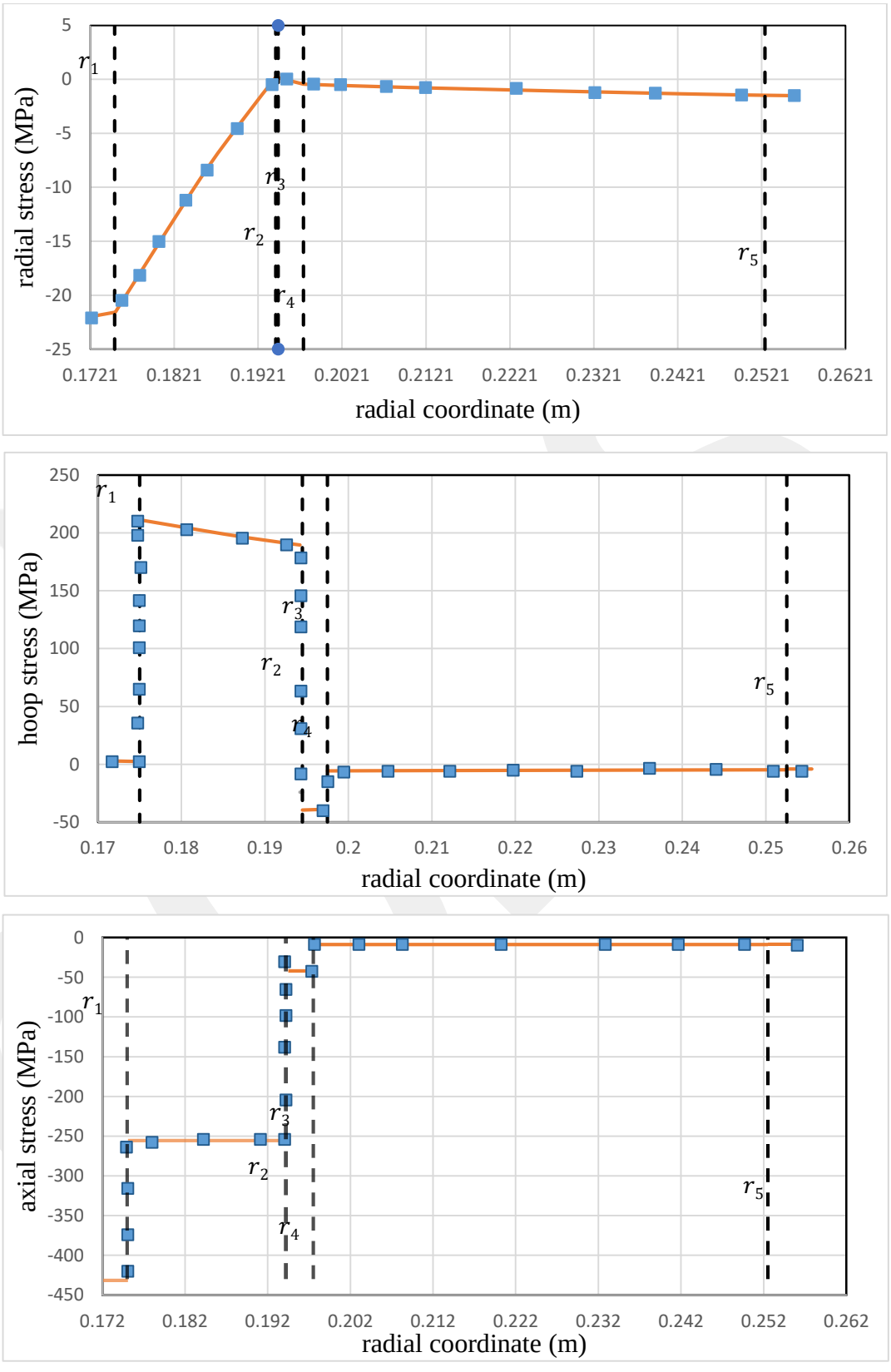

Fig 3.38. Comparison of stress distributions of the six-layer tube and the results in Sollund et al. [31] ($a = 0.1721\ mm,\ ,\ b = 0.255\ mm\ ,\ P_{int} = 220$ bar , $P_{ext} = 15$ bar).

CHAPTER 4

SUMMARY AND CONCLUSION

The aim of this study was to investigate the stress response of multilayer and FGM fixed-ended tubes under thermal and mechanical loads. In the first part, the expressions of temperature distribution, stress components and radial displacement for a single layer tube under thermal and/or mechanical loading are obtained analytically for different boundary conditions. Afterwards, these analytical expressions are used in a simple and efficient numerical method to find the distributions of temperature, stresses and radial displacement of multilayer tubes under thermal loading (with or without heat generation) and under pressure loads. In all derivations and numerical solutions, MATHEMATICA software is used. Using this procedure, some example problems solved previously by several researchers, including multilayer and FGM tubes with different geometries and loading conditions are solved for the validation studies. The numerical results obtained by using the proposed method perfectly agreed with the results given in other studies. It is also found in this study that, increasing the number of layers in FGM tube problems gives better and closer results.

This solution procedure is different from other methods given in other closely related studies, as it suggests a quite easy way to find solutions in elastic state for not only multilayer but also FGM tube problems with different loading and boundary conditions. In addition, one can solve FGM tube problems where all thermal and mechanical properties such as Poisson's ratio are variable using this method.

For future studies, this procedure can be used to determine elastic-plastic response of multilayer and FGM tubes under thermal and mechanical loads. In addition, problems including rotation and shrink fit may also be solved using this method. Lastly, it can be used for finding the solutions of thermal and mechanical problems with different geometries including spheres, disks, and sold cylinders made of functionally graded materials.

REFERENCES

[1] Timoshenko, S.P., Goodier, J.N., Theory of Elasticity. 3rd ed. New York: McGraw-Hill Book Company;1970.

[2] Boresi, A.P, Schmidt, R.J., Sidebottom, O.M., Advanced Mechanics of Materials. Wiley 5th ed., New York, 1993.

[3] Mendelson, A., Plasticity: Theory and Application. Macmillan, New York, 1968.

[4] Boley. B.A., Weiner, J. Fr., Theory of Thermal Stresses. New York: Wiley, 1960.

[5] Nadai, A., Plasticity. New York: Mc-Graw-Hill, 1931.

[6] Durban, D., Kubi, M. A., General solution for the pressurized elastoplastic tube. Journal of Applied Mechanics (1992) 59:20-26.

[7] Lazzarin, P., Livieri, P., Different solutions for stress and strain fields in autofrettaged thick walled cylinders. International Journal of Pressure Vessels and Piping (1997) 71:231-238.

[8] Parker, A.P., Autofrettage of open-end tubes–pressures, stresses, strains, and code comparisons. J Pressure Vessel Technol-Trans ASME (2001) 123:271-281.

[9] Perry J., Aboudi J., Elasto–plastic stresses in thick walled cylinders. J Pressure Vessel Technol—Trans ASME (2003) 125:248-252.

[10] Akis T., Eraslan, A.N., Yielding of long concentric tubes under radial pressure based on von Mises criterion. J Fac Eng Archit Gazi Univ (2005) 20: 365-372 (In Turkish).

[11] Eraslan, A.N., Akış, T., Yielding of two-layer shrink-fitted composite tubes subject to radial pressure. Forsch Ingenieurwes (2005) 69: 187–196.

[12] Qiu J., Zhou M., Analytical solution for interference fit for multi-layer thick-walled cylinders and the application in crankshaft bearing design. Applied Sciences (2016) 6,167.

[13] Eraslan, A.N., Akış, T., Stress analysis in strain hardening two-layer composite tubes subject to cyclic loading of internal pressure. International Journal of Advances in Applied Mathematics and Mechanics (2015) 3: 65–76.

[14] Eraslan, A.N., Akis, T., Akis, E., Deformation analysis of two-layer composite tubes under cyclic loading of external pressure. Journal of Basic and Applied Research International (2016) 13:107-119.

[15] Eraslan A.N., Sener E., Argeso H., Stress distributions in energy generating two-layer tubes subjected to free and radially constrained boundary conditions. International Journal of Mechanical Sciences (2003) 45: 469–496.

[16] Horgan, C.O., Chan, A.M., The pressurized hollow cylinder or disk problem for functionally graded isotropic linearly elastic materials. J Elasticity (1999) 55:43-59.

[17] Tutuncu, N., Ozturk, M., Exact solutions for stresses in functionally graded pressure vessels. Composites: Part B (2001) 32:683-686.

[18] Jabbari, M., Sohrabpour S., Eslami, M.R., Mechanical and thermal stresses in a functionally graded hollow cylinder due to radially symmetric loads. Int J Pressure Vessels Piping (2002) 79:493-497.

[19] Ma, L., Feng, X.Q., Gau, K.W., Yu, S.W., Elastic and plastic analyses of functionally graded elements. Functionally Graded Materials VII Materials Science Forum (2003) 423–424:731-736

[20] Zhifei, S., Taotao, Z., Hongjun, X., Exact solutions of heterogeneous elastic hollow cylinders. Composite Structures (2007) 79: 140–147.

[21] Chen, Y.Z., Lin, X.Y., Elastic analysis for thick cylinders and spherical pressure vessels made of functionally graded materials. Computational Materials Science (2008) 44: 581-587.

[22] Eraslan, A. N., Akis, T., Plane strain analytical solutions for a functionally graded elastic–plastic pressurized tube. International Journal of Pressure Vessels and Piping (2006) 83: 635–644.

[23] Li, X., Peng, X., A Pressurized functionally graded hollow cylinder with arbitrarily varying material properties. Journal of Elasticity (2009) 96: 81–95.

[24] Nie, G.J., Zhong, Z., Batra, R.C., Material tailoring for functionally graded hollow cylinders and spheres. Composites Science and Technology (2011) 71: 666–673.

[25] Sburlati, R., Analytical elastic solutions for pressurized hollow cylinders with internal functionally graded coatings. Composite Structures (2012) 94: 3592–3600.

[26] Xin, L., Dui, G., Yang, S., Zhang, J., An elasticity solution for functionally graded thick-walled tube subjected to internal pressure. International Journal of Mechanical Sciences (2014) 89:344–349.

[27] Akis, T., Yielding of functionally graded long tubes under thermal loading. J. Fac. Eng. Arch. Gazi University (2006) 21: 737-743.

[28] Ozturk, A., Gulgec, M., Elastic–plastic stress analysis in a long functionally graded solid cylinder with fixed ends subjected to uniform heat generation. International Journal of Engineering Science (2011) 49: 1047–1061.

[29] Sadrabadi, S. A., Rahimi, G.H., Citarella, R.J., Karami, S., Sepe, R., Analytical solutions for yield onset achievement in FGM thick walled cylindrical tubes undergoing thermomechanical loads. International Journal of Pressure Vessels and Piping (2018) 161: 10–16.

[30] Sollund, H. A., Vedeld, K., Hellesland, J., Efficient analytical solutions for heated and pressurized multi-layer cylinders, Ocean Engineering, (2014) 92: 285–295.

[31] Vedeld, K., Havar, A., Sollund, H. A., Stresses in heated pressurized multi-layer cylinders in generalized plane strain conditions. International Journal of Pressure Vessels and Piping (2014) 120-121: 27-35.

[32] Yeo, W.H., Purbolaksono, J., Aliabadi, M.H., Ramesh, S., Liew, H.L., Exact solution for stresses/displacements in a multilayered hollow cylinder under thermo-mechanical loading. International Journal of Pressure Vessels and Piping, (2017) 151: 45-53.

[33] Wolfram Research, Inc., Mathematica, Champaign, IL (2003).